INTERPRETATION AND SCALING OF POSITIONAL INFORMATION DURING DEVELOPMENT

Thesis by

Marcos Nahmad Bensusan

In Partial Fulfillment of the Requirements

for the Degree of

Doctor of Philosophy

California Institute of Technology

Pasadena, California

2011

(Defended September 27, 2010)

© 2011

Marcos Nahmad Bensusan

All Rights Reserved

To Michelle,

for her love and support

Acknowledgments

Getting involved in research on developmental biology coming from a theoretical background was not an easy task. It not only required learning new specialized language and technical expertise, but also required me to "think" in a very different way. I am grateful to many people that have made this process an enjoyable and exciting experience. First of all, I would like to thank Angela Stathopoulos, my mentor, for all her patience, support, and guidance throughout my graduate career. She not only ensured that my transition to the "bench" was a smooth process, but also taught me to "think as a biologist" throughout many hours of interesting discussions. I am also very grateful to my CDS advisor, John Doyle, for his full support and encouragement to pursue my interests in biology and for deep scientific discussions. Also, I want to express my more sincere gratitude to Arthur Lander, who agreed to come all the way from UC-Irvine every year to participate in my committee meetings. His contributions and suggestions have been very valuable. I also would like to thank my colleague, Greg Reeves, for many interesting discussions during our weekly lunch hour. Greg and I share the first authorship of the data in Chapter 4, so I would like to acknowledge his contributions to this work. I also thank Ellen Rothenberg and Richard Murray for their participation in my committee and for their ideas and suggestions.

This work is the result of a collective effort of many special people in my life. I would like to thank the most my wife, Michelle, for accompanying me on this journey, for her love and patience, and for supporting me in good and difficult times. This thesis is dedicated to her in appreciation for sharing with me each moment of my life. I also thank

my kids, Orly, Elias, and Shelly, for their unconditional love, and for turning tough days into special moments with their smiles and hugs. Lastly, I also want to thank my family, especially my mom, for always being supportive of my career goals –even if that meant living far away from home.

Abstract

Cells in a developing animal require information about their relative position in order to function and differentiate appropriately. In the classical view, cellular positional information is interpreted from the concentration of chemical signals known as morphogens. However, recent studies have questioned the ability of morphogens to establish gene expression patterns in a concentration-dependent manner. Here we combine theoretical tools and experimental work in *Drosophila melanogaster* to investigate the mechanisms by which positional information is interpreted from a morphogen gradient and the ability of patterns to scale with respect to the size of the system.

First, we study how a concentration gradient of the signaling molecule Hedgehog establishes multiple patterns of gene expression along the anterior-posterior axis of the *Drosophila* wing disc. Using mathematical modeling as a hypotheses-generating tool, we predicted that positional information cannot be explained by different concentration thresholds from a static Hedgehog gradient. Instead, we propose that cells take into account their history of Hedgehog signaling exposure to determine patterns of gene expression. We provide experimental evidence that supports our model and conclude that gradient dynamics, resulting from the gene network architecture of the Hedgehog signaling pathway, determine pattern formation in the wing disc.

Second, we introduce a theoretical formalism to study the role of morphogen gradient dynamics in developmental patterning. Given a mathematical model of pattern formation, we define and compute parameter perturbations that leave invariant the steady-state distribution of the relevant morphogen. We propose that this approach can be

used as a tool to design genetic experiments that assay the function of morphogen dynamics.

Lastly, we use dorsal-ventral patterning of the early *Drosophila* embryo as a model to study scaling of gene expression patterns with respect to natural variations in axis length, that is, the ability to establish positional information relative to the size of the system. We provide evidence that gene expression patterns that depend on the maternal factor Dorsal, scale along the dorsal-ventral axis. Our data suggest that scaling in this system is a gene-dependent rather than a position-dependent property. We propose that the mechanisms for scaling depend on feedback interactions downstream of Dorsal.

Table of Contents

Chapter 1. Introduction **1**

1.1 Historical Perspective 2

1.2 Positional Information and Morphogen Gradients 7

1.3 The Problem of How Extracellular Morphogens are Interpreted 15

1.4 The Problem of How Gradient Dynamics Affect the Interpretation of Morphogen Signals 18

1.5 The Problem of Size-Dependent Scale Invariance of Pattern 21

1.6 A Multidisciplinary Approach to the Study of Developmental Pattern Formation 25

Chapter 2. Dynamic Interpretation of Hedgehog Signaling in the *Drosophila* Wing Disc **27**

2.1 Introduction 28

2.2 Materials and Methods 31

2.3 Results 34

2.4 Discussion 51

Chapter 3. Steady-State Invariant Genetics: Probing the Role of Morphogen Gradient Dynamics in Developmental Patterning **63**

3.1 Introduction 64

3.2 Methods 67

3.3 Theoretical Framework: Definitions and Examples 68

3.4 Analysis of Steady-State Invariant Sets 80

3.5 Concluding Remarks 83

3.6 Outlook 84

Chapter 4. Spatial Scaling of Dorsal-Ventral Patterns in the Early *Drosophila* Embryo 86

4.1 Introduction 87

4.2 Materials and Methods 90

4.3 Results 95

4.4 Discussion 104

Chapter 5: Discussion 110

Chapter 6: Future Directions 119

6.1 Future Directions for Chapter 2 119

6.2 Future Directions for Chapter 3 124

6.3 Future Directions for Chapter 4 124

Bibliography 127

Appendices 150

Supporting Materials for Chapter 2 150

Supporting Materials for Chapter 3 178

Supporting Materials for Chapter 4 185

Chapter 1

Introduction

"Development starts off from a more or less spherical egg, and from it an animal develops that is anything but spherical; it has legs, a head, a tail, etc. and internal organs that also have determined constant forms…"

C. H. Waddington (The Nature of Life, 1961)

It is difficult to think of a natural process that displays a more elegant combination of efficiency, complexity, and self-organization than animal development. The species that today populate our planet are the result of the most spectacular experiment in natural history; through millions of generations, organisms have adapted their body plans to coexist with each other, often in unfavorable or hostile environments. The final product of this long evolutionary process is not only a plethora of living shapes and forms, but also the precise "instructions" of how they develop and come to be. These "instructions" or principles have only become available to us recently, thanks to the advancement of microscopy, molecular biology, and genetics. In fact, much of the research in modern developmental biology relates to finding and interpreting the principles underlying animal design (Carroll et al., 2005; Davidson, 2006; Lawrence, 1992). A central aspect to the understanding of animal development is the study of pattern formation, this is, the spatiotemporal specification and organization of cell types in a developing group of cells. Although there has been much scientific interest in developmental patterning during the past 40 years, the mechanisms by which cells interpret the signals that control gene expression patterns remain controversial. This chapter introduces the ideas and models

that have played a key role in trying to explain the formation of pattern in developing systems and highlights some fundamental problems that will be the focus of this work.

1.1 Historical Perspective

For centuries, scientists and naturalists have been fascinated by the complexity of animal development and have speculated about the origin of life forms and functions. While the importance of embryonic pattern formation was well recognized by embryologists in the late 19th century, the models of how cells in a developing embryo or tissue acquire a precise spatial organization have changed dramatically in the history of biology. Today we know that all cells in a developing animal carry the same genetic information and that the spatial organization of cells during development depends on their ability to control, in space and time, the expression of a set of key genes. But for much of the first half of the 20th century, the genetic basis of spatial order in development was a controversial subject. This brief historical remark does not intend to summarize the complex history of embryonic pattern formation, but tries to trace the origin of some of the concepts that are currently widely used in developmental patterning, such as the concepts of organizer, embryonic field, and morphogen gradient.

Much of the early efforts to explain pattern formation originate from regeneration experiments in insects (Morgan, 1897) and the concept of embryonic induction in vertebrates (Spemann, 1938). These experiments revealed the amazing ability of embryos to self-organize their developmental programs upon external manipulations. The global properties of spatial order were captured in the concept of embryonic field, first postulated by Boveri in 1910 (reviewed by Sander, 1994). In its simplest form, an

embryonic field refers to a system that, as long as it remains in contact with some substratum, is able to spatially reorganize its developmental program in response to changes in size or mass. Although the concept of embryonic field was not precisely defined and the mechanisms of action of the field were not known in the early 20th century, many sources of experimental evidence favored the existence of embryonic fields and the concept rapidly became a paradigm of experimental embryology.

Strong support for the embryonic field concept came from spectacular transplantation experiments in newts and salamanders. In 1924, Hans Spemann and Hilde Mangold performed a famous experiment using salamander eggs from two different species (Spemann and Mangold, 1924). They transplanted dorsal cells from one embryo (the donor) and introduced them into the ventral region of the other embryo (the host). As revealed by the difference in cell pigmentation between the two species, the donor cells were able to induce dorsal neural fates in the surrounding host tissue. The experiment suggested the presence of an "organizing" substance emanating from the donor tissue that acts at the distance to orchestrate patterning in the host. The discovery of the "Organizer" could have had an immediate impact on the problem of pattern formation, but the lack of success in identifying the organizing substance over many decades obscured the interest in the problem (Witkowski, 1985).

Almost at the same time that Spemann popularized the concept of induction, the field of genetics began to demonstrate that its tools had much to offer to the problem of pattern formation. The identification of mutants in fruit flies and mice with morphological defects and the discovery of genetic mosaics provided a fantastic opportunity to study the problem of developmental patterning. Thomas Hunt Morgan,

who established the modern school of genetics in the fruit fly *Drosophila melanogaster*, was also an influential embryologist. In 1934, Morgan wrote a review entitled *Embryology and Genetics* with the objective to set a ground of contact for the two disciplines (Morgan, 1934). However, only a few embryologists at that time believed that genes could have a developmental role and Morgan's attempt to initiate crosstalk between geneticists and embryologists was not very fruitful. The most significant efforts to integrate genetics and embryology came from Conrad Hal Waddington, a British paleontologist by training that was attracted to embryology by the Organizer problem. As many embryologists and biochemists that turned their attention to the Spemann Organizer, Waddington failed to find the chemical nature of the organizing substance, but in the late 1930s, he uncovered another aspect of the Organizer problem. In Spemann's work, too much attention was given to the inducer tissue (the Organizer) rather on the response of the surrounding cells to the organizing substance. Waddington realized that in order for ventral cells in the host tissue to develop into ectopic dorsal tissue in the Spemann and Mangold experiment, they must be competent to respond to the inducing signal. This idea prompted Waddington to propose that the development potential of cells to adopt a particular fate should be under the control of the genes. The idea that genes were under control of developmental patterning was not entirely new, but was very unpopular among embryologists who claimed that different patterns could not be explained by the action of genes whose DNA template was the same in every cell type of the embryo. By 1940, Waddington was able to gather a series of analogies to support the equivalence of organizers and genes (Waddington, 1940). A celebrated example was that of the gene *aristapedia* which is responsible for the transformation of legs into antennas

in *Drosophila* (since in *aristapedia* mutants, legs develop in place of the antennas). He argued that in the same way that host cells in the Organizer experiment adopt different fates in the presence or absence of the organizing substance, *aristapedia* was able to *induce* the "antenna" fate instead of the default "leg" fate. In 1956, Waddington presented a genetic model of embryonic cell differentiation suggesting that organizing substances in the cytoplasm influence the activation of genes in the nucleus (Waddington, 1956). With his ideas, Waddington founded the genetic basis of embryonic induction and pattern formation, but his work received full consideration by embryologists only after Jacob and Monod demonstrated that cell differentiation in bacteria was under the transcriptional control of gene activity (Jacob and Monod, 1961).

The synthesis of genetics and embryology opened a new research era in the problem of developmental patterning. During this new stage, organisms that were extensively used for the study of embryology, such as flat worms, salamanders, and frogs, were replaced by emerging genetic "model" organisms such as fruit flies and mice. Genetic screens prompted the discovery of new genes with developmental phenotypes, but the technology was still somewhat immature to reveal the molecular mechanisms underlying the spatial control of gene expression. These conditions favored the development of theoretical and mathematical models of pattern formation. The main challenge of these theoretical studies was to introduce a conceptual framework to explain the stable generation of patterns and their self-organizing properties. An almost universal feature of the theories of pattern formation (that prevails until today) was to postulate the existence of chemical gradients (or gradient-fields), which were considered particular cases of morphogenetic fields in the 1920s and 1930s. Gradients of different kinds were

originally considered in theories by Huxley and de Beer (1934), Dalcq (1938), and Child (1941); but perhaps the most influential theoretical contributions to the current understanding of pattern formation came in the 1950s and 1960s with Turing's reaction-diffusion model of morphogenesis (Turing, 1952), Stern's prepattern hypothesis (Stern, 1954), and Wolpert's positional information theory (Wolpert, 1969).

The use of reaction-diffusion dynamics in developmental patterning is due to the famous mathematician, Alan Turing, a pioneer in the development of mathematical models in embryonic pattern formation. In his 1952 seminal paper, Turing used partial differential equations to model the concentrations of two chemical species diffusing and reacting with one another. It was shown that under certain conditions on the parameters (e.g., assuming short-range activation and long-range repression) a broad variety of periodic patterns (such as "spots" or "stripes") could be generated using Turing's formalism. In his paper, Turing also coined the term "morphogen" to refer to the chemical species that work as "generators of form," a concept that is prevalent in the modern literature. Meinhardt and Gierer later expanded the efforts of Turing and applied them to patterning of *Hydra* (Meinhardt and Gierer, 1972). A recent application of Turing's concept is the case of Spätzle, a ligand that activates the Toll receptor in the early *Drosophila* egg. Spätzle is "freely" diffusible in the extracellular space surrounding the embryo known as the perivitelline fluid where it interacts with other factors that regulate its activity. These peculiar characteristics make the system suitable for modeling by using Turing's formalism (Meinhardt, 2004). In fact, reaction-diffusion models have successfully explained some intriguing properties of this system such as axis duplication when Spätzle is over-expressed (Morisato, 2001). Turing' reaction-diffusion models are

very influential today in mathematical biology and have also been shown to have experimental significance in the formation of skin and pigmentation patterns (Kondo and Asai, 1995).

On the other hand, one of the first attempts to explain pattern formation based on genetic evidence is the work on genetic mosaics in *Drosophila* and the theory of prepatterns proposed by Curt Stern (Stern, 1954). The theory postulates the existence of genetic prepatterns and suggests that final patterns in a tissue result from the competence of cells to respond to the prepattern cues (or 'singularities'). In a mutant clone, for example, mutant cells may not affect the prepattern, but may cause a change in their competence to respond to it. With the prepattern concept, Stern was able to explain the phenotypes resulting from genetic mosaics of homeotic mutants in *Drosophila* (i.e., mutants transform one tissue identity into another). Stern's prepattern hypothesis was very influential in the 1960s, especially on insect patterning (Sondhi, 1963; Lawrence, 1966; Stumpf, 1967). However, the prepattern hypothesis lost general applicability when it was found to be insufficient to explain bristle patterns in different *Drosophila* tissues (Bryant, 1969; Tokunaga, 1978). Nonetheless, Stern's theory had a profound influence on Wolpert's positional information theory and was also later proposed to apply to patterning of the *Drosophila* segmentation network (Akam, 1987).

1.2 Positional Information and Morphogen Gradients

The prevailing view about developmental pattern formation comes from Lewis Wolpert's theoretical work on positional information (Wolpert, 1969). In contrast to previous models of pattern formation, Wolpert's goal was to propose a general conceptual

framework in which the common properties of pattern formation could be explained. Wolpert reasoned that in the same way that universal principles govern the synthesis of proteins from a DNA template (cf. the central dogma of molecular biology), there should be general principles involved in the translation of genetic information into spatial patterns of cellular differentiation; if cells depend on their spatial location to determine their fate, what are the general principles by which cells acquire and interpret their "positional information"?

According to the theory of positional information, developmental patterning is the process by which each cell, based on its genetic information and developmental history, determines its pattern of molecular differentiation according to its location in the system. Hence, pattern formation is regarded as a sequential two-step process comprising the specification and the interpretation of positional information. The specification of positional information in an embryonic field is the equivalent of choosing a coordinate system (a notion proposed originally by Hans Driesch in 1894). Coordinate systems are defined with respect to reference points and depend on the polarity of the system, i.e., the direction in which positional information is to be measured. One mechanism (originally proposed by Stumpf in 1966) by which cells may acquire their positional coordinates is by measuring the concentration of a chemical substance that is present in a concentration gradient across the field of cells (Stumpf, 1966). A concentration gradient capable of specifying positional information in a concentration-dependent manner is referred to as a morphogen gradient in the modern literature. Although this is not the only way to specify positional information, the existence of morphogen gradients and their role in

developmental patterning was later strongly supported by many experimental studies and constitutes one of the paradigms of modern developmental biology.

The second step in the process of pattern formation is the interpretation of positional information, that is, how "positional values" are converted into discrete states of cellular differentiation. The interpretation step must depend on a regulatory code by which cells translate positional information signals into differentiation genes, but may also depend on cellular competence to positional signals, developmental history, and cell-cell interactions.

Perhaps the most important contribution of Wolpert's positional information theory is the postulate that the coordinate systems required for positional specification may be universal (at least within the same animal). For example, the specification of positional values in two developing tissues may be the same, but they give rise to two different adult parts because cells interpret positional coordinates in a different manner within each tissue. Evidence for this universality hypothesis was provided by genetic mosaics of homeotic mutants (Roberts, 1964) or from transplantation experiments in insect segments (Stumpf, 1967). For example, clones of cells lacking the gene *aristapedia* produce leg structures in the antenna that correlate with their corresponding position in the leg (Roberts, 1964). One corollary of the universality hypothesis of coordinate systems is that the process of positional specification is independent from its interpretation. In particular, the specification of positional information should be -in principle- independent of the field's genome or its developmental history.

The original motivation of the theory of positional information was to address the problem of size-dependent scale invariance in embryonic patterning. This problem can be

abstracted by the famous French flag problem, which Wolpert introduced a year earlier and can be stated as follows (Wolpert, 1968). Consider an embryonic field that is subdivided in three contiguous patterns such that the first third contains cells of "blue" type, the second third contains cells of "white" type, and the remaining third contains cells of "red" type (resembling the pattern of a French flag). The problem consists of explaining how the patterns maintain their proportions over large deviations in the original size of the field (i.e., after the field has been 'cut' into half or after two fields have been fused). It is evident that to generate a French flag pattern irrespective of the size of the field, each cell must poses information about its location, not only with respect to a reference point, but also relative to the length of the axis. Wolpert offered a solution in terms of a diffusible substance (morphogen) that is secreted at one end of the embryonic field (source) and destroyed at the other (sink) (Wolpert, 1968). This solution of the problem suggests the existence of two or more 'thresholds' in positional information values that cause any two adjacent cells to adopt the same pattern when their positional values are within the same threshold domain, but another pattern if they correspond to different threshold regions [an idea originally proposed by Dalcq and Pasteels (1937)]. For its simplicity, the formation of pattern as a result of concentration thresholds from a morphogen gradient rapidly became a classical textbook model of developmental patterning (popularly known as Wolpert's French flag model[*] or "Classical Morphogen" model). Subsequent theoretical work explored the biological

[*] The use of the name Wolpert's French Flag *model* in the modern literature is unfortunate because it does not necessarily refer to the solution of Wolpert's French Flag *problem* described above (i.e., the size-dependent scale invariance problem), but simply to the existence of morphogen concentration thresholds that define boundaries of gene expression patterns. Perhaps, the name "Dalcq-Pasteels Thresholds" model would have made more historical sense. In the rest of this work, I will use the term "classical" morphogens to distinguish morphogens that specify positional information in a concentration-dependent manner from (non-classical) morphogens that do not employ multiple thresholds (see below).

feasibility of morphogen gradients to be established by diffusion (Crick, 1970) and discussed the mechanisms in which concentration thresholds could lead to sharp boundaries of gene expression (Lewis et al., 1977). However, the existence of morphogens and their mechanisms of action remained a theoretical speculation until the first morphogen was discovered experimentally 20 years later.

The molecular identification of morphogen gradients in the late 80s and 90s provided the first opportunity to test their proposed role as carriers of positional information. The first genetic gradient to be observed experimentally was the maternal product, Bicoid (Bcd), in the early *Drosophila* embryo (Driever and Nusslein-Volhard, 1988a). In their studies, Driever and Nusslein-Volhard were able to show not only that the Bcd protein forms a concentration gradient that peaks at the anterior pole and decreases posteriorely in an exponential fashion, but they provided genetic evidence that patterning of the anterior-posterior axis in the embryo depends on Bcd concentrations (Driever and Nusslein-Volhard, 1988b). The news that Bcd apparently behaves as a classical morphogen provided strong support to Wolpert's positional information theory and initiated the "hunt" for additional morphogens in other systems. In the following 10 years, many other morphogen candidates were identified in different systems, including Activin in the frog embryo (Green and Smith, 1990), Decapentaplegic (Dpp) in the *Drosophila* embryo and developing wing (Ferguson and Anderson, 1992; Nellen et al., 1996), and Sonic Hedgehog in the chick limb and spinal cord (Riddle et al., 1993; Roelink et al., 1995). Moreover, comparative studies across different phyla have revealed that most morphogens belong to just a few families of signaling molecules, namely, the Hedgehogs, the Wnts, and the families of Transforming, Epithelial, and Fibroblast

Growth Factors (TGFs, EGFs, and FGFs, respectively). This remarkable fact shows that, in some sense, the specification of positional information is universal; despite the vast repertoire of animal body plans, positional information is established using essentially the same molecular machinery.

However, morphogens are by no means the only way to establish positional information. For example, in the sea urchin embryo, it is possible to explain cell differentiation solely from the dynamics of transcriptional networks (Smith et al., 2007; Bolouri, 2008). Another intriguing case of developmental patterning without morphogens is that of the slime mold *Dictyostelium discoideum* in which cells first differentiate at scattered locations and then sort themselves in the aggregate to form a reproducible "French flag" pattern (Thompson et al., 2004). Conversely, the role of morphogens is not limited to pattern formation. For example, morphogens are also recognized to participate in cell affinity, polarity, and tissue growth (Lawrence, 2001).

Recent advances in genetic, molecular, and microscopy tools have provided the opportunity to study the mechanisms underlying morphogen-mediated patterning in high resolution and have favored some experimental model systems over others. The experimental studies in this work are based on two systems that lead much of the current research in developmental patterning, the early *Drosophila* embryo and the developing *Drosophila* wing (or wing imaginal disc). One of the advantages of the first system as a model to study the role of morphogens is the fact that during the first ~4 hours (known as the syncytial blastoderm stage), the *Drosophila* embryo is a giant cell comprising nuclei that share a common cytoplasm and are encompassed by a single cell membrane. (Individual cell membranes form later during a stage known as cellularization). This

means that the early gradients in the *Drosophila* embryo are intracellular. In fact, the maternal factors Bcd and Dorsal (dl) that initiate patterning of the embryo are transcription factors, meaning that they directly bind DNA and control gene expression. This suggests that the interpretation of positional information in the early *Drosophila* embryo is much simpler than in other systems in which patterning is orchestrated by extracellular morphogens that depend on complex signal transduction pathways. Another advantage of the early *Drosophila* embryo is that its size does not change over time, that is, once an embryo is laid, it will retain its size during embryonic development; this provides the advantage that positional coordinates will not need to change over time as a result of embryo growth. On the other hand, the wing imaginal disc has proven to be one of the most convenient models to study extracellular morphogens because powerful genetic toolkits permit a precise spatiotemporal tuning of morphogen activity. One example is the increasing stock collection libraries employing the Gal4-UAS system (Fischer et al., 1988; Brand and Perrimon, 1993). Gal4 is a yeast protein that, when expressed in a particular pattern in flies, can activate transcription of any gene that is under the control of the "Upstream Activation Sequence" (UAS). The Gal4-UAS system can be combined with other genetic techniques such as mitotic recombination to express any desired gene in genetic mosaics, or can be enhanced for temporal control when expressed in conjunction with a temperature-sensitive form of Gal80 yeast protein which, at permissive temperature, binds Gal4 and blocks the transcription of the gene under UAS control (McGuire et al., 2004; see Chapter 2 for an example).

One important difference between morphogen-mediated patterning in the early *Drosophila* embryo and in imaginal discs is the origin of positional information. Unlike

in the early embryo in which the morphogens are established maternally (i.e., mother cells deposit *bcd* and *dl* RNA into the egg when it is still in the female's abdomen), the classical paradigm by which imaginal discs are patterned can be described as a three-step process (Lawrence and Struhl, 1996). In the first step, positional information from both the anterior-posterior (AP) axis and the dorsal-ventral (DV) axis of the embryo defines the location of a subset of cells that will become the disc primordium. The second step consists of forming 'compartments' within the disc primordium. For example, cells located at the posterior side of the disc primordium express the 'selector' gene *engrailed* (Morata and Lawrence, 1975) that distinguishes them from cells at the anterior side of the primordium that do not express it. In this case, the restriction of *engrailed* expression to posterior cells is defined earlier during the patterning of the embryo segments. The expression of selector genes is inherited after cells divide and also influences cell affinity to result in sharp boundaries between compartments. In this way, cells segregate into distinct compartments and maintain their identity as the tissue grows (García-Bellido, 1975). Third, cells in each compartmental boundary are instructed to serve as the source of morphogens, which establish positional information within the disc (Meinhardt, 1983).

In recent years, the study of how morphogen gradients are established and interpreted is at the very front of research in developmental biology. Yet, our progress on understanding their mechanisms of action as organizing molecules of pattern formation has been frustratingly slow. The study of morphogen-mediated patterning can be conceptually subdivided into two classes of problems: how morphogen gradients are established (specification of positional information; reviewed by Zhu and Scott, 2004; Kornberg and Guha, 2007), and how morphogen gradients specify patterns (interpretation

of positional information; reviewed by Gurdon and Bourillot, 2001; Ashe and Briscoe, 2006). In this thesis, I present the results of my investigations on three fundamental problems regarding how morphogen signals are interpreted to control developmental patterning. These problems, which are briefly discussed and justified in the following sections, are the driving force and motivation of my multidisciplinary research program.

1.3 The Problem of How Extracellular Morphogens are Interpreted

The advancement of molecular and genetic tools in developmental biology has left no doubt about the importance of organizing molecules or morphogens in the formation of patterns of gene expression. Although the progress regarding the identification and localization of the relevant morphogens that orchestrate patterning in different experimental systems has been spectacular in the past 10 years, the problem of how morphogens act, that is, how signaling gradients give rise to different cellular responses, still deserves much additional consideration.

The Classical Morphogen model provides a simple and elegant mechanism by which graded spatial information can be converted into discrete patterns of gene expression. This mechanism depends on the existence and interpretation of morphogen concentration thresholds, but the molecular basis of how thresholds from a graded input give rise to multiple discrete responses remains poorly understood. Theoretical models can mimic concentration thresholds by assuming high cooperative binding of the morphogen or imposing positive feedback on gene responses (Lewis et al., 1977; Meinhardt, 1978). On the other hand, experimental studies in many systems have shown that chemical gradients often correlate with the position of gene expression patterns.

These observations provide support to the Classical Morphogen model, but do not conclusively demonstrate that patterning is a concentration-dependent process. In fact, with the exception of a few cases in which the interpretation of the morphogen signal has been studied in detail, it is largely unclear if the position of different patterns actually corresponds to different concentration thresholds. One such exception is the case of Activin in the frog embryo (Green and Smith, 1990; Gurdon et al., 1998). Activin is a member of the TGF-β family that patterns the dorsal mesoderm in the frog embryo. Through a series of elegant studies, John Gurdon and his colleagues have been able to convincingly show that Activin works as a classical morphogen by directly activating the genes *goosecoid* (*gsc*) and *Xenopus brachyury* (*Xbra*) in a dose-dependent manner. First, Gurdon et al. observed that glass beads soaked in Activin transplanted into the embryo result in the expression of *gsc* next to the beads followed by an expression domain of *Xbra* (Gurdon et al., 1994; Gurdon et al., 1995). Second, using radioactively labeled Activin protein, it was shown that signal responses depend on absolute receptor occupancy (in particular, about 100 Activin-bound receptors are sufficient to activate *Xbra*, while approximately 300 are required for *gsc*; Dyson and Gurdon, 1998). Third, changes in Activin dosage correspond to similar concentration changes in the intracellular transducer of the signal, Smad2 (Shimizu and Gurdon, 1999). Furthermore, Gurdon and collegues ruled out that other mechanisms played a role in Activin patterning. For example, they showed that once activin signaling is stabilized, increased temporal exposure to the signal does not affect the patterning outcome (Dyson and Gurdon, 1998). In addition, cells appear to respond to Activin signaling levels independent of the levels of their neighbors (Gurdon et al., 1999). Taken together, this

detailed body of data provides strong evidence that Activin acts as a classical morphogen in the frog embryo.

However, not all the gradients that have been studied in detail support the Classical Morphogen model. For example, the specification of digits in the developing vertebrate limb depends on the temporal exposure to Sonic Hedgehog (Shh) signaling. A group of cells in the posterior limb bud produces Shh, which forms a gradient along the AP axis of the limb. In vivo studies in which the fate of Shh producing cells is genetically marked have demonstrated that many of the cells that initially express Shh are displaced anteriorely as a result of tissue growth away from the region of Shh-expressing cells. This process results in populations of cells that experience different temporal exposures to Shh and suggests that the identity of posterior digits depends on their temporal exposure to Sonic Hedgehog signaling (Ahn and Joyner, 2004; Harfe et al., 2004). Follow up studies confirmed that temporal exposure rather than Shh signaling "strength" is the predominant factor in the specification of posterior digits (Scherz et al., 2007; Towers et al., 2008) and concluded that Shh acts as a "non-classical" morphogen in the vertebrate limb.

Although the Classical Morphogen model remains as a paradigm of modern developmental biology, the importance of concentration thresholds remains doubtful in many systems that are often considered "classical." Regardless of whether or not the Classical Morphogen model can be verified or ruled out in other systems, a more detailed study of morphogen signaling will provide the opportunity to uncover the precise mechanisms in which positional information give rise to form and pattern in developing systems. In Chapter 2, I present our study of how a gradient of Hedgehog (Hh) is interpreted to give rise to at least three patterns of gene expression in the *Drosophila*

wing disc. Hh belongs to a family of widely conserved signaling molecules that organize patterning in different developmental contexts (reviewed by Ingham and McMahon 2001, Jiang and Hui, 2008; Varjosalo and Taipale, 2008; see Box 1.1). We demonstrate that patterning by Hh in the *Drosophila* wing disc largely depends on the properties of the Hh gene network architecture rather than in the "shape" of the Hh concentration. Our results suggest that, contrary to what was previously thought, Hh does not seem to act as a classical morphogen in this system and we introduce a novel mechanism in which patterns of gene expression can be established during development (Nahmad and Stathopoulos, 2009).

1.4 The Problem of How Gradient Dynamics Affect the Interpretation of Morphogen Signals

Developing systems exhibit various sorts of dynamic behaviors. For example, some cells grow and divide, while other cells die prior to reaching maturity; some cells remain in their original locations while others migrate several cell diameters away from the site from which they originated. Yet, the resulting morphogenetic pattern in adult animals is usually invariant and highly reproducible from individual to individual suggesting that the interpretation of positional information takes into account these dynamical processes. One idealization of the Classical Morphogen model, at least in its naïve "textbook" version, is its static nature. In this view, patterns correspond to the read out of concentration thresholds from a stable morphogenetic landscape. However, morphogen gradients are more likely dynamic entities rather than fixed systems of coordinates. In fact, several experimental studies in many systems have shown that morphogen gradients remain changing in time during and even after the process of pattern formation takes

Box 1.1. Brief overview of the Hedgehog signaling pathway.

hegehog (*hh*) was discovered in genetic screens that affect early *Drosophila* patterning (Nusslein-Volhard and Wieschaus, 1980). Since its discovery, the Hh pathway has been central in the study of development and disease. Unlike other signaling pathways, activation of Hh signaling depends on the interruption of an inhibitory signaling cascade, rather than on leading the activation of a pathway. In the absence of Hh, the 12-span receptor Patched (Ptc) maintains the signaling pathway inactive by repressing phosphorylation of the 7-transmembrane effector Smoothened (Smo). Although the precise mechanism of how Ptc inhibits Smo activation remains unclear, Ptc and Smo do not seem to interact directly (Denef et al., 2000). Instead, Ptc seems to repress Smo catalytically (Taipale et al., 2003), probably by secreting a small molecule that results in Smo repression (Bijlsma et al., 2006). Upon Hh binding to Ptc, the Hh-Ptc complex is internalized via endocytosis and degraded in lysosomes (Torroja et al., 2004). This leads to removal of Ptc and activation of the pathway. However, activation of Hh signal does not seem to depend on the absolute levels of unliganded Ptc, but also on the levels of the Hh-Ptc complex which can activate the signal by titrating unliganded Ptc molecules (Casali and Struhl, 2004). Hh signal activation induces phosphorylation of Smo by Protein Kinase A (PKA) (Jia et al., 2004; Zhao et al., 2007) which enhances the recruitment of a series of kinases that include the kinesin-like molecule Costal2 (Cos2) and the kinase Fused that prevents PKA-dependent phosphorlylation and cleavage of the zinc-finger transcription factor *cubitus interruptus* (*ci*). In the absence of Hh signaling, the cleaved Ci fragment (known as Ci75) acts as a repressor of Hh target genes. Activation of the Hh pathway inhibits the processing of Ci into Ci75 and permits full-length Ci to enter the nucleus as a transcriptional activator of Hh target genes (Vervoort, 2000). A key feature of Hh signaling is that *ptc*, the gene that encodes the Hh receptor, is transcriptionally activated by Hh signaling. This feedback gives Ptc the dual function of receiving the signal and limiting its range of action (Chen and Struhl, 1996). Although most key aspects Hh signaling are generally conserved from flies to vertebrates, there are some differences. For example, vertebrates have three Hh ligands and transcriptional activation depends on the balance of three *ci* homologs, known as Gli's. Moreover, unlike in *Drosophila,* Hh signaling in mammals depends on a cellular structure called the primary cilium (Huangfu, et al. 2003). In addition to its role as a morphogen in many developmental contexts, Hh has also been implicated in tissue homeostasis, stem cell maintenance, and growth control (reviewed by Jiang and Hui, 2008).

place (Bergmann et al., 2007; Harvey and Smith, 2009; Kanodia et al., 2009; Liberman et al., 2009). The problem of how the dynamics of morphogen gradients contributes to the establishment and interpretation of pattern is little understood and only recently has received full consideration (Jaeger and Reinitz, 2006; Kutejova et al., 2009).

How is a stable pattern established from a gradient that changes in time? And moreover, how do morphogen dynamics contribute to the interpretation of positional information? The first question has been recently studied in detail in some systems. For example, temporal changes in Activin concentrations in the frog embryo are rapidly reflected in concentration changes of the transducer, Smad2 (Bourillot et al., 2002). In this case, cells may switch from *Xbra* to *gsc* expression as Activin levels are temporally established. Therefore, Activin signaling is continuously transduced; a transient signal corresponding to transient pattern of gene expression that converge to stable patterns once the Activin gradient reaches a steady-state distribution. Furthermore, the role of transient morphogen gradients is especially relevant in systems in which patterning takes place within a short window of time. For instance, in the early *Drosophila* embryo, patterning along the AP axis takes about 90 minutes, while the rates of Bcd gradient formation in diffusion models is estimated to take on the order of a few hours. This has led to the proposal that the interpretation of the Bcd gradient takes place prior to reaching its steady state (Bergmann et al., 2007).

However, the problem of whether or not morphogen gradient dynamics *per se* encodes some sort of positional information has not been carefully explored experimentally. For example, it is conceivable that cells respond to the rate of change of a morphogen signal or that a transient exposure to the signal changes the context in which

cells respond to the morphogen at later times (Pages and Kerridge, 2000). In our study of Hh signaling in the *Drosophila* wing disc (presented in Chapter 2), we provide experimental evidence that changes in the distribution of the Hh gradient are essential for the formation of different patterns of gene expression and that the establishment of Hh-dependent gene expression patterns depends on the history of Hh signaling exposure, rather on the steady-state profile of the gradient (Nahmad and Stathopoulos, 2009).

In general, the study of the role of morphogen dynamics in pattern formation remains technically challenging because genetic manipulations cannot be finely tuned enough to selectively perturb transient gradients in a reproducible way, without affecting the steady-state distribution of the morphogen. In Chapter 3, I present a modeling-based experimental design framework to isolate the roles of transient and equilibrium dynamics in morphogen-mediated patterning. Although the experimental implementation of this idea is left for future studies, these theoretical tools are not limited to the study of morphogen dynamics, in particular, and might be applicable to a wide variety of problems.

1.5 The Problem of Size-Dependent Scale Invariance of Pattern

Many animals exhibit an extraordinary ability to re-organize their developmental programs in response to changes in embryo size. For example, sea urchins embryos are subdivided along their animal-vegetal axis into three germ layers (mesenchyme, endoderm, and ectoderm) and several embryological studies show that the proportions of this pattern are preserved when the size of the embryo is manipulated up to 8-fold

(Hörstadius, 1939; Gustafson, 1965). This ability to adapt pattern to the size of the embryo is commonly referred as size-dependent scale invariance or, simply, scaling.

The problem of scaling can naturally be stated in terms of positional information (Wolpert, 1969), this is, how do cells acquire information about their *relative* location in a developing field? One way to illustrate the concept of establishing positional information in relative rather than absolute coordinates is provided by the famous French flag problem introduced above (Wolpert, 1968): Is it possible to establish a pattern in which three sequential states can be established in equal proportions independently of the size of the system? A simple solution of the French flag problem is to postulate the existence of a morphogen gradient established by diffusion that is produced at one end of the embryo and destroyed at the other (Wolpert, 1968). However, this solution assumes that the distal end of the embryo works as a "perfect sink", a scenario that is likely unrealistic. Other theoretical and empirical models that have been proposed to explain the problem of scaling include the double gradient theory of Dalcq (Dalcq, 1938; Hörstadius, 1939; Needham, 1942; Wolpert, 1969) that suggests that patterning depends on the concentration of two gradients emanating from opposing ends of the embryo (an idea that was recently explored further using mathematical modeling by McHale et al., 2006), and the "short-range activator, long-range inhibition" model of Gierer and Meinhardt (1972). Although these models provide plausible solutions to the scaling problem in general, they lack experimental significance because they were based on hypothetical gradients rather than on real morphogens. Since the spatial distribution of different cell types ultimately depends on patterns of gene expression, the problem of scaling is equivalent to the

question of how morphogen gradients determine patterns that correlate with changes in the size of the system.

The most extreme manifestation of scaling is observed in experiments in which embryo size is externally manipulated resulting in well-proportioned animals that are much smaller or much bigger than the average adult. For instance, classical experiments in amphibians reveal that bisected embryos that contain a portion of the dorsal lip result in smaller, but anatomically normal tadpoles (Spemann, 1938). Conversely, adding extra tissue to a frog embryo results in a bigger animal but its overall anatomy is preserved (Waddington, 1938). Recent progress on the problem of scaling in frogs revealed that the mechanisms of scaling depend on protein-protein interactions of morphogens from the family of Bone Morphogenetic Proteins (BMPs) and their inhibitors (reviewed by De Robertis, 2006). In particular, it was found that Admp, a BMP ligand whose expression is inhibited by BMP signaling, is essential for scaling (Reversade and De Robertis, 2005). Further, mathematical modeling suggest that scaling in this system depends on shuttling of BMPs to the ventral midline by binding the inhibitor Chordin, coupled with Admp auto-repression (Ben-Zvi et al., 2008).

A different aspect of scaling is exhibited across a population of animals in which the proportions of gene expression patterns are maintained despite natural variations in embryo size. In Chapter 4, I present results on the problem of scaling due to natural variations in embryo size along the DV axis in *Drosophila*. Patterning of the DV axis in *Drosophila* depends on the nuclear distribution of the maternal factor Dorsal (dl), a homolog of vertebrate NF-κB (reviewed by Moussian and Roth, 2005; Reeves and Stathopoulos, 2009; see Box 1.2). Our results show that the dorsal borders of DV patterns

Box 1.2. Brief overview of dorsal-ventral patterning in the *Drosophila* embryo.

The establishment of dorsal-ventral (DV) positional information in the early *Drosophila* embryo is largely under maternal control and originates early during oogenesis.
The signaling cascade that provides DV asymmetry in the oocyte arises from the dorsally restricted activation of EGFR in the follicular epithelium, a group of somatic cells that cover the surface of the developing egg (Price et al., 1989; Schejter and Shilo, 1989). This asymmetry restricts the transcription of *pipe*, a gene that encodes a glycosaminoglycan-modifying enzyme, to the ventral side of the egg chamber (Sen et al., 1998). Pipe localization initiates a cascade of reactions that involve complex interactions of proteases in the perivitelline fluid, a space that separates the embryo from the follicular epithelium (reviewed by Moussian and Roth, 2005). The protease cascade results in the formation of a gradient of Spätzle in the perivitelline space. The process of translating maternal signals into the embryo is afforded by the Spätzle-dependent activation of the Toll signaling pathway, which also plays a pivotal role in the immune response of insects and vertebrates (reviewed by Imler and Zheng, 2004). Toll activation recruits a complex that includes the serine/threonine kinase Pelle (Towb et al., 1998). This process leads to Pelle accumulation and auto-phosphorylation and results in a gradient of activated Pelle in the ventral region of the embryo that is known to be sufficient for DV patterning of the embryo (Towb et al., 2001; Stathopoulos and Levine, 2002). In the cytoplasm, Pelle likely phosphorylates and promotes the proteolysis of the IκB homolog, Cactus (Edwards et al., 1997; Drier et al., 1999). Destruction of Cactus releases the NF-κB homolog, Dorsal (dl) and permits its nuclear import where it acts as a transcription factor (Belvin et al., 1995; Bergmann et al., 1996; Reach et al., 1996). The end result of the pathway is a graded nuclear distribution of dl that organizes the subdivision of the DV axis in distinct domains of gene expression (Roth et al., 1989; Rushlow et al., 1989; Steward, 1989). High levels of dl lead to transcription of *twist* and *snail* that define mesodermal precursor cells in the ventral-most region of the embryo (Jiang et al., 1991; Pan et al., 1991). Intermediate to low levels of nuclear dl activate *short of gastrulation* (*sog*) and *rhomboid* in ventrolateral regions that define the neurogenic ectoderm (Bier et al., 1990; François et al., 1994; Ip et al., 1992). Finally, *decapentaplegic* (*dpp*) and *zerknült* (*zen*) are activated in the dorsal and dorso-lateral regions of the embryo that correspond to the precursors of the amnioscerosa and the dorsal ectoderm (Rushlow et al., 1987). Although this view fits well with the hypothesis that dl acts as a classical morphogen, patterning of the DV axis depends on a complex transcriptional network in which dl-target genes interact with each other to establish precise domains of gene expression (Stathopoulos and Levine, 2005).

that depend on the maternal factor dl scale with respect to embryo size. Furthermore, we provide evidence that scaling in this system depends on dl but not in a direct manner. We propose that additional factors downstream of dl are required to determine relative coordinates along the DV axis.

1.6 A Multidisciplinary Approach to the Study of Developmental Pattern Formation

In his famous Lectures on Physics, the great Caltech physicist Richard Feynman wrote:

If our small minds, for some convenience, divide a glass of wine, this universe, into parts –physics, biology, geology, astronomy, psychology, and so on- remember that nature does not know it!

Feynman was obviously not talking about multidisciplinary "wine" science, but he was referring to the human obsession of classifying knowledge into categories. Scientific questions are "traditionally" studied using the tools and views of the discipline that they were classified into, rather than using a broad, unbiased perspective. The multidisciplinary philosophy followed in this work is, as much as possible, interest-driven towards the fundamental question of how cells interpret their positional information in order to acquire a specific pattern or fate, rather than limited by the tools or concepts from a certain discipline. The history of the problem of pattern formation has facilitated its study using both theoretical and experimental viewpoints (Ibañez and Izpizúa-Belmonte, 2008; Green, 2002; Lander, 2007), but the interplay between theory and experiment is often forced to exhibit its usefulness instead of being truly motivated by scientific questions.

We are now witnessing a second major revolution in developmental biology (the first one was the synthesis of embryology and genetics in the first half of the 20th

century). I am referring to the post-genomic revolution. This new era is not only facilitating whole-genome tools for the study of biological systems and expanding the availability of unexplored experimental systems, but is changing the way we think about developmental mechanisms in terms of gene regulatory networks (Levine and Davidson, 2005). Furthermore, the post-genomic revolution is also bringing a new multidisciplinary viewpoint to the study of biological systems that promotes the use of tools from different disciplines. This viewpoint is already affecting the way we study the developing embryo and will hopefully bring new light to the understanding of the "building blocks" underlying animal design.

Chapter 2

Dynamic Interpretation of Hedgehog Signaling in the *Drosophila* Wing Disc*

Morphogens are classically defined as molecules that control patterning by acting at a distance to regulate gene expression in a concentration-dependent manner. In the *Drosophila* wing imaginal disc, secreted Hedgehog (Hh) forms an extracellular gradient that organizes patterning along the anterior–posterior axis and specifies at least three different domains of gene expression. Although the prevailing view is that Hh functions in the *Drosophila* wing disc as a classical morphogen, a direct correspondence between the borders of these patterns and Hh concentration thresholds has not been demonstrated. Here, we provide evidence that the interpretation of Hh signaling depends on the history of exposure to Hh and propose that a single concentration threshold is sufficient to support multiple outputs. Using mathematical modeling, we predict that at steady state, only two domains can be defined in response to Hh, suggesting that the boundaries of two or more gene expression patterns cannot be specified by a static Hh gradient. Computer simulations suggest that a spatial "overshoot" of the Hh gradient occurs, i.e., a transient state in which the Hh profile is expanded compared to the Hh steady-state gradient. Through a temporal examination of Hh target gene expression, we observe that the patterns initially expand anteriorly and then refine, providing in vivo evidence for the overshoot. The Hh gene network architecture suggests this overshoot results from the Hh-

* © 2009, Nahmad and Stathopoulos. This chapter, originally published as "Nahmad M. and Stathopoulos A. (2009) Dynamic Interpretation of Hedgehog Signaling in the Drosophila Wing Disc. PLoS Biol 7(9): e1000202. doi:10.1371/journal.pbio.1000202," is reproduced under the Creative Commons Attribution License (http://creativecommons.org/licenses/by/2.5/).

dependent up-regulation of the receptor, Patched (Ptc). In fact, when the network structure was altered such that the *ptc* gene is no longer up-regulated in response to Hh-signaling activation, we found that the patterns of gene expression, which have distinct borders in wild-type discs, now overlap. Our results support a model in which Hh gradient dynamics, resulting from Ptc up-regulation, play an instructional role in the establishment of patterns of gene expression.

2.1 Introduction

Pattern formation in many developing systems depends on the formation and interpretation of morphogen gradients (Gurdon and Bourillot, 2001). The classical model of pattern formation conveyed by morphogens is typically illustrated by Wolpert's French Flag model (Wolpert, 1968). In the context of Wolpert's model, cells capable of sensing an extracellular gradient will adopt one of three different regulatory states depending on their local readout of the morphogen concentration. Based only on the input (ligand gradient) to output (target gene expression) relationship, several signaling molecules appear to operate in the context of Wolpert's Classical Morphogen model (Cooke, 1995; Gurdon et al., 1998; Tabata and Takei, 2004); however, the underlying mechanisms regarding how gradients of these signaling molecules are translated into discrete patterns of gene expression remain unclear. One example of such a signaling molecule is Hedgehog (Hh), as in the *Drosophila* wing disc, where the distribution of Hh clearly correlates with gene expression patterns (Fig. 2.1A) (Strigini and Cohen, 1997). Yet, it has not been demonstrated definitively that different Hh concentrations define the positions of distinct borders of gene expression patterns.

Hedgehog molecules are secreted proteins that control patterning pervasively during animal development (Jiang and Hui, 2008). In the *Drosophila* wing imaginal disc, *hh* is expressed exclusively in cells of the posterior compartment. After several posttranslational modifications, Hh is secreted from the posterior compartment, forming a concentration gradient within the anterior compartment with highest levels present at the anterior–posterior (AP) boundary. Although the range of Hh signaling is short compared to that of Decapentaplegic (Dpp), 10–15 cells compared with approximately 40 cells, respectively, at least three different patterns are established by Hh signaling (Strigini and Cohen, 1997; Mullor and Guerrero, 2000; Vervoort et al., 1999; Ho et al., 2005; Mullor et al., 1997). Target genes activated by Hh signaling include *dpp*, *collier* (*col*), *patched* (*ptc*), and *engrailed* (*en*) (Fig. 2.1A).

A simplified network of genetic interactions involved in the Hh signaling pathway is shown in Figure 2.1B. Hh signaling is maintained in a default OFF state by the Hh receptor Patched (Ptc), which is constitutively expressed in cells of the A compartment. Ptc expression inhibits the activation of the transmembrane protein Smoothened (Smo) through a mechanism that is still not well understood and is likely indirect (Denef et al., 2000; Taipale et al., 2002). Extracellular Hh binds to Ptc and induces its internalization and degradation. In the absence of Ptc, Smo accumulates and is phosphorylated, a step required to activate Hh signaling (Apionishev et al., 2005; Jia et al., 2004). The details regarding how phosphorylated Smo (pSmo) results in activation of the pathway are complex and not well defined, but require Smo-mediated recruitment of a series of kinases that prevent processing of the transcription factor Cubitus interruptus (Ci). In the absence of Hh or pSmo, Ci is cleaved, and one of the fragments, known as Ci75, acts to

repress particular Hh target genes (Méthot and Basler, 1999). Activation of the Hh pathway stabilizes pSmo expression, which in turn inhibits the cleavage of Ci into Ci75, to permit full-length Ci to enter the nucleus and activate the transcription of Hh target genes.

Activation of Hh signaling in the wing disc appears to depend not only on the concentration of free Ptc, but also on the amount of Ptc bound to Hh (Casali and Struhl, 2004). Thus, it has been proposed that transduction of Hh signaling depends on the ratio of liganded to unliganded Ptc (Casali and Struhl, 2004). Furthermore, an evolutionarily conserved property of the Hh signaling pathway is that *ptc*, the gene that encodes the Hh receptor, is transcriptionally up-regulated by Hh signaling (see Fig. 2.1B). This feedback gives Ptc the dual function of both receiving the signal as well as limiting the spatial range of the Hh gradient (Chen and Struhl, 1996).

In this study, we investigated the mechanisms by which the Hh gradient is interpreted to pattern the *Drosophila* wing disc. Our approach was to use mathematical modeling to formulate hypotheses that can be tested directly through experimentation. Surprisingly, our mathematical analysis suggested that the steady-state Hh gradient is insufficient to determine more than two gene expression patterns in a concentration-dependent manner. We propose that Hh-dependent Ptc up-regulation causes a transient expansion (or "overshoot") of the Hh gradient before approaching its final distribution. Through experiments conducted in vivo, we provide evidence that this transient overshoot exists and that it is required to distinguish different spatial domains of gene expression in response to Hh. Taken together, our data suggest a new model of pattern

formation, which takes into consideration gradient dynamics to explain Hh-dependent patterning of the wing disc.

2.2 Materials and Methods

Numerical Simulations

A Forward-in-Time-Centered-in-Space (FTCS) algorithm (Δx = 2.5 μm, Δt = 0.5 s) was implemented to solve Equations (2.1)–(2.5) numerically in MATLAB using the parameters in Supporting Table 2.1. Numerical solutions approximately reach steady state in less than 8 hours. To simulate the outputs in *ptc*-TPT (Fig. 2.3H), we use Equation (S4) in Supporting Text instead of Equation (2.2) (see Supporting Text for further details).

Fly Crosses and Transgenes

Fly crosses were conducted at 25 °C, except where otherwise indicated. For the experiments using the hh^{ts2} allele (Fig. 2.2E, 2.5, 2.6A,B, and Supporting Fig. 2.2), fly stocks of genotype *dpp10638*/CyO; hh^{ts2}/TM6B, Tb were crossed at 18 °C. *dpp10638* is a transgene on II containing a lacZ reporter (dppZ) that produces nuclear β-galactosidase (β-gal). hh^{ts2} homozygous animals are marked by the Tb^{+} phenotype. A Tubulin1>*ptc*>Tubulin1α 3′UTR (TPT) transgenic line located on chromosome III has previously been shown to rescue *ptc* mutant animals (Chen and Struhl, 1996). To obtain *ptc*-TPT discs, we crossed ptc^{9};TPT / SM6; TM6B, Tb males to ptc^{16}, dpp10638; + / SM6; TM6B, Tb females. ptc^{16} has been previously characterized as a null allele (Capdevila et al., 1994), and ptc^{9} produces a product that is defective in reaching the plasma membrane and binding to Hh (Strutt et al., 2001). Tb^{+} marks *ptc* mutant larvae

that carry a copy of both the TPT and *dpp10638* transgenes (Fig. 2.3D–F and Supporting Fig. 2.5). In Figure 2.4D–F, TPT transgenic discs in a wild-type background (*ptc*+TPT discs) were obtained from third instar larvae of the genotype *dpp10638*; TPT / SM6; TM6B, Tb. In Figure 2.6C–H, males of genotype *dpp10638;* UAS-Ptc / SM6; TM6B, Tb were crossed to females of genotype TubGal80^{ts}; TubGal4 / SM6; TM6B, Tb at 18 °C. TubGal80^{ts} is a transgene on chromosome II that expresses a temperature-sensitive form of the Gal80 protein. In these experiments, third instar larvae of Tb^{+} phenotype were selected, representing mutants of genotype TubGal80^{ts}/*dpp10638*; TubGal4/UAS-Ptc. *dpp*^{hr56} / *dpp*^{hr4} transheterozygotes animals are defective in Dpp signaling at 29 °C (Hsiung et al., 2005). We crossed *dpp*^{hr56}; + / SM6; TM6B, Tb to *dpp*^{hr56}; dppZ / SM6; TM6B, Tb animals at 18 °C. Third instar larvae marked by Tb^{+} are normal at 18 °C, but defective in Dpp signaling after 24 h at 29 °C (Supporting Fig. 2.3).

Reinitialization of the Hh Gradient Using a Temperature-Sensitive *hedgehog* Allele

hh^{ts2} flies were placed at 18 °C. After 2 d, adults were removed and progeny were kept at 18 °C for an additional 7 d. Hh signaling was then interrupted by placing the resulting larvae at 29 °C for 24 h. Finally, larvae were placed back at 18 °C to induce Hh signaling for a period of time, τ. Third instar larvae homozygous for the *hh*^{ts} allele were fixed immediately for immunostaining at the designated time points τ. A graphical depiction of this scheme is presented in Figure 2.2D.

Fixation, In Situ Hybridization, and Immunostaining

Third instar wing discs were dissected, fixed, and immunostained using standard techniques. The following primary antibodies were used: monoclonal mouse anti-Ptc

(developed by I. Guerrero, and was obtained from the Developmental Studies Hybridoma Bank at the University of Iowa), rabbit anti-β-gal (Invitrogen Molecular Probes), monoclonal mouse anti-Col (M. Crozatier), rabbit anti-En (P. O'Farrell), and guinea pig anti-pMad (E. Laufer). The secondary antibodies used were rabbit Alexa 647, mouse Alexa 488, and guinea pig Alexa 555 (Molecular Probes). Samples were mounted in Mowiol 4-88 (Molecular Biosciences). Fluorescent in situ hybridization for data in Figure S2 was performed using standard techniques using a digoxigenin-labeled riboprobe for *dpp*. Primary and secondary detection of the *dpp* probe was done using a polyclonal sheep anti-digoxigenin (Roche) and sheep Alexa 555 (Molecular Probes) antibodies, respectively.

Image Analysis

Images were acquired using a confocal microscope (Zeiss Pascal) and processed in Adobe Photoshop. Images in Supporting Figure 2.2 were taken using a 20× objective (Zeiss). Images in other figures and supporting figures were taken using a 40× oil objective (Zeiss). Imaging parameters for each set of data were selected for the control or wild-type experiment, and the same imaging conditions were used throughout the rest of each dataset. Discs compared in Figure 2.2E were chosen such that they met the following conditions: (1), approximately the same size, (2), similar average background intensity in the posterior compartment, and (3), similar average intensity in the anterior compartment away from the AP boundary. For the intensity profiles in Figure 2.2E, images were processed in ImageJ and quantified in MATLAB (see Supporting Protocol for further details).

2.3 Results

Mathematical Modeling of Hh Signaling Interpretation

We devised a mathematical model of Hh signaling based on the simplified network presented in Figure 2.1B (see Supporting Text for further details). The dynamics of gene (and protein) concentrations along the AP axis are modeled using the following system of reaction-diffusion equations:

$$\frac{\partial[\mathrm{Hh}]}{\partial t} = D\frac{\partial^2[\mathrm{Hh}]}{\partial x^2} + S^{-}(x)\alpha_{\mathrm{Hh}} - \gamma_{\mathrm{Hh\_Ptc}}[\mathrm{Hh}][\mathrm{Ptc}] - \beta_{\mathrm{Hh}}[\mathrm{Hh}], \tag{2.1}$$

$$\frac{\partial[ptc]}{\partial t} = S^{+}(x)\alpha_{ptc0} + \frac{\alpha_{ptc}[\mathrm{Signal}]^{\mathrm{m}}}{k_{ptc}^{\mathrm{m}} + [\mathrm{Signal}]^{\mathrm{m}}} - \beta_{ptc}[ptc], \tag{2.2}$$

$$\frac{\partial[\mathrm{Ptc}]}{\partial t} = T_{\mathrm{Ptc}}[ptc] - \gamma_{\mathrm{Hh\_Ptc}}[\mathrm{Hh}][\mathrm{Ptc}] - \beta_{\mathrm{Ptc}}[\mathrm{Ptc}], \tag{2.3}$$

$$\frac{\partial[\mathrm{Hh\_Ptc}]}{\partial t} = \gamma_{\mathrm{Hh\_Ptc}}[\mathrm{Hh}][\mathrm{Ptc}] - \beta_{\mathrm{Hh\_Ptc}}[\mathrm{Hh\_Ptc}], \tag{2.4}$$

$$\frac{\partial[\mathrm{Signal}]}{\partial t} = \frac{S^{+}(x)\alpha_{\mathrm{Signal}}\left(\frac{[\mathrm{Hh\_Ptc}]}{[\mathrm{Ptc}]}\right)^{\mathrm{n}}}{k_{\mathrm{Signal}}^{\mathrm{n}} + \left(\frac{[\mathrm{Hh\_Ptc}]}{[\mathrm{Ptc}]}\right)^{\mathrm{n}}} - \beta_{\mathrm{Signal}}[\mathrm{Signal}], \tag{2.5}$$

where [Hh], [*ptc*], [Ptc], and [Hh_Ptc] are the concentrations of Hh, *ptc* (mRNA), Ptc (protein), and the Hh-Ptc complex, respectively. The coefficients α, β, γ, and *T* represent the rates of synthesis, degradation, complex formation, and translation, respectively. We use a system of coordinates centered on the AP boundary with the anterior compartment on the positive side (Fig. 2.1A). $S^{+}(x)$ (or $S^{-}(x)$) is a step function of the form $S^{+}(x) = 1$ if

$x > 0$ [or $S^{-}(x) = 1$ if $x < 0$] and zero otherwise (see Supporting Text for further model details).

We use the variable [Signal] (instead of a particular effector such as pSmo, for example) to represent the concentration of Hh signaling activity and assume that [Signal] reflects the propensity to activate Hh target gene expression. Our model of signal activation is based on the phenomenological observations that Hh-dependent gene expression depends on the ratio of liganded (Hh_Ptc) to unliganded Ptc [Equation (2.5)] (Casali and Struhl, 2004). Unlike other models of Hh signaling conducted in the past (Saha and Schaffer, 2006; Gunbin et al., 2007; Lai et al., 2004; Eldar et al., 2003; Gonzalez et al., 2008), our model is not based on any particular molecular mechanism regarding how Ptc and Smo interact. A mechanistic model would require additional knowledge of the specific biochemical interactions, including how Ptc interacts with Smo and how Smo interacts with other pathway components, which are currently not completely understood. Our goal was to use mathematical modeling as a tool to formulate experimentally testable hypotheses in order to study how a gradient of Hh is interpreted by a field of cells.

Theoretical Analysis Suggests That the Steady-State Hh Gradient Is Interpreted as a "Switch-Like" Response

At steady state, the system of equations [Equations (2.1)–(2.5)] reduces to a single second-order equation for [Hh] with boundary conditions (see Supporting Text), and all other concentrations can be written as a function of [Hh]. For example, setting the left-hand side of Equations (2.4) and (2.5) to zero, and substituting Equation (2.4) into (2.5), we obtain the following expression valid at steady state in the anterior compartment:

$$[\text{Signal}]_{ss} = \left(\frac{\alpha_{\text{Signal}}}{\beta_{\text{Signal}}}\right)\frac{[\text{Hh}]_{ss}^{\,n}}{\varepsilon^n + [\text{Hh}]_{ss}^{\,n}} \text{ with } \varepsilon = \frac{k_{\text{Signal}}\beta_{\text{Hh\_Ptc}}}{\gamma_{\text{Hh\_Ptc}}}. \quad (2.6)$$

Equation (2.6) is a nonlinear input-output relationship between the (unbound) $[\text{Hh}]_{ss}$ gradient and the $[\text{Signal}]_{ss}$ profile, in which the subscript ss refers to steady-state concentrations. It reveals that the steady-state interpretation of the Hh gradient, in terms of the [Signal] profile, depends qualitatively on the Hill coefficient n. For n ~ 1, an extracellular [Hh] gradient corresponds to a monotonic [Signal] gradient, but as n increases, the spatial distribution of [Signal] rapidly acquires a step-like profile (Fig. 2.1C). Let F be the rate of Signal activation (first term on the right in Equation (2.5)):

$$\text{F}\left(\frac{[\text{Hh\_Ptc}]}{[\text{Ptc}]}\right) = \frac{\alpha_{\text{Signal}}\left(\frac{[\text{Hh\_Ptc}]}{[\text{Ptc}]}\right)^n}{k_{\text{Signal}}^{\,n} + \left(\frac{[\text{Hh\_Ptc}]}{[\text{Ptc}]}\right)^n},$$

which is assumed to be a sigmoidal function of the [Hh_Ptc] to [Ptc] ratio (Casali and Struhl 2004), then the value of n is proportional to the slope of the line tangent to the graph of F at the point of half-maximal activation (Fig. 2.1D). Thus, it is possible to obtain a lower-bound estimate of n using any two data points on this curve (Supporting Text). Using published data (Casali and Struhl, 2004), we estimated that n > 6.8 (Fig. 2.1D). The quantitative details of this approximation depend on several unknown parameters as well as the quantitative accuracy of the data used (see Supporting Text). Nevertheless, the qualitative behavior when n >> 1 is clear. Most cells interpret either maximal signaling levels (ON state) or little to no signal (OFF state), and the transition between these two states is sharp (Fig. 2.1E and Supporting Text). However, this analysis

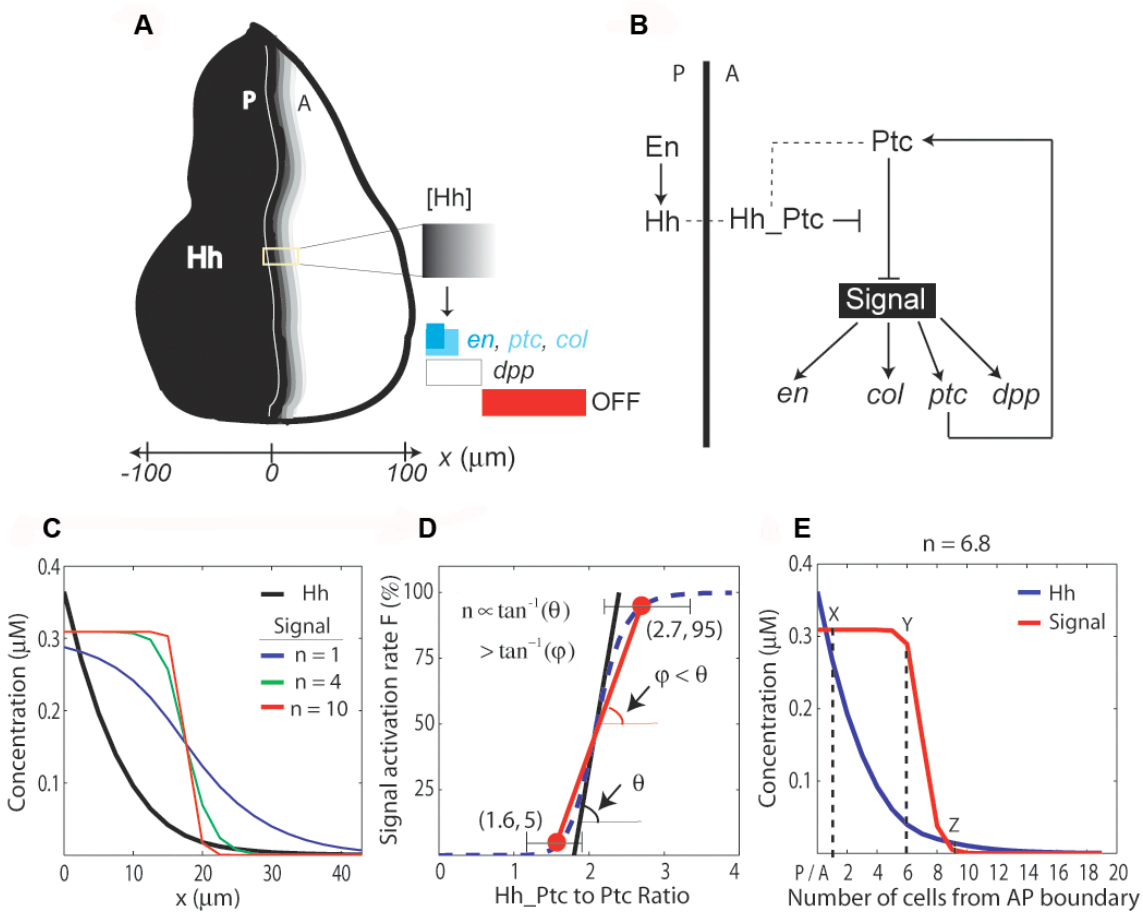

Figure 2.1 Mathematical modeling proposes the Hh steady-state gradient is translated into a step-like signal response.

(A) In the wing disc, Hh emanates from the posterior (P) compartment and forms a concentration gradient within the anterior (A) compartment to organize three different domains of gene expression: (I) *engrailed* (*en*), *patched* (*ptc*) and *collier* (*col*): blue; *en* is initially expressed in a narrow domain (dark blue), but it later expands to encompass the same domain as *ptc* and *col* (light blue). (II) *decapentaplegic* (*dpp*): white. (III) Cells beyond the *dpp* domain do not respond to the signal (OFF: red). Here and in subsequent figures, wing discs are oriented with posterior to the left and position along the AP axis is measured relative to the AP boundary ($x = 0$). (B) Simplified gene network of Hh signaling in the *Drosophila* wing disc as modeled in this study. Arrows represent activation; blunt-end lines represent repression. (C) Simulated steady-state (ss) profiles of [Hh] and [Signal]. The $[Hh]_{ss}$ profile (black curve) is approximately invariant to changes in the parameter n, whereas the $[Signal]_{ss}$ profile is qualitatively different for different values of n.

(D) Estimation of n from published data (Casali and Struhl, 2004). The dashed line is the graph of, $F(\text{Ratio}) = \frac{(\text{Ratio})^n}{k_{\text{Signal}}^n + (\text{Ratio})^n}$ with $\text{Ratio} \equiv \frac{[\text{Hh\_Ptc}]}{[\text{Ptc}]}$. Ratio = 1.6 produces no signaling response (~5%), whereas Ratio = 2.7 gives full activation of the pathway (~95%) (Casali and Struhl, 2004). A lower-bound value of n can be estimated by the slope of the line through these data points [red line; slope = $\tan^{-1}(\varphi) = \frac{0.95 - 0.05}{2.7 - 1.6} = 0.8$]. Therefore, $n = 4k_{\text{Signal}} \tan^{-1}(\theta) > 4k_{\text{Signal}} \tan^{-1}(\varphi) \approx 6.8$. The minimum lower-bound estimate, taking into account error bars (drawn according to published data (Casali and Struhl, 2004), is n > 4.0. (E) Simulated steady-state profiles of [Hh], blue line, and [Signal], red line, for n = 6.8. Cell position relative to the AP boundary is indicated on the horizontal axis (*x*-axis). "X," "Y," and "Z" denote three arbitrary positions along the x-axis.

---

fails to explain how three (or more) domains of gene expression might be specified by the Hh gradient (see Fig. 2.1A).

Computer Simulations Suggest That Hh Gradient Dynamics May Contribute to Differential Gene Expression

Our mathematical analysis supports the hypothesis that at steady state, a graded extracellular input of [Hh] is interpreted into a switch-like profile of signal activation [Signal], in which two domains of gene expression could easily be supported by the ON versus OFF states. Although morphogens are often considered as static gradients or their transient dynamics are largely ignored (Tabata and Takei, 2004; Kicheva and González-Gaitán, 2008), recent studies have highlighted the importance of morphogen gradient dynamics in supporting differential gene expression (Saha and Schaffer, 2006; Bergmann et al., 2007; Harfe et al., 2004; Jaeger et al., 2004). In order to reconcile the apparent switch-like profile of Hh signaling with the fact that at least three domains of gene expression are specified, we asked whether dynamics of the Hh gradient contribute to patterning of the *Drosophila* wing disc.

We examined the dynamic establishment of the Hh gradient through numerical simulations of Equations (2.1)–(2.5) (see Materials and Methods section). We observed that the gradient expands transiently to a position further from its steady-state distribution and then refines towards its source, the posterior compartment, as it approaches its final form (Fig. 2.2A). This dynamic behavior of the gradient is most likely due to the dynamics of Hh-dependent Ptc expression. During the formation of the gradient, Ptc is expressed only at low levels throughout the anterior compartment, and therefore, the range of Hh is largely unrestricted by Ptc; once Ptc is up-regulated, then Hh mobility is affected. As a consequence, we observe that a transient expansion of the gradient, or overshoot, results. Cells in more anterior positions receive the Hh-dependent signal for a limited amount of time, but they no longer receive the signal once the gradient has reached its steady-state position (Fig. 2.2B).

On the basis of this theoretical analysis, we proposed an Overshoot model to explain the three states observed in the system: (State 1) cells that are never exposed to Hh above a "switching threshold," the level necessary to activate Hh signaling, are always in the OFF state (Fig. 2.2C, red); (State 2) those cells that are only transiently exposed to levels above the switching threshold may transiently turn gene expression ON, but only certain genes subject to additional regulation will be able to maintain expression (Fig. 2.2C, white); and (State 3) those cells that are exposed constantly to levels above the switching threshold exhibit an ON state (Fig. 2.2C, blue). Interpretation of Hh signaling in the context of the Overshoot model requires only a single concentration threshold (the switching threshold) and takes into account each cell's dynamic history of Hh exposure (see Discussion).

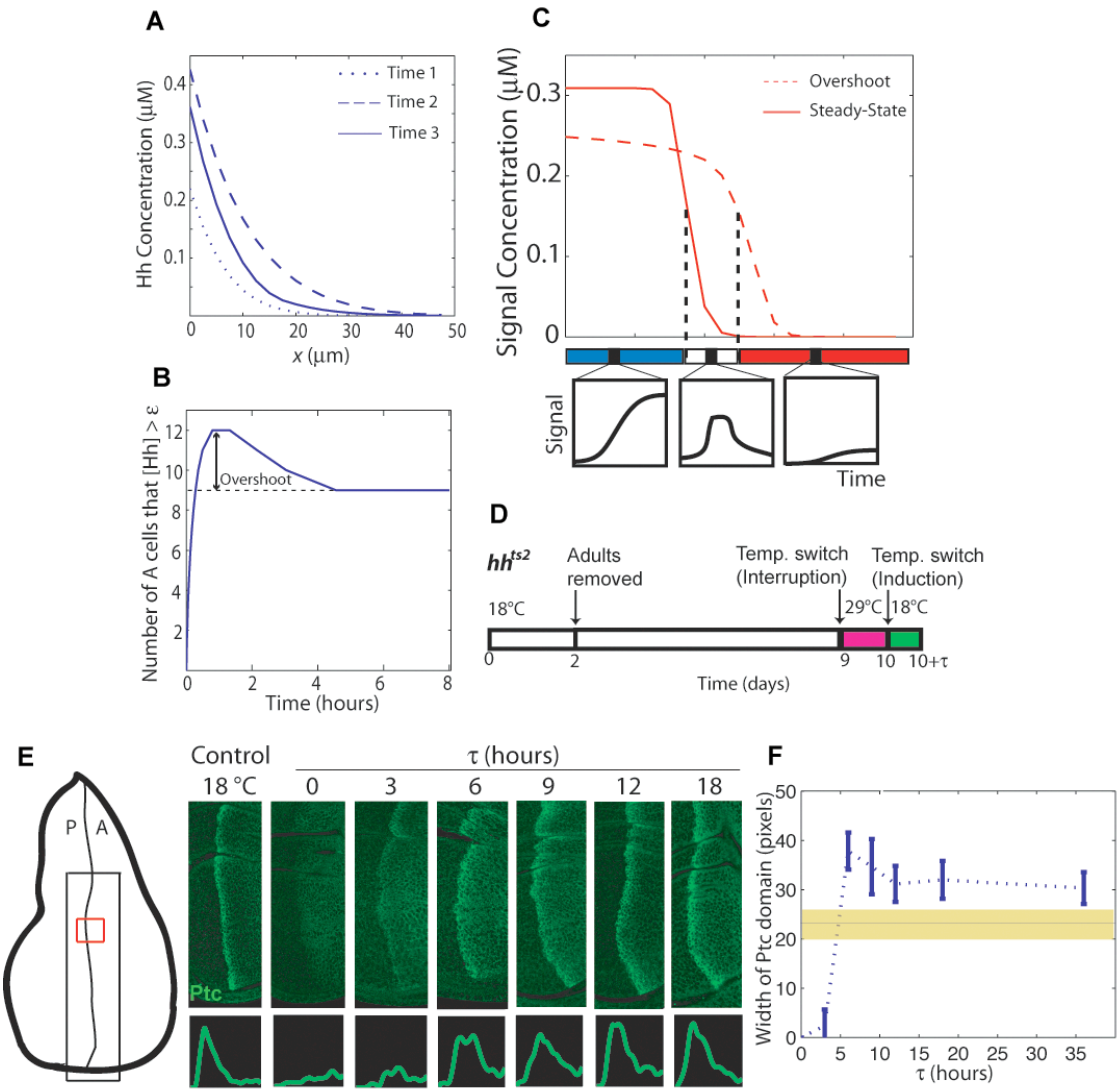

Figure 2.2.Temporal analysis of Hh signaling in vivo reveals the existence of a spatial overshoot.

(A) Simulated profile of [Hh] gradient at three different time-points: Time 1 < Time 2 < Time 3. The gradient transiently expands anteriorly (Time 2) and then refines towards its steady-state shape (Time 3). (B) Number of cells that experience higher concentrations of [Hh] than the ON/OFF switch threshold, ε, as a function of time based on the simulated [Hh] profiles. This diagram defines an overshoot, a spatial domain of cells that are exposed transiently to [Hh]. (C) The dashed and solid red lines represent the [Signal] profiles resulting from the "overshoot" and "steady-state" gradients, respectively. Cells experience three qualitatively different dynamic trajectories of [Signal] exposure depending on their spatial location (lower boxes). (D) Experimental setup to reinitialize the Hh gradient using a temperature sensitive *hedghog*

allele (hh^{ts2}; see Materials and Methods for details). Induction at 18 °C to induce Hh signaling was conducted for different intervals of time (τ). (E) Ptc immunostaining of hh^{ts2} homozygous discs from the experiment described in (D) for different induction times τ compared to a disc from a larva raised solely at 18 °C. The large box in the illustration shows the entire region imaged; the small red box corresponds to a sample region used to generate the profiles using the Supporting Protocol, displayed in the bottom panels. Discs were fixed, immunostained, and imaged under identical conditions (see Materials and Methods). (F) Width of the Ptc domains as the Hh gradient is developed. At least four discs at each time point were used. Mean widths were computed, and error bars indicate standard deviations (see Supporting Protocol 1). Yellow area indicates the width range for Ptc in control discs at 18 °C.

Taken together, our mathematical modeling enabled us to formulate the following hypotheses. First, the Hh gradient at steady state is insufficient to generate more than two states, and, thus, Hh patterning cannot be explained using the Classical Morphogen model. Second, the formation of the gradient exhibits a transient overshoot. This dynamic behavior would be a consequence of the gene network architecture; in particular, it is effected by Hh-dependent up-regulation of Ptc. And third, that the overshoot is necessary to specify more than two domains of gene expression in the system. These hypotheses are experimentally testable, and once they are supported by in vivo experimentation, we contend that the details of the mathematical model (parameter values, equation terms, etc.) are less important.

In Vivo Evidence for a Transient Expansion of the Hh Signaling Response

First, we designed an in vivo approach to test the existence and function of a Hh overshoot in wing disc patterning. Experimental evidence for the Hh gradient overshoot can be inferred from a recent study in which Hh was visualized using inducible Hh-GFP, though the existence of the overshoot was not highlighted by the authors (Su et al., 2007).

We investigated whether or not an overshoot at the level of extracellular Hh protein would also have an effect on target gene expression.

To test this idea, we used a system in which Hh signaling in the wing disc can be reinitialized and target gene expression assayed in time through the use of a temperature-sensitive *hedgehog* allele, hh^{ts2} (Ma et al., 1993) (Fig. 2.2D). After 24 h at restrictive temperature, no Hh protein is detected by Western blot analysis suggesting that Hh protein synthesis is impaired at the restrictive temperature (S. Eaton, personal communication). As the *ptc* gene itself is a target of Hh signaling, we investigated Ptc recovery in time after the Hh gradient is re-established (Fig. 2.2D). We found that Hh-dependent Ptc expression transiently expands, followed by a posterior refinement (Fig. 2.2E). The refinement observed is not simply due to changing the temperature, because no differences in Ptc expression are observed in equivalently treated wild-type discs (Supporting Fig. 2.1). This overshoot of Ptc expression is observed as soon as 6 h after reinitialization of the gradient, and even after 36 h, refinement of the Ptc pattern is not complete (Fig. 2.2F). The dynamic states of this pattern support that a Hh gradient overshoot exists and, more importantly, demonstrate that an overshoot can be detected at the level of target gene expression.

Hh-Dependent Ptc Up-Regulation Is Required for the Establishment of Different Domains of Gene Expression

Previous studies have conclusively demonstrated that Ptc restricts the range of the Hh gradient (Chen and Struhl, 1996). As the Hh gradient expands further in *ptc* clones, we hypothesized that a Hh overshoot is likely to depend on signal-induced Ptc up-regulation. Therefore, we investigated how Hh-patterning is affected in discs that lack the ability to

up-regulate Ptc. *ptc* mutant animals die during embryogenesis but can be rescued, remarkably, by introducing ubiquitous levels of *ptc* through a Tubulin1α>*ptc*>Tubulin1α (TPT) transgene (Chen and Struhl, 1996). In *ptc* mutant discs carrying a copy of the TPT transgene (*ptc*-TPT; see Materials and Methods), it has been previously documented that Hh target genes are expressed in a broader domain compared to wild type (Chen and Struhl, 1996), but no information regarding the relative positions of target genes has been reported.

In *ptc*-TPT discs, there is no Hh-dependent *ptc* expression, and consequently, discs are not expected to exhibit a Hh overshoot. We found that the expression domains of Collier (Col) and a *dpp* reporter, dppZ, which are expressed in different domains in wild-type discs (Fig. 2.3A–C), are almost completely overlapping in *ptc*-TPT discs, save a single row of cells (Fig. 2.3D–F). This result provides insights into the mechanism of patterning, because in contrast to the wild type (Fig. 2.3G), the Overshoot model and the Classical Morphogen model make different predictions regarding target gene expression in *ptc*-TPT discs (Fig. 2.3H). The Classical Morphogen model predicts that these genes will continue to be differentially expressed in *ptc*-TPT discs because distinct concentration thresholds define their boundaries (Fig. 2.3H). In contrast, the Overshoot model predicts that Col and dppZ borders would overlap in *ptc*-TPT discs; in the absence of a spatial overshoot, we predict that there are no cells that are only transiently exposed to the signal (Fig. 2.3H and see Fig. 2.3C).

As Ptc up-regulation also results in Hh signal inactivation, we considered the possibility that the almost overlapping patterns of Col and dppZ observed in *ptc*-TPT discs are simply a consequence of increased levels of Ptc introduced by the TPT

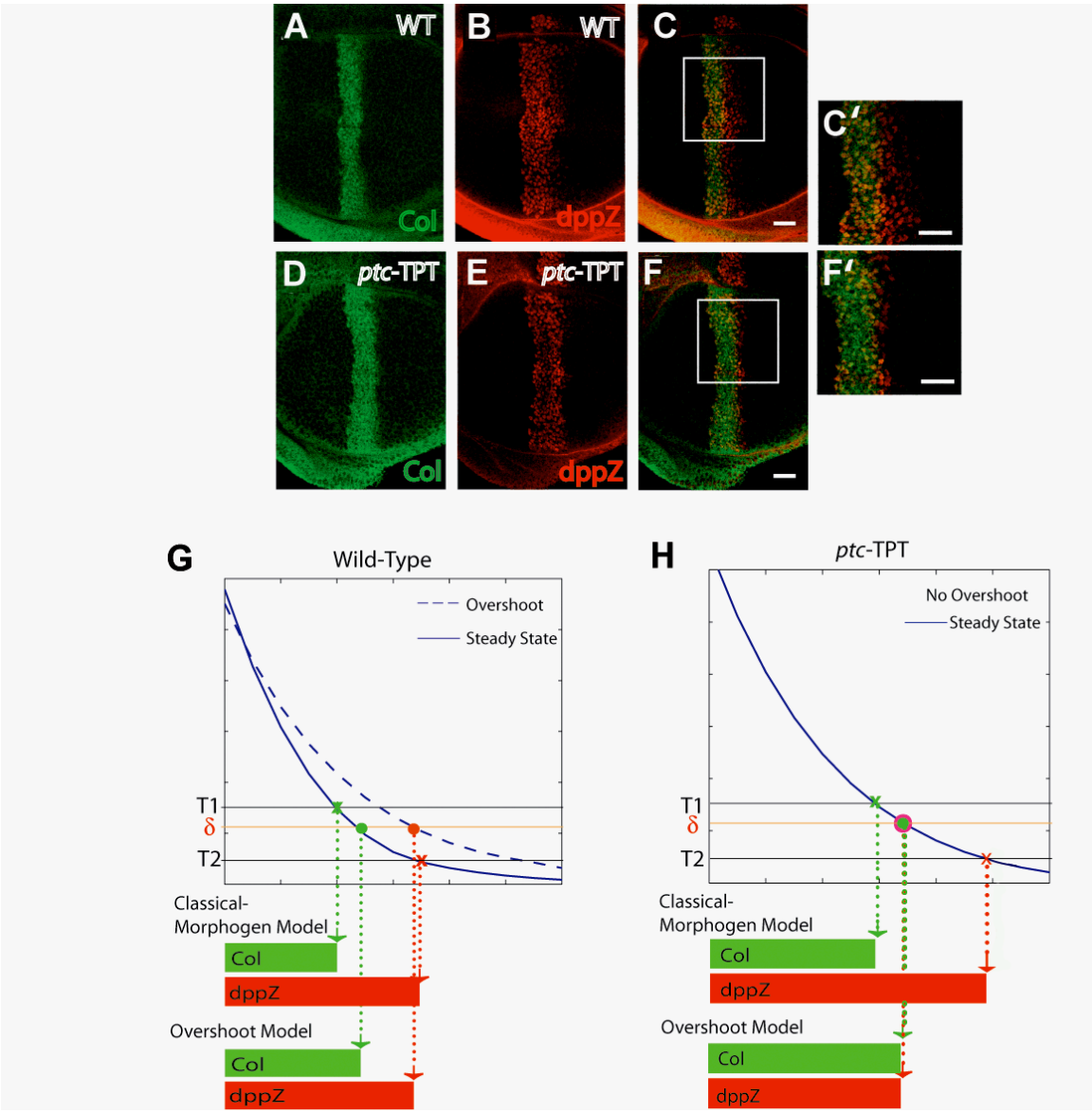

Figure 2.3 Hh-dependent Ptc is required for the specification of more than two domains of gene expression.

(A–F) Immunostaining of third instar wing discs carrying the dppZ reporter using anti-Col ([A and D] green) and anti-β-gal ([B and E] red) antibodies. (C and F) Merge of images in (A and B) and (D and E), respectively. Stainings within wild-type (WT) discs or *ptc*- discs carrying a single copy of the TPT transgene are depicted in (A–C) and (D–F), respectively. (C′ and F′) 2.25× magnification of white boxed regions in (C and F), respectively. Scale bar indicates 10 μm. (G) Interpretation of the wild-type Hh gradient according to the Classical Morphogen model or Overshoot model; Col and dppZ are shown as

examples. The Classical Morphogen model assumes the existence of concentration thresholds (T1 and T2) in the steady-state gradient of Hh that define different domains of gene expression (marked by "x") . In the Overshoot model, patterning depends on a single "switching threshold," δ, that differentiates between ON/OFF states of the pathway (see Supporting Text). Because of the overshoot, some cells will be exposed to the signal (above δ for a transient period of time (red solid circle), whereas others will be constantly exposed (green solid circle). Either model has the potential to explain gene expression in wild-type. The dashed and solids lines represent the two different time points corresponding to the overshoot and steady-state profiles, respectively. (H) In *ptc*-TPT discs, the Hh gradient is not expected to exhibit an overshoot. The Hh gradient profiles converge to the steady-state location directly, and no posterior shift of the gradient occurs. Using the same concentration thresholds T1 and T2 defined in (G), the Classical Morphogen model predicts different Col and dppZ domains even in the absence of Ptc up-regulation. According to the Overshoot model, in contrast, no cells would be exposed to the signal only transiently and, thus, an overlap of Col and dppZ patterns is predicted.

---

transgene. In fact, we noted that in *ptc*-TPT discs, the predicted distance between the anterior borders of Col and dppZ [$X_{dpp} - X_{ptc/col}$], in the context of the Classical Morphogen model, is reduced with respect to the wild-type case if levels of Ptc introduced by the TPT transgene are higher than the endogenous Ptc levels expressed in wild-type discs away from the boundary (see Fig. 2.4A,B and Supporting Text). In order to address this possibility, we considered a system in which Ptc is expressed at even higher levels than in *ptc*-TPT discs. For instance, within wild-type discs that carry a copy of the TPT transgene (*ptc*+TPT), the levels of Ptc are higher in anterior cells away from the boundary compared with *ptc*-TPT discs. If the Ptc levels introduced by the TPT were the cause of the small difference between Col and dppZ expression patterns in *ptc*-TPT discs, the prediction is that [$X_{dpp} - X_{ptc/col}$] in *ptc*+TPT discs will reduce even further (see Figure 2.4C and Supporting Text). We observed that dppZ expands at least three cells

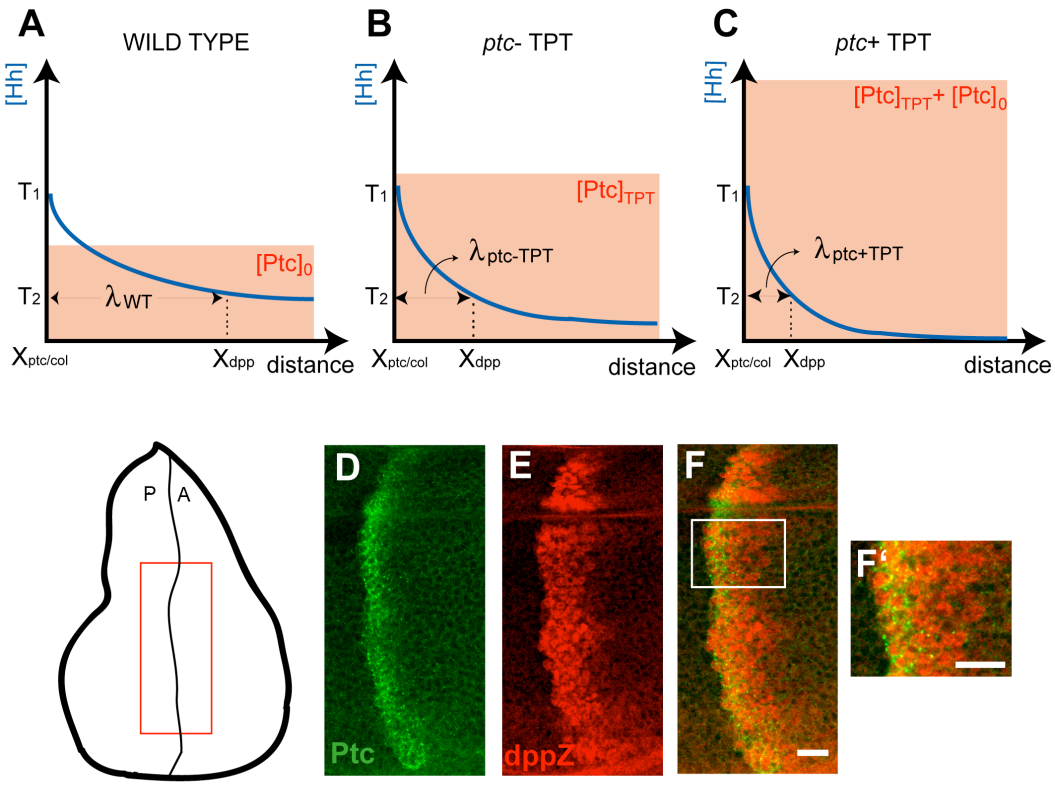

Figure 2.4 Ptc and dppZ are expressed in different domains in *ptc*+TPT discs.

(A–C) Comparison of the range of the Hh gradient in wild-type (A), *ptc*-TPT (B), and *ptc*+TPT discs (C) in the region anterior to the expected *ptc* and *col* borders ($X_{ptc/col}$). In this region the gradients are exponential, with characteristic length given by $\lambda = \sqrt{\frac{D}{\gamma_{Hh\_Ptc}[Ptc]_A + \beta_{Hh}}}$, with $[Ptc]_A$ defined as the Hh-independent concentration of Ptc in the anterior compartment. On the basis of reported measurements of the TPT transgene with respect to wild type (Chen and Struhl, 1996), we assumed that $[Ptc]_A$ in *ptc*-TPT discs ($[Ptc]_{TPT}$ is higher than in wild-type discs ($[Ptc]_0$). In the context of the Classical Morphogen model, the Hh gradient in (A–C) has the same amplitude (T_1) at $X_{ptc/col}$ even though that the actual value of $X_{ptc/col}$ may be different for each case. Therefore, λ is representative of the width of the domain in which Ptc and dppZ do not overlap ($[X_{dpp} - X_{ptc/col}]$). $[Ptc]_A$ should be higher in *ptc*-TPT than in *ptc*-TPT discs and, thus, λ in *ptc*+TPT disc is a lower-bound estimate of $[X_{dpp} - X_{ptc/col}]$ in *ptc*-TPT discs (see Supporting Text). (D and E) Immunostaining of wing discs carrying the *dpp10638* reporter and a single copy of the TPT transgene using anti-Ptc (D) and anti-β-gal (E) antibodies. (F) Merge of images in (D and E). (F′) Magnification of the white box shown in (F). Scale bar indicates 10 μm.

beyond the Ptc border in *ptc*+TPT discs (Fig. 2.4D–F). These data reveal that the overlapping patterns in *ptc*-TPT discs do not result from a dominant-negative effect of the TPT transgene and argue strongly against the Classical Morphogen model (see Discussion).

Dynamics of Hh Target Gene Expression

In light of the Overshoot model (Fig. 2.2C), we predicted that (1) *dpp* would respond rapidly to a transient exposure to Hh, because the transient overshoot likely occurs in a relatively short amount of time (e.g., see Fig. 2.2F); and (2) *dpp*, but not *ptc*, expression would be predicted to persist after the transient signal is discontinued.

We investigated the response of Ptc and dppZ expression after Hh signal was restored only transiently in hh^{ts2} homozygous discs. Consistent with previous data (Fig. 2.2E), Ptc is fully expressed after only 6 h of signal re-initialization; in contrast, dppZ expression is limited to only one row of cells under these conditions (Fig. 2.5B; compare to Fig. 2.5A). The full domain of Ptc is reached after 12 h of induction (Fig. 2.5C), but this expression can be completely eliminated after a loss of Hh activity of only 8 h (Fig. 2.5E). In contrast, even after 12 h of induction, only partial dppZ expression appears (Fig. 2.5C). Expression of dppZ within its entire expression domain is approached after 20 h of exposure (Fig. 2.5D). Importantly, a similarly full dppZ expression pattern is supported when the signal is only induced for 12 h but followed by an additional interruption of 8 h (Fig. 2.5E, compare with Fig. 2.5D). This result suggests that additional time of exposure to the signal is not required to support the full expression of dppZ, but instead that 12 h of exposure to Hh are sufficient for approximately normal dppZ expression, but an additional waiting period is required for the pattern to fully develop (Fig. 2.5E; compare

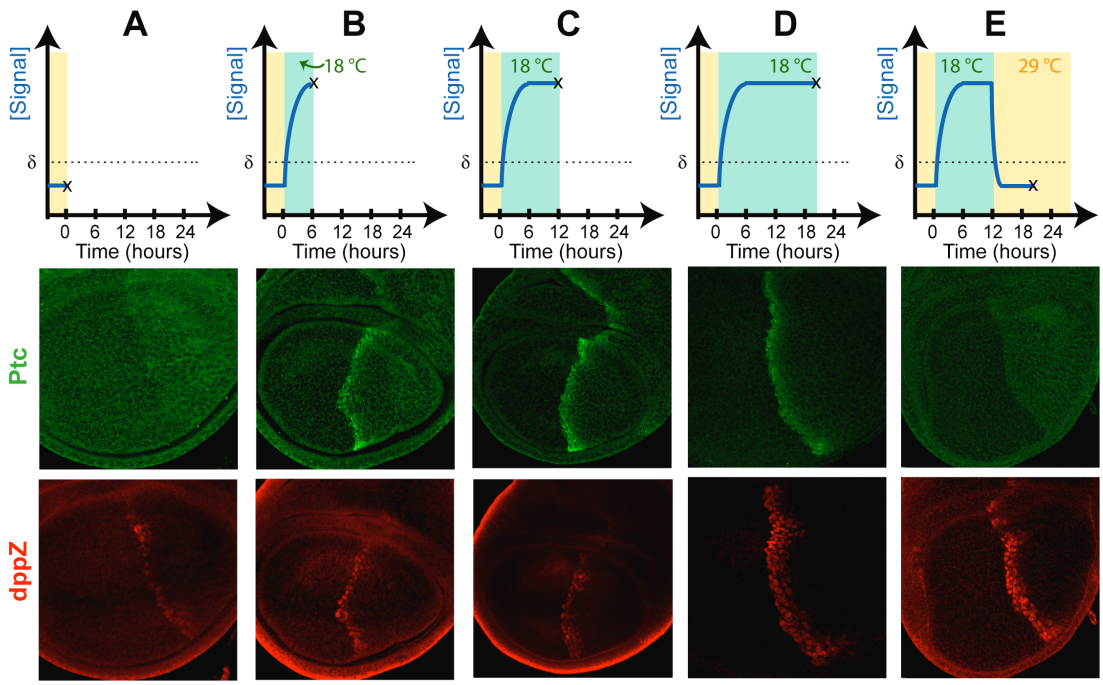

Figure 2.5 Dynamic response of Hh target genes.

Third instar larvae from hh^{ts2} homozygous animals initially grown at 18 °C and obtained along a time course of Hh exposure at particular times indicated in the diagrams. The time course (also illustrated in the panels above the images) is defined by notation (*y*,*z*): homozygous animals were grown for grown at 18 °C for 8 d, followed by 48-h signal interruption at 29 °C, followed by *y* hours of signal induction at 18 °C, followed by an additional *z* hours of interruption at 29 °C: (A) = (0,0); (B) = (6,0); (C) = (12,0); (D) = (20,0); and (E) = (12,8). In the lower panels, immunostainings depict Ptc (green) and dppZ (red) expression in discs subject to the different histories of Hh exposures as outlined in the time-course.

---

with Fig. 2.5C). These data also suggest that whereas sustained exposure to the signal is required to maintain Ptc expression, dppZ expression is maintained after Hh signaling has ceased (Fig. 2.5E and see below). Collectively, these data demonstrate that *ptc* responds rapidly to changes in Hh signaling activity and suggest that although the *dpp* response is much slower, additional regulatory mechanisms may ensure its ability to capture the full dynamics of the gradient (see Discussion).

We investigated further the fact that dppZ expression perdures after Hh signal is interrupted using the hh^{ts2} genetic background and found that dppZ persists after 24 h at restrictive temperature, although the intensity of expression is significantly reduced (Fig. 2.6A,B). Through in situ hybridization, we confirmed that dppZ perdurance is not a consequence of β-galactosidase (β-gal) stability, as *dpp* transcript similarly persists after 24 h of signal interruption (Supporting Figure 2.2).

Previous studies have used Ptc overexpression to repress Hh signaling in the wing disc (Johnson et al., 1995). Using the Gal4-UAS system and a temperature-inducible Gal80 protein, we were able to interrupt Hh signaling (via strong Ptc overexpression) in a temporally-controlled manner. At permissive temperature, Gal80 blocks Gal4's ability to drive Ptc expression such that wing discs from animals developing at permissive temperature exhibit normal patterns of Ptc, Col, and dppZ (Fig. 2.6C,E,G). However, animals exposed to restrictive temperature for the last 24 h of larval development (Fig. 2.6D) ectopically express Ptc ubiquitously, which abrogates Hh signaling, as confirmed by the loss of Col expression (Fig. 2.6F). In contrast, we found that low levels of dppZ expression persist under these conditions (Fig. 2.6H). Taken together, these data (Fig. 2.5 and Fig. 2.6) suggest that whereas *ptc* (or *col*) and *dpp* expression are each initiated by Hh signaling, only *ptc* and *col* expression require sustained exposure for maintenance.

In an effort to identify the molecular machinery responsible for maintenance of *dpp* expression, we considered a role for *dpp* autoregulation. If Dpp autoregulation were responsible for maintaining expression of *dpp* in the most anterior part of its domain (that which is not overlapping with the Col/Ptc), then Ptc and dppZ would be expected to overlap in discs in which Dpp signaling is lost. To test this assertion, we used a *dpp*

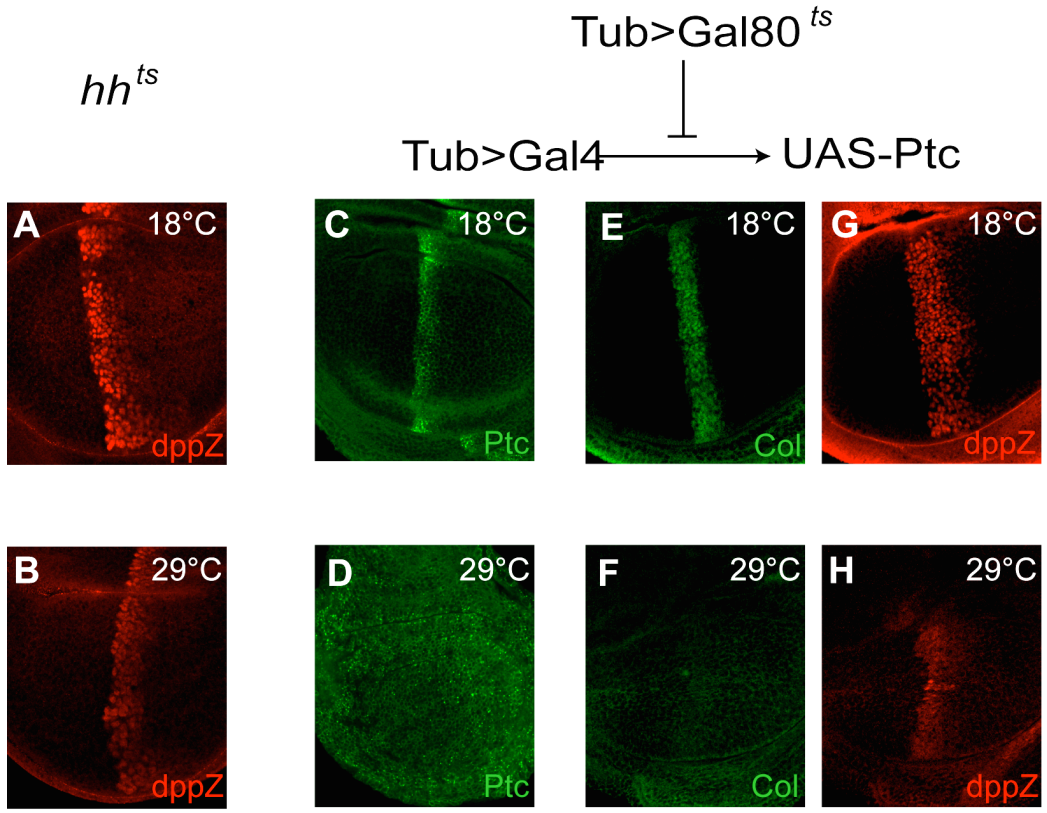

Figure 2.6 Persistence of dpp expression after Hh signaling interruption.

(A and B) Antibody staining using anti-β-gal antibody to detect dppZ expression in hh^{ts2} homozygous third instar wing discs at 18 °C (A), or exposed to restrictive temperature 29 °C for the last 24 h (B). The domain of dppZ expression is similar in (A and B), but the intensity of expression is higher in wild type. (C–H) Immunostaining using anti-Ptc (C and D), anti-Col (E and F), and anti-β-gal (G and H) antibodies within discs that overexpress Ptc using the Gal4-UAS system, and controlled by a temperature-sensitive Gal80. At 18 °C, Gal80 inactivates ectopic Ptc expression, so discs grown at this temperature exhibit essentially normal patterns of Ptc (C), Col (E), and dppZ (G). A 24-h exposure to 29 °C, however, causes high levels of Ptc expression ubiquitously (D), and consequently, the Col pattern is completely lost (F), whereas low levels of dppZ remain (H).

---

temperature-sensitive system (dpp^{ts}) (Hsiung et al., 2005). dpp^{ts} discs develop normally at permissive temperature; in particular, they have normal patterns of phosphorylated Mad (pMAD), a direct indicator of Dpp signaling activity, as well as normal expression of Ptc

and dppZ (Supporting Fig. 2.3A-C). However, *dpp*^{ts} discs, exposed to restrictive temperature for the last 24 h of larval development, exhibit a loss of pMAD expression (Supporting Fig. 2.3E), but Ptc and dppZ genes are expressed in their normal domains (Supporting Fig. 2.3F,G); in particular, these patterns do not overlap (Supporting Fig. 2.3H). Thus, this result argues against the idea that Dpp autoregulation is the main mechanism that controls *dpp* maintenance.

2.4 Discussion

In this study, we investigated how the Hh gradient is interpreted in the *Drosophila* wing imaginal disc. In particular, we explored whether or not concentration thresholds in the Hh gradient correspond to different borders of target gene expression. We used mathematical modeling as a hypotheses-generating tool. Although our mathematical model makes strong claims about the interpretation of Hh signaling, it is through in vivo experimentation that these hypotheses were tested. The predictions of the mathematical analysis present a novel mechanism for Hh signal interpretation by a field of cells. This model can be summarized by three main claims (see Fig. 2.2C): (1) At steady state, a monotonic Hh gradient is translated into a step-like signal response. This suggests that only two states ("blue"/"red," corresponding to fully ON/OFF expression of Hh target genes) can be discriminated at steady state. (2) The dynamics of the Hh gradient (and therefore the signal response) exhibit a spatial overshoot. This raises the possibility that a third state ("white," corresponding to *dpp* ON; *ptc*/*col* OFF expression) may be established by the transient signal provided by the overshoot. (3) This third state (white) may require additional mechanisms to sustain gene expression after the transient

exposure to Hh ceases. Here, we discuss these predictions in the light of our experimental data.

Existence of a Hh Overshoot and Dynamics of Target Gene Expression

We provide in vivo evidence that Hh signaling responds to dynamical changes of the gradient. Upon Hh signaling reinitialization (using the hh^{ts2} system), the establishment of the Hh gradient is dynamic and exhibits an "overshoot behavior" (Fig. 2.2E,F). Although the existence of the Hh overshoot can be predicted from the gene network architecture, it was not clear if the timescale of gradient formation would be slow enough such that the overshoot could be detected at the level of target gene expression. Using Ptc expression as a reporter of Hh signaling activity, we demonstrated that a Hh overshoot can influence Hh-dependent patterning. Ptc is fully up-regulated within 6–9 h of reinitialization of the system (Fig. 2.2E), therefore, we estimate that the transient overshoot occurs on a similar timescale; in contrast, refinement of the gradient likely happens at a much slower pace (Fig. 2.2F). Furthermore, it is not clear from our data whether the refinement occurs progressively (as predicted in Fig. 2.2B) or in a stepwise manner (i.e., oscillating towards a final state), and either scenario would be consistent with an Overshoot model.

However, the natural timing of an overshoot during the course of normal development remains in question. As *hh* is expressed in the early embryo, one possibility is that the Hh gradient forms early during embryonic development and is retained within the wing disc. Of note, however, is the fact that several factors are required for Hh secretion and distribution (Han et al., 2004; Burke et al., 1999; Panakova et al., 2005; Chamoun et al., 2001). As it remains unclear at which developmental time point Hh mobility might be afforded by one or more of these factors, it is difficult to speculate on

the timing of an overshoot. In the future, live examination of the distribution of Hh from early larval development and throughout maturation of wing disc development will provide insights, but currently, this remains a technical challenge.

Our data also revealed that *ptc* expression is up-regulated faster than *dpp* expression (Fig. 2.5). Moreover, the temporal response of *dpp* expression in response to Hh signaling (12–20 h) is much slower than the predicted timescale of the occurrence of the overshoot (6–9 h). This result is counterintuitive with regards to the Overshoot model because it predicts that the domain of *dpp* expression can be specified by a transient Hh signal. Interestingly, our data demonstrate that only a short transient exposure to Hh appears to be required to support *dpp* expression, but it can only be detected some time thereafter (see Fig. 2.5). Thus, additional regulation above that of Hh is likely to influence the timing of gene expression. For example, the kinetics of *dpp* expression may be controlled by a feed-forward loop, in which a factor required for its activation introduces a time delay with respect to the time in which exposure to the Hh signal takes place (see below).

Signal-Dependent Ptc Up-Regulation Is Required to Generate Multiple Patterns

Our in vivo data demonstrated that in the absence of Hh-dependent Ptc up-regulation, the borders of Col and dppZ coincide (Fig. 2.3F). We contend that this result is not due to higher levels of Ptc supported by the TPT transgene, because wild-type discs expressing this same TPT transgene (*ptc*+TPT discs) should express even higher concentrations of Ptc in the anterior compartment (due to additional contributions from the endogenous *ptc* gene), and yet these discs clearly exhibit different domains of Ptc and dppZ expression (Fig. 2.4). Thus, the Classical Morphogen model cannot explain the patterns observed in

ptc-TPT and *ptc*+TPT discs. Importantly, the nonoverlapping domains of Ptc and dppZ in *ptc*+TPT (Fig. 2.4D-F) are consistent with the Overshoot model, as Hh-dependent Ptc up-regulation is supported within these discs.

Nonetheless, other interpretations to explain the overlapping patterns in *ptc*-TPT discs are plausible. For example, we observed that whereas the Col domain of expression expands in *ptc*-TPT discs relative to wild-type discs (Fig. 2.3D, compare with Figure 2.3A), the dppZ expression domain does not (Fig. 2.3B,E). It is formally possible that the Col and dppZ borders may coincide in the *ptc*-TPT discs due to a postulated repressor that blocks Hh target gene expression beyond a certain position within the anterior compartment. However, we suggest this scenario is unlikely, as a significant expansion of the dppZ domain is observable both in *ptc* mutant clones located near the AP boundary or when lower levels of Ptc are present (Chen and Struhl, 1996). Furthermore, Hh-expressing clones located anywhere in the anterior compartment are able to support expression of target genes within and around the clone (Strigini and Cohen, 1997).

Another possible interpretation is provided by a recent study of Hh signaling in the vertebrate spinal cord in which signal-dependent Ptc up-regulation provides cells the ability to adapt after sustained exposure to the Hh signal ("desensitization") (Dessaud et al., 2007). This "Temporal Adaptation model" also invokes feedback by up-regulated Ptc; however, the role of the Ptc protein in this model is quite different. The Temporal Adaptation model relies on Ptc to down-regulate the signaling pathway; in contrast, the Overshoot model depends on the ability of Ptc to sequester the ligand. Supposing that desensitization is in effect, Ptc up-regulation could convert different Hh concentrations into a more graded signal response (Supporting Fig. 2.4A), but such an effect would be

limited to the domains in which Ptc is expressed, as desensitization is cell autonomous in nature. Thus, cells that express dppZ (but not Col) should not be affected by Ptc-dependent desensitization (Supporting Fig. 2.4B). We argue, therefore, that the Temporal Adaptation model cannot explain the patterning changes we observe in *ptc*-TPT discs, i.e., the overlap between *dpp* and *ptc/col* expression domains (see Supporting Fig. 2.4). Alternatively, *en* is considered responsive to the highest levels of Hh signaling (see Fig. 2.1A) (Strigini and Cohen, 1997; Blair, 1992; de Celis and Ruiz-Gomez, 1995), and En and Col overlap in expression within *ptc*-TPT discs (Supporting Fig. 2.5). However, we cannot be sure that this is due to loss of desensitization, because a careful examination of En expression in wild-type discs shows that Col and En in fact overlap even in wild-type discs, provided that gene expression is assayed late enough in development (Supporting Fig. 2.6). Nevertheless, it is still plausible that Hh-dependent Ptc up-regulation may control the boundary position of other Hh target genes in two ways: by Ptc-dependent desensitization within the domain of *ptc* expression and through gradient dynamics (overshoot) in cells located anteriorly to the *ptc* domain.

Although the Overshoot model is largely consistent with our observations, the fact that Col and dppZ patterns in *ptc*-TPT discs do not completely overlap (Fig. 2.3F′) requires additional discussion. Because the Overshoot model strictly assumes a unique threshold, δ, that distinguishes between ON and OFF states of the system (Fig. 2.2C), in theory, the model would predict a full overlap of Col and dppZ within *ptc*-TPT discs. Though we contend that gradient dynamics, driven by signal-dependent Ptc up-regulation, encodes the predominant mechanism by which gene expression boundaries are established, additional mechanisms could also subtly influence patterning outputs. For

instance, interpretation of the ON/OFF threshold at the *cis*-regulatory level cannot be infinitely accurate, and thus, different binding affinities (i.e., concentration-dependent effects) might account for small differences in the observed expression domains (Fig. 2.3F).

A State-Space Model for the Overshoot Model of Patterning

Our results can be summarized by a state-space diagram, which integrates dose-dependent effects with gradient formation dynamics (Fig. 2.7A). The history of Hh signaling activity over time for a given cell is represented by a trajectory within the state-space diagram. Cells in the anterior compartment adopt one of *three* final territories (I, III, and IV) depending on their history of Hh exposure rather than their final Hh concentration. Territory II is a transient state in which the cell expresses *ptc*, but not *dpp*. An unusual topological property of this state-space diagram is that Territory IV can only be reached through Territory III. A further requirement is that cells that enter Territory IV be able to maintain *dpp* expression, for instance through a positive feedback loop that allows cells to retain *dpp* expression even once Hh signaling has been discontinued. In support of this requirement, our data show that *dpp* expression is maintained long after Hh signaling is interrupted (Fig. 2.6).

Autoregulatory feedback is an attractive hypothesis to explain this maintenance of *dpp* expression, as previous studies suggest *dpp* exhibits autoregulation in the wing disc (Hepker et al., 1999) and in the early embryo (Jazwinska et al., 1999; Biehs et al., 1996). However, we see no change in the dppZ pattern when Dpp signaling is transiently impaired (Supporting Fig. 2.3), arguing against autoregulatory feedback as a major mechanism supporting “memory” of *dpp* expression. However, other possible molecular

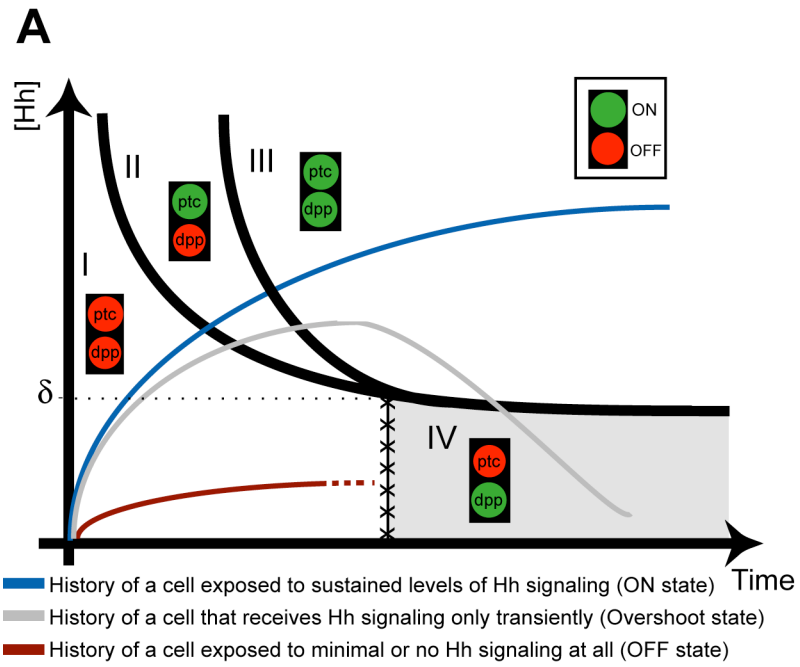

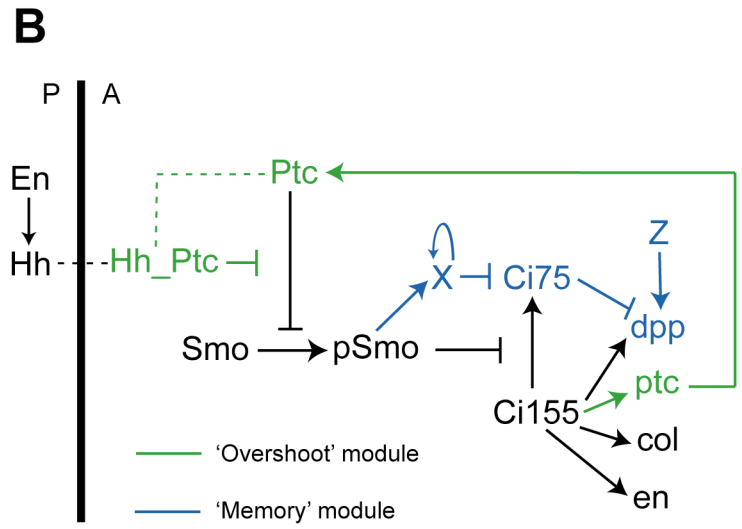

Figure 2.7 State-space diagram and network architecture for the Overshoot model.

(A) The state-space diagram consistent with the Overshoot model is divided into four territories (I–IV) defined by the expression levels of *ptc* (or *col*) and *dpp*, consistent with the data in Figure 5. All cells in the anterior compartment are initially in Territory I (*ptc* OFF; *dpp* OFF) but only cells relatively far from the AP boundary, in which signaling levels are below the switching threshold, δ, remain in this territory (red trajectory). During the formation of the Hh gradient, cells located sufficiently close to the AP boundary visit transiently Territory II and express *ptc*, but not *dpp*. From the subset of cells that enter Territory II,

those that remain exposed to the signal will continue expressing *ptc* and will eventually express *dpp* when crossing to Territory III (blue trajectory). However, cells in which Hh signaling ceases (for example, as a result of gradient refinement after the overshoot) will maintain *dpp* expression, but will stop expressing *ptc*. These cells will cross to Territory IV and remain there (gray trajectory). Note that Territory IV is not simply connected to Territory I (see boundary line demarcated by X's) as it is only accessible from Territory III. An additional territory (V) may be considered to include *engrailed* in the state-space model (see Figure S6G). (B) The Overshoot model is inherent within the Hh network architecture. The overshoot of Hh depends exclusively on Hh-dependent Ptc-upregulation ("Overshoot" module). However, distinct *ptc/col* and *dpp* can only be realized if *dpp* (but not *ptc* and *col*) expression is maintained in cells in which exposure of Hh is only transient. One way in which this can be effected at the molecular level is if a "Memory" module operates in the network. For example, *dpp* expression can be maintained specifically if a stable protease "X" that degrades the repressor form of Ci (Ci75) is up-regulated in response to Hh signaling; "Z" represents a Hh-independent activator that supports *dpp* expression (see Discussion).

---

mechanisms to maintain *dpp* expression are conceivable (see below and Fig. 2.7B, for example).

Towards the Molecular Basis of the Overshoot Model

Our data are consistent with a model in which Hh-dependent Ptc up-regulation is necessary to shift the initial Hh gradient posteriorly, generating a zone of transient signal exposure that is required to specify different domains of gene expression. Unlike other models of patterning, the Overshoot model is based on two properties of the Hh gene network architecture: first, a negative feedback loop mediated by Ptc that controls the spatial range of the Hh gradient (Fig. 2.7B; "Overshoot" module) (Chen and Struhl, 1996), and second, a positive feedback loop that maintains gene expression of *dpp* in the region in which only a transient Hh signal is received (Fig. 2.7B; "Memory" module).

Although we contend that the molecular players within the Overshoot module are known, we do not have a molecular understanding of the genes that relate to the Memory module. One possible molecular mechanism to explain "memory" may involve the differential functions of Ci. *ptc*, *col*, and *en* require the activator form of Ci (Ci155) for expression; whereas in the absence of Ci155, *dpp* still exhibits low-level expression (Méthot and Basler, 2001). Evidence exists that the repressor form of Ci (Ci75) is more critical for *dpp* expression and that another activator "Z" may support low level *dpp* expression (Méthot and Basler, 2001). A putative Memory module, for example, could involve Hh-dependent regulation of a protease, "X," that degrades Ci75 and is stable. In this scenario, the overshoot gradient would be sufficient to activate X in the *dpp* expression domain, which in turn will maintain the absence of Ci75 in this region even after the overshoot has occurred. This molecular model is appealing in light of our data for the following reasons. First, it suggests that the slow temporal response of the *dpp* pattern after signal reinitialization may be due to the delay in producing X; and second, it explains why *dpp* can only be maintained at low levels after Hh signaling is removed (Fig. 2.6 and Supporting Fig. 2.2).

Implications of the Overshoot Model

We have discussed how the Overshoot model proposed here explains *ptc/col* and *dpp* differential expression, but how might expression of *en* be controlled? We observed that the En boundary falls in the middle of the Ptc domain in the wing disc of a crawling third instar larva (Supporting Fig. 2.6A–C), but the patterns tend to overlap when discs are taken from larvae close to pupariation (Supporting Fig. 2.6D–F). These results suggest that the En pattern forms very slowly and may also be explained in the context of our

three-state overshoot model: En is patterned in a manner similar to *ptc* and *col* genes, encompassing similar domains of expression, but the En pattern is realized later (Supporting Fig. 2.6G).

These observations raise an important point regarding the interplay of gradient dynamics and Hh concentration levels. Although the Overshoot model does not require multiple concentration thresholds in order to determine different boundaries of gene expression, the rate of signal activation likely depends on the Hh concentration. The influence of concentration on patterning through the Overshoot model is explicitly taken into account within the state-space diagram; different territories are delineated by curved domains (instead of straight vertical lines) to indicate responsiveness to concentration differences (Fig. 2.7A and Supporting Fig. 2.6G). For example, cells exposed to two different Hh concentrations (provided that they are both higher than the switching threshold, δ) will both eventually turn *en* expression ON, but the cell exposed to the higher concentration will support expression first. This would also explain why the dppZ pattern forms in a sequential manner, with fewer cells closer to the AP boundary expressing the reporter first (Fig. 2.5). To be clear, this concentration-dependent influence on the rate of pattern formation is *not* related to concentration thresholds as defined by the Classical Morphogen model.

Another implication of the Overshoot model is that the decision to activate *dpp* is irreversible. This implies that once cells receive sufficient Hh levels to turn on the pathway and express *dpp*, they will continue to do so even if Hh signaling is removed (Fig. 2.6). This idea is similar to early theoretical studies based on the classical French Flag model that proposed that the ability to reach a certain concentration threshold is not

sufficient to support a specific response, but that instead additional feedback interactions are required to "lock down" that response (Lewis et al., 1977; Meinhardt, 1978). We find support for this idea as we observe that *dpp* expression is retained even 24 h after Hh protein is removed (Fig. 2.6B and Supporting Fig. 2.2).

Although the Overshoot model as presented here (Fig. 2.7A) can only specify three states (i.e., a "French Flag"), it is conceivable that this model may be generalizable to support more than three distinct domains of expression. For example, an additional state in the system may be incorporated if additional proteins are considered, ones that, like Ptc, regulate Hh mobility and are up-regulated in response to the signal. In vertebrates, targets of Hh have been identified that include proteins that sequester Hh itself. Hedgehog-interacting-protein 1 (Hhip1) can limit the range of the Hh gradient, and *Hhip1* transcription is also slowly up-regulated by Hh signaling (Chuang and McMahon, 1999). In this case, for instance, the full refinement of the Hh gradient could occur in two discrete steps (in vertebrates this could be mediated by Ptch1 and a Hhip1) that generate two transient zones of different temporal exposures to Hh able to support multiple patterns of gene expression. In fact, in *Ptch1* mutant mouse embryos that express low levels of Ptch1 ubiquitously, neural tube patterning is affected in ventral regions (close to the source of Hh), but patterning of intermediate regions is approximately normal (Jeong and McMahon 2005). However, in *Ptch1; Hhip1* double mutants, ventral patterns expand and overlap intermediate patterns (Jeong and McMahon, 2005). These observed patterning changes share similarity with the overlap of patterns observed for *ptc*-TPT discs (Fig. 2.3D–F); thus, we suggest that the Overshoot model may apply to Hh patterning in vertebrates as well.

Conclusion

The significance of the Overshoot model presented here relies on the architecture of a particular gene regulatory network, in which a morphogen activates the expression of a molecule affecting its distribution. As this network property has been identified in other systems (Chuang and McMahon, 1999; Golembo et al., 1996; Nakagoshi et al., 2002; Drossopoulou et al., 2000), it is possible that evolution has selected upon this network architecture to support patterning of other developing systems in a similar manner to Hh-mediated patterning of the *Drosophila* wing disc, through gradient dynamics.

Chapter 3

Steady-State Invariant Genetics: Probing the Role of Morphogen Gradient Dynamics in Developmental Patterning

Morphogen-mediated patterning is the predominant mechanism by which positional information is established during animal development. In the classical view, the interpretation of morphogen gradients is assumed to be at equilibrium and the dynamics of gradient formation are generally ignored. The problem of whether or not morphogen gradient dynamics contribute to developmental patterning has not been explored in detail, in part, because genetic experiments that selectively affect signaling dynamics while maintaining unchanged the steady-state morphogen profile are difficult to design and interpret. Here, I present a theoretical approach to identify genetic mutations in developmental patterning that may affect the transient, but leave invariant the steady-state signalling gradient. As a case study, I illustrate how these tools can be used to explore the dynamic properties of Hedgehog signaling in the developing wing of the fruit fly, *Drosophila melanogaster*. This analysis provides insights into how different properties of the Hedgehog gradient dynamics, such as the duration of exposure to the signal or the width of the gradient prior to reaching the equilibrium, can be genetically perturbed without affecting the local steady-state distribution of the gradient. I propose that this method can be generally applicable as a tool to design experiments to probe the role of transient morphogen gradients in developmental patterning and discuss potential applications of these ideas to a wide variety of problems.

3.1. Introduction

A classical paradigm in developmental biology is that cells in a developing embryo or tissue acquire information about their relative spatial location by interpreting the local concentration of chemical signals in their environment called morphogens. The key idea is that the interpretation of positional information results in the establishment of gene expression patterns whose boundaries correspond to concentration thresholds of the morphogen gradient (Wolpert, 1971; Gurdon et al., 1998; Ashe and Briscoe, 2006). A common implicit assumption of the Classical Morphogen model is that gradients are interpreted approximately at the steady state in order to produce stable patterns of gene expression (Nellen et al., 1996; Kicheva et al., 2008). However, recent quantitative imaging studies in some systems have demonstrated that morphogens are more dynamic than previously thought and have raised criticisms to the classical morphogen concept (Gregor et al., 2007; Harvey and Smith, 2009; Liberman et al., 2009). For instance, if gradient formation evolves in time, how and when are concentration thresholds interpreted? Or more generally, how do morphogen dynamics contribute to positional information? One possibility is that patterns evolve as the gradient develops, giving rise to transient patterns that converge to stable gene expression domains as the gradient approaches the equilibrium (Bourillot et al., 2002). This scenario supports a 'no-role' model for transient gradients (Fig. 3.1A), but this seems not always to be the case. For example, we recently reported that in the wing disc of the fruit fly, *Drosophila melanogaster*, the specification of different spatial domains of expression in response to Hedgehog (Hh) signalling depends on the dynamics of the Hh gradient (Nahmad and Stathopoulos, 2009). In particular, we showed that cells exposed to Hh only transiently

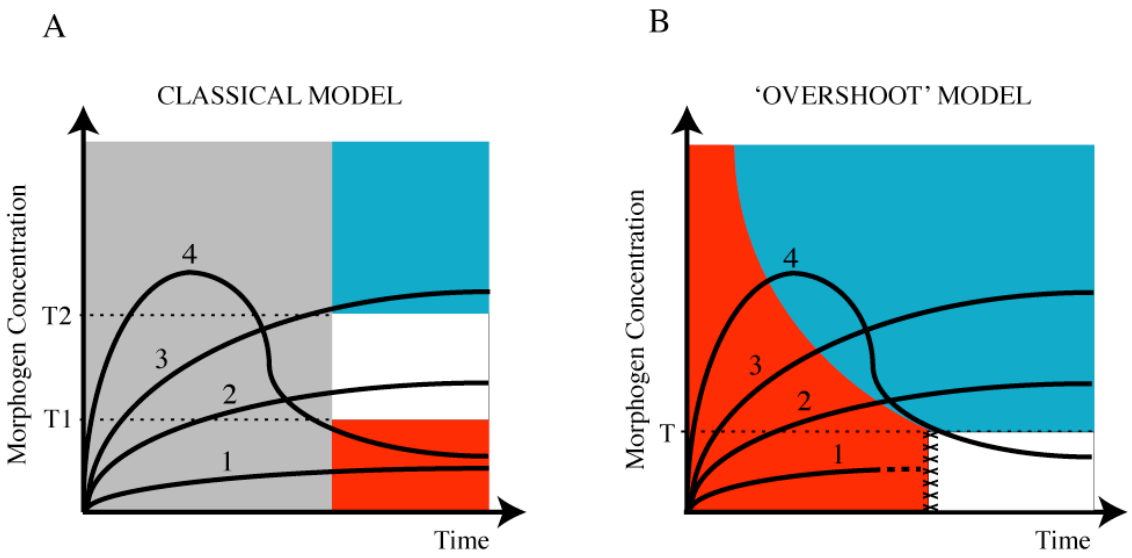

Figure 3.1 Static vs. dynamic models of morphogen-mediated patterning.

(A) In the classical view, morphogens are assumed at equilibrium and cellular states (blue, white, or red) depend on morphogen concentration thresholds (T1 and T2). In this model, the dynamics of the gradient prior to reaching the equilibrium (gray region) does not have a role in patterning. For example, cells transiently exposed to the morphogen, but that cease receiving the signal at the steady state acquire the same state (red) than cells always exposed to low signaling levels (trajectories 1 and 4). (B) In the 'Overshoot' Model (Nahmad and Stathopoulos, 2009), the dynamics of the gradient are essential for pattern formation. Cells receiving the morphogen will change from a red (OFF) to a blue (ON) state. As in (A), those cells that keep receiving the signal will maintain their blue fate (trajectories 2 and 3), but cells that lost their transient signal (trajectory 4) will adopt a different state (white) than cells that never reach the switching threshold T (trajectory 1). In (B), the red and white domains are not simple-connected, i.e. trajectories cannot cross the red-white boundary.

---

express a different combination of genes compared to cells constantly receiving the signal or cells that never receive it at all. In contrast to the Classical Morphogen Model (Fig. 3.1A), this case provides an example in which patterns are not only defined based on the steady-state readout of the morphogen concentration, but also on their history of exposure to the signal (Fig. 3.1B). In general, the problem of whether or not the dynamics of

gradient formation are required for morphogen interpretation remains largely unexplored experimentally because mutants that affect gradient dynamics are also likely to perturb the steady-state morphogen distribution. Despite the recent introduction of techniques to quantify and measure the dynamic properties of morphogen gradients in living embryos or tissues (Kicheva et al., 2007; Yu et al., 2009), the identification of mutants that selectively affect gradient dynamics with little or no effect on the equilibrium profile remains challenging.

For more than 50 years, mathematical modeling and theoretical biology have provided powerful tools to identify potential mechanisms of morphogen gradient formation and interpretation in developmental patterning (Turing, 1952; Meinhardt, 1978; von Dassow et al., 2000; Lander et al., 2002; Eldar et al., 2003; Bollenbach et al., 2008). However, much of this literature has been built on the assumption that morphogens are interpreted at the steady state and transient gradients are often completely ignored. Reducing a dynamical system to its steady state is usually mathematically convenient as the equations of the model often simplify considerably and theoretical tools are readily available to study the stability of solutions. In contrast, much less analytical tools exist to investigate the temporal evolution of a gradient and studies that have taken morphogen dynamics into consideration usually rely on exhaustive numerical explorations of high-dimensional parameter spaces (Jaeger et al., 2004; Saha and Schaffer, 2006).

In this paper, I present theoretical tools to study transients of dynamical systems in general and the role of the dynamics of morphogen gradients in particular. Given a mathematical model of a particular morphogen-based pattern formation system, we

consider parameter perturbations that may change the transient shape of a morphogen without effectively affecting its steady-state distribution. I introduce a theoretical framework to study these perturbations in a geometric way and discuss how they could be analyzed systematically. As an example, I investigate the dynamics of the Hh gradient in the *Drosophila* wing disc and show how this approach may lead to predict genetic mutants that provide insights into the role of Hh gradient dynamics during development. Other applications of these concepts and their theoretical and biological implications are also highlighted.

3.2. Methods

Wing Disc Immunostaining

In Figure 3.3A, a third instar wing disc of genotype *dpp10638/CyO* was immunostained with mouse anti-Ptc (Hybridoma Bank Developmental Studies at the University of Iowa) and rabbit anti-β-Galactosidase (Invitrogen) antisera following standard techniques. *dpp10638* is a lacZ enhancer trap reporter that expresses nuclear β-Galactosidase under the control of the *dpp* enhancer.

Analytical Solutions

The analytical solution of equation (3.1) was derived by Bergmann et al. (2007) and is given by:

$$[\mathrm{A}](x,\,t) = \mathrm{A}_0\left[\exp\left(\frac{-x}{\lambda}\right) - \frac{1}{2}\exp\left(\frac{-x}{\lambda}\right)erfc\left(\frac{\frac{2Dt}{\lambda} - x}{2\sqrt{Dt}}\right) - \frac{1}{2}\exp\left(\frac{x}{\lambda}\right)erfc\left(\frac{\frac{2Dt}{\lambda} + x}{2\sqrt{Dt}}\right)\right],$$

with *erfc*, the complementary error function, $erfc(z) = \frac{2}{\pi}\int_{z}^{\infty} \exp(-\tau^2) d\tau$. This solution was used to generate the gradient profiles in Figure 3.2C-E. An approximate analytical solution of Equation (3.6) near the AP boundary (Equation (3.8)) was obtained by linearization and the full details of this approximation are given in the Supporting Text.

Numerical Simulations

Our model of Hh-dependent patterning of the wing disc is assumed one-dimensional along the AP axis. We used a system of coordinates centered at the AP boundary (x=0) where the posterior and anterior ends of the disc were assumed at $x = -L_P$ and $x = L_A$, respectively (with L_P+L_A=200 μm, the length of the AP axis). Equations (3.5) were numerically solved with the parameters values as in Supporting Table 1 and using a Forward-in-Time-Centered-in-Space algorithm implemented in MATLAB. As in previous work (Nahmad and Stathopoulos, 2009), we use zero initial conditions, except for [*ptc*] and [Ptc] that were taken as:

$$[ptc](x, 0) = \frac{\alpha_{ptc0}}{\beta_{ptc}}, \text{ for } x > 0 \text{ and zero otherwise; } [\text{Ptc}](x, 0) = \frac{T_{\text{Ptc}}}{\beta_{\text{Ptc}}}[ptc](x, 0).$$

Furthermore, we imposed zero-flux boundary conditions at the disc extremes ($x = -L_P$; $x = L_A$), and assumed continuity of the $[\text{Hh}]_{SS}$ profile and its derivative at the AP boundary (x = 0; see Supporting Text).

3.3. Theoretical Framework: Definitions and Examples

One way to study the role of signaling dynamics is to consider perturbations that maintain certain steady-state properties of a system unchanged, but affect the history of how those

equilibrium states are reached. In this section, I introduce a general theoretical framework to define this class of perturbations, referred here as *steady-state invariant perturbations*, and use a practical example to illustrate how this approach can be used as a tool for experimental design in the context of developmental genetics.

Steady-State Invariant Perturbations: An Example

In order to introduce the concept of steady-state invariant perturbations, consider a simple example, namely, a naïve model of a one-dimensional morphogen produced at a point source (x=0) that establishes a concentration gradient by diffusion and linear degradation,

$$\frac{\partial\,[\mathrm{A}]}{\partial t} = D\frac{\partial^2[\mathrm{A}]}{\partial x^2} + \alpha\delta(x) - \beta[\mathrm{A}], \qquad (3.1)$$

where [A] denotes the concentration of morphogen A, $\delta(x)$ is the Dirac delta distribution, and α, β and D are the production, degradation, and diffusion rates of A, respectively. At the steady state, the shape of the [A] gradient is exponential* and given by

$$[\mathrm{A}]_{ss}(x) = \mathrm{A}_0 \exp\left[-\frac{x}{\lambda}\right], \qquad \text{with } \mathrm{A}_0 = \frac{\alpha}{2\sqrt{D\beta}} \text{ and } \lambda = \sqrt{\frac{D}{\beta}}. \qquad (3.2)$$

In Equation (3.2), A_0 and λ represent the amplitude and characteristic length of the steady-state gradient, and their values determine uniquely this solution. As A_0 and λ are defined in terms of the parameters of the system, a perturbation on the wild-type parameter values will maintain the steady-state solution invariant if and only if the values of A_0 and λ remain unchanged. To formalize, let $(\tilde{\alpha}, \tilde{\beta}, \tilde{D})$ be the wild-type parameter values and consider a mutant that perturbs the system such that the effective parameter

* In this example, we ignore boundary conditions by assuming that the system is infinitely long and diffusion occurs in both directions from the source. These assumptions allow us to solve the full time-dependent problem (3.1) exactly using the method of Fourier transforms (Bergmann et al., 2007; see Methods section) and solution (3.2) arises as a limit of the time-dependent solution when $t \to \infty$.

values of the system change to (α', β', D'). We say that the mutant preserves the steady-state gradient or is *steady-state invariant* if the following equations hold:

$$\frac{\alpha'}{\sqrt{D'\beta'}} = \frac{\tilde{\alpha}}{\sqrt{\tilde{D}\tilde{\beta}}} \equiv \text{constant1}$$
$$\sqrt{\frac{D'}{\beta'}} = \sqrt{\frac{\tilde{D}}{\tilde{\beta}}} \equiv \text{constant2}. \qquad (3.3)$$

The set of all steady-state invariant perturbations can be represented geometrically in parameter space and will be referred to as the *steady-state invariant set* of the system. In general, a steady-state invariant perturbation Δ can be denoted as a vector in parameter space that is based on the point of wild-type parameter values and ends on the steady-state invariant set (Fig. 3.2A). In this example, it follows that any perturbed parameter vector (α', β', D') satisfying Equation (2.3) must be of the form,

$$(\alpha', \beta', D') = (\delta\tilde{\alpha}, \delta\tilde{\beta}, \delta\tilde{D}) \quad \text{for some } \delta > 0. \qquad (3.4)$$

Equation (3.4) represents a straight line in parameter space that crosses through the origin and contains the wild-type parameter vector ($\tilde{\alpha}$, $\tilde{\beta}$, $\tilde{D}$) (Fig. 3.2B). Thus, the line defined by Equation (3.4) is the steady-state invariant set of this system. Importantly, a perturbation that keeps the parameter values within the steady-state invariant set may affect the transient evolution of the gradient but maintains the steady-state morphogen gradient unchanged. In this simple example, the effects on morphogen dynamics along the steady-state invariant set are simple to interpret; for $\delta < 1$, gradient formation is slower compared to the wild-type case, while for $\delta > 1$ the steady-state gradient is approached faster than in the wild type (Fig. 3.2C-E). In addition, the rates in which the steady state is approached are space-dependent; cells adjacent to the source approach equilibrium faster than cells away from it and this property also holds after steady-state

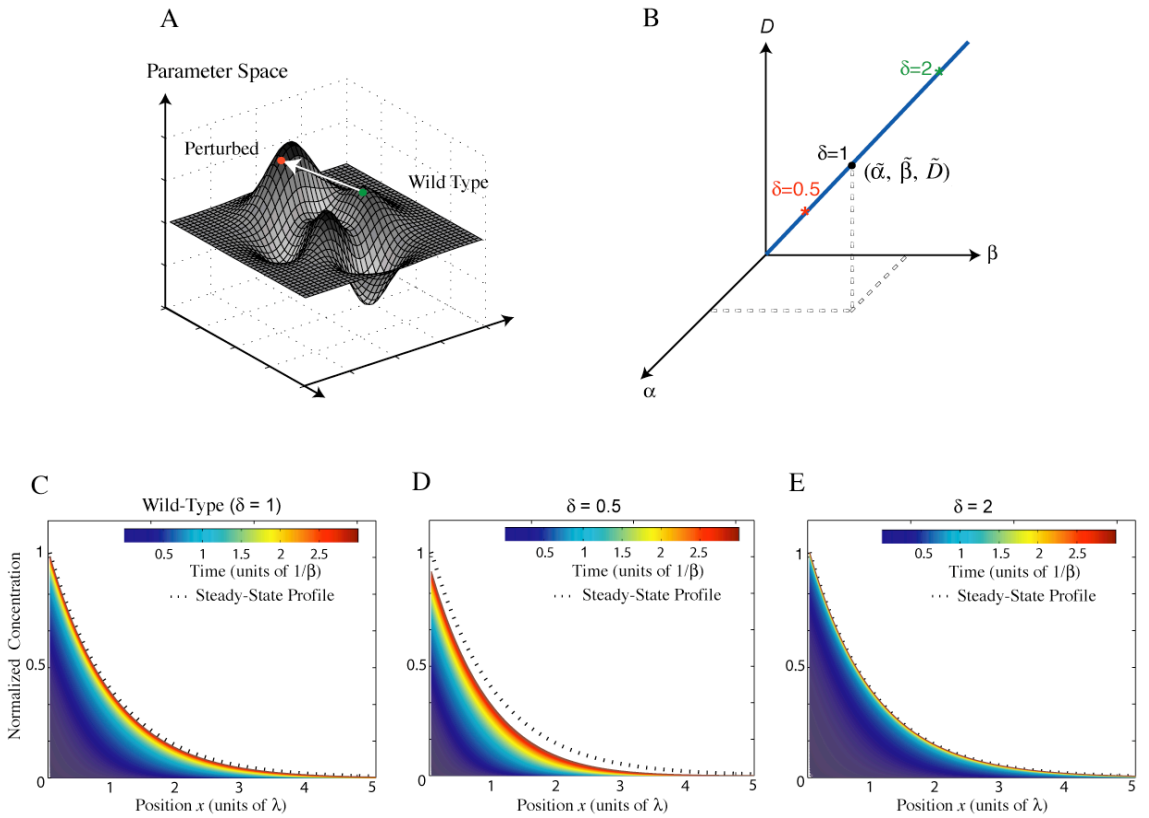

Figure 3.2 Analysis of steady-state invariant perturbations in the case of a morphogen established by diffusion and uniform linear degradation.

(A) Steady-state invariant sets can be generally described as subsets of parameter space. A steady-state invariant perturbation is represented by a vector in parameter set based on the point of wild-type parameter values (green) and ending on another point of the steady-state invariant set (red). (B) The steady-state invariant set of the morphogen modelled by Equation (1) is the straight line defined by Equation (3.4) with δ>0. (C-E) Temporal dynamics of the morphogen concentration [from Equation (3.1)] when parameter values α, β, and D are perturbed along the steady-state invariant set by varying the value of δ. (C) δ=1 (unperturbed case); (D) δ=0.5; (E) δ=2. For comparison purposes, gradients in (C-E) are plotted using the same colour-coded timescale and the (invariant) steady-state profile is displayed in all three panels.

---

invariant perturbations (see Supporting Fig. 3.1). Despite the simplicity of this example, the definition of steady-state invariant sets and the method to compute them can be generalized (see Box 3.1).

BOX 3.1

Consider the following general model of developmental patterning. Let $\mathbf{G}=([g_1], [g_2], \ldots, [g_k])$ a vector denoting concentrations of gene products $g_1, \ldots, g_k$ and assume that the dynamics of gene concentrations is described by a reaction-diffusion equation of the form

$$\frac{\partial \mathbf{G}}{\partial t} = \mathbf{D}\nabla^2\mathbf{G} + \boldsymbol{f}(\mathbf{G}, \boldsymbol{\mu}). \qquad \text{(B1)}$$

In this equation, ∇^2 denotes the Laplacian operator ($\nabla^2 \equiv \frac{\partial^2}{\partial x^2} + \frac{\partial^2}{\partial y^2} + \frac{\partial^2}{\partial z^2}$), $\mathbf{D}$ is a vector of diffusion coefficients, $\boldsymbol{f}$ is the reaction function that describes the interactions of gene products, and $\mathbf{m}$ is a vector of kinetic rates or parameters of the system. Note that the systems considered in the text (Equations (3.1) and (3.5)) are particular cases of Equation (B1). At the steady state, we set the time derivatives to zero so that the steady-state concentrations, $\mathbf{G}^{ss}$, obey the following equation,

$$0 = \mathbf{D}\nabla^2\mathbf{G}^{SS} + \boldsymbol{f}(\mathbf{G}^{SS}, \boldsymbol{\mu}). \qquad \text{(B2)}$$

Assume that the solution of (B2) exists and let us denote it as $\mathbf{G}_{\mathbf{x}}^{SS}(\boldsymbol{\mu})$.

A parameter perturbation (e.g., a genetic perturbation) of the system is a function D of the form $D(\mathbf{m})=(d_1m_1, d_1m_2, \ldots, d_rm_r) \equiv (\mu'_1, \mu'_2, \ldots, \mu'_r)$ for some positive constants $d_1, \ldots, d_r$. We are interested in the study of perturbations that leave the steady-state solution $\mathbf{G}_{\mathbf{x}}^{SS}(\boldsymbol{\mu})$ unchanged at least in a region of space **S**. A *steady-state invariant perturbation* is a parameter perturbation D that satisfies the following property:

$$\mathbf{G}_{\mathbf{x}}^{SS}(\boldsymbol{\mu}) = \mathbf{G}_{\mathbf{x}}^{SS}(\Delta(\boldsymbol{\mu})) \qquad \text{for all } \mathbf{x} \in \mathbf{S}. \qquad \text{(B3)}$$

Our goal is to find the set of steady-state invariant perturbations satisfying Equation (B3). For this purpose, it is useful to consider the following geometric representation. Note that there is a one-to-one correspondence between parameter perturbations and points in parameter space (i.e points of the form $(\mu'_1, \mu'_2, \ldots, \mu'_r)$ with $m'_i \geq 0$, i=1,…, r). For each **x** (fixed), $\mathbf{G}_{\mathbf{x}}^{SS}(\boldsymbol{\mu}) = \text{constant}$ and therefore, we can consider the points $(\mu'_1, \mu'_2, \ldots, \mu'_r)$ in parameter space that satisfy

$$\mathbf{G}_{\mathbf{x}}^{SS}(\mu'_1, \mu'_2, \ldots, \mu'_r) = \mathbf{G}_{\mathbf{x}}^{SS}(\boldsymbol{\mu}) = \text{constant}, \qquad \text{for } \mathbf{x} \text{ fixed}. \qquad \text{(B4)}$$

Denote by $W_{\mathbf{x}}$ the set of points in parameter space satisfying (B4) for a given **x**, and define the *steady-state invariant set,* **W**, of the system (in **S**) as the set that results from the intersection of $W_{\mathbf{x}}$ for all $\mathbf{x} \in \mathbf{S}$, i.e.

$$\Omega = \bigcap_{\mathbf{x} \in \mathbf{S}} \Omega_{\mathbf{x}}, \qquad \text{(B5)}$$

(see Supporting Figure 3.2). Hence, the steady-state invariant set is a geometric representation of the set of mutants that leave invariant the equilibrium gene concentrations in cells located within the region **S**.

Hh Signaling in the *Drosophila* Wing Disc: A Case Study

In order to motivate the applications of the concept of steady-state invariant sets to practical cases, the dynamic properties of Hh signaling in the *Drosophila* wing imaginal disc were investigated. In a recent study, we provided experimental evidence for the existence of a transient expansion (or 'overshoot') of the Hh gradient in the *Drosophila* wing disc which is required to define three different regions of signal exposure (Fig. 3.3A; Nahmad and Stathopoulos, 2009). However, how specific properties of this transient overshoot (e.g., its duration) contribute to patterning has not been established. Here, I use the concept of steady-state invariant perturbations to make predictions about which genetic perturbations of the system may affect the dynamic properties of this overshoot without affecting the equilibrium profile of the gradient.

Consider the mathematical model of the Hh signaling pathway originally presented in Nahmad and Stathopoulos (2009):

$$
\begin{aligned}
\frac{\partial[\mathrm{Hh}]}{\partial t} &= D\frac{\partial^2[\mathrm{Hh}]}{\partial x^2} + S^{-}(x)\alpha_{\mathrm{Hh}} - \gamma_{\mathrm{Hh\_Ptc}}[\mathrm{Hh}][\mathrm{Ptc}] - \beta_{\mathrm{Hh}}[\mathrm{Hh}] \\
\frac{\partial[ptc]}{\partial t} &= S^{+}(x)\alpha_{ptc0} + \frac{\alpha_{ptc}[\mathrm{Signal}]^{\mathrm{m}}}{k_{ptc}^{\mathrm{m}} + [\mathrm{Signal}]^{\mathrm{m}}} - \beta_{ptc}[ptc] \\
\frac{\partial[\mathrm{Ptc}]}{\partial t} &= T_{\mathrm{Ptc}}[ptc] - \gamma_{\mathrm{Hh\_Ptc}}[\mathrm{Hh}][\mathrm{Ptc}] - \beta_{\mathrm{Ptc}}[\mathrm{Ptc}] \\
\frac{\partial[\mathrm{Hh\_Ptc}]}{\partial t} &= \gamma_{\mathrm{Hh\_Ptc}}[\mathrm{Hh}][\mathrm{Ptc}] - \beta_{\mathrm{Hh\_Ptc}}[\mathrm{Hh\_Ptc}] \\
\frac{\partial[\mathrm{Signal}]}{\partial t} &= \frac{S^{+}(x)\alpha_{\mathrm{Signal}}\left(\frac{[\mathrm{Hh\_Ptc}]}{[\mathrm{Ptc}]}\right)^{\mathrm{n}}}{k_{\mathrm{Signal}}^{\mathrm{n}} + \left(\frac{[\mathrm{Hh\_Ptc}]}{[\mathrm{Ptc}]}\right)^{\mathrm{n}}} - \beta_{\mathrm{Signal}}[\mathrm{Signal}],
\end{aligned}
\tag{3.5}
$$

where [Hh], [*ptc*], [Ptc], [Hh_Ptc] are the concentrations of Hh, *ptc* (mRNA), Ptc (protein), and the Hh-Ptc complex, respectively. The coefficients α, β, γ, and T,

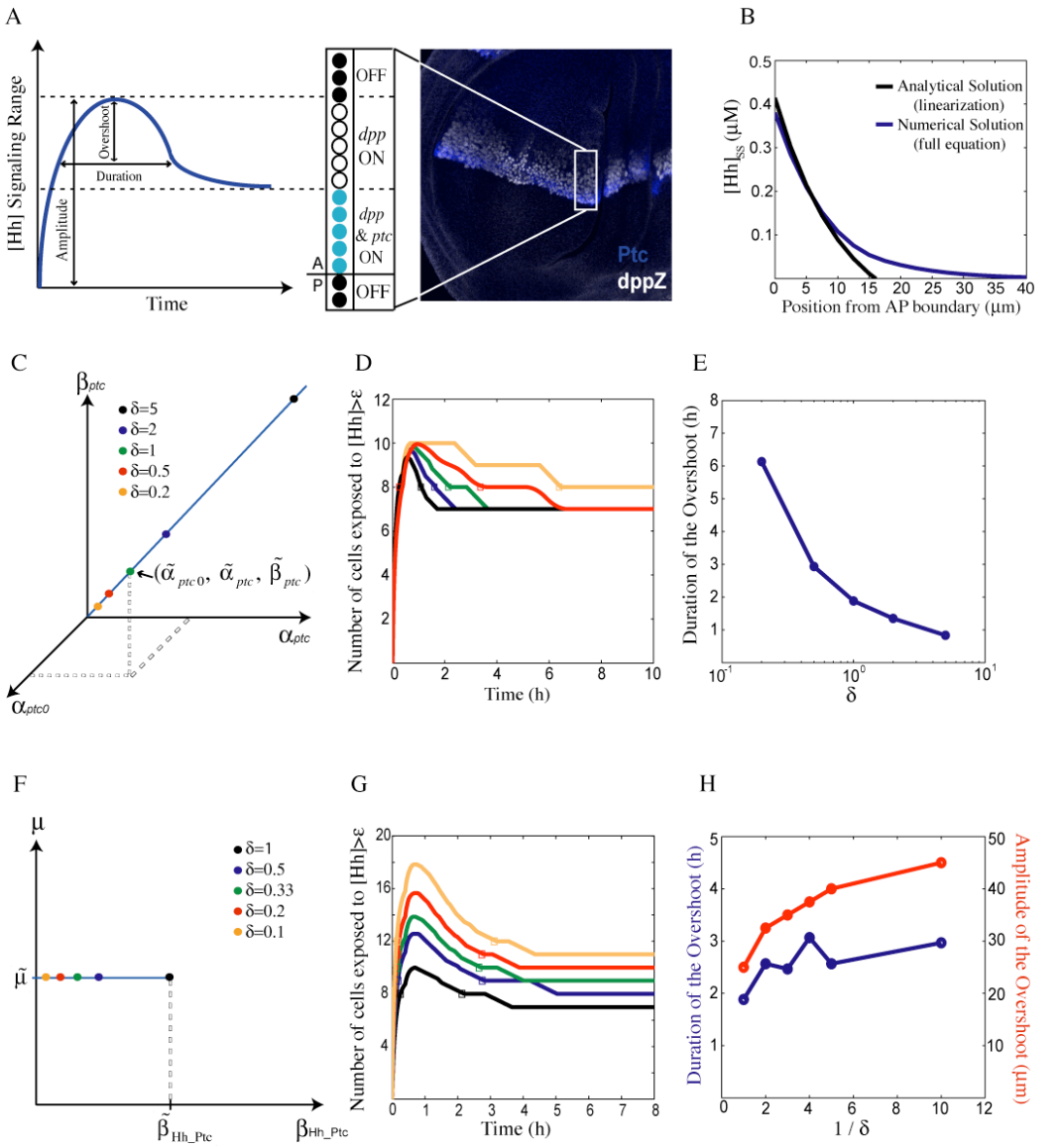

Figure 3.3 Analysis of steady-state invariant perturbations of the Hh morphogen in the *Drosophila* wing disc.

(A) Summary of the 'Overshoot' Model (Nahmad and Stathopoulos, 2009). An overshoot of the Hh gradient determines patterning of the *Drosophila* wing disc. Three gene expression domains are established by this overshoot. Cells that do not receive the signal or that receive sustained signalling levels are denoted by red and blue, respectively. Certain cells that are only transiently exposed to the signal are denoted by the white state and characterized by *dpp* (but not *ptc*) expression. The photo displays wild-type expression patterns of *ptc* and *dpp* in a third-instar wing disc (with the anterior compartment oriented upwards) carrying a *dpp*-lacZ reporter immunostained using Ptc (blue) and β-Galactosidase (white) antibodies. (B)

Comparison of the Hh steady-state profiles as obtained from the numerical solution of equation (6) or the exact solution of the linearization [Equation (3.8)]. Note that the approximation is good only near the AP boundary. (C) The steady-state invariant subset described by equation (3.10) represents a line parameterised by the variable δ. (*d*) Analysis of the overshoot in selected steady-state invariant mutants. Colour coding of the curves correspond to different values of δ as shown in (C). Note that the amplitude of the overshoot is unaffected by these steady-state invariant perturbations. (E) The duration of the overshoot (in hours) as extracted from (D) (squares) as a function of δ. (F) Representation of the steady-state invariant subset from equation (11) in two dimensions. The vertical axis denoted by μ, represents any other dimensions of parameter space. (G) Similar analysis as in (D), but corresponding to the approximate steady-state invariant subset in (F). (H) Steady-state invariant perturbations in (F) considerably affect the amplitude (red), but not the duration of the overshoot (blue).

---

represent the rates of synthesis, degradation, complex formation, and translation, respectively. $S^+(x)$ (or $S^-(x)$) is a step function of the form $S^+(x) = 1$ if $x > 0$ (or $S^-(x) = 1$ if $x < 0$), and zero otherwise that is used to represent compartment-specific reactions. For example, in this model, extracellular Hh is produced in the posterior compartment ($x<0$) and diffuses across the anterior-posterior (AP) boundary ($x=0$). In the anterior compartment ($x>0$), Hh binds its receptor, Patched (Ptc), and Hh signaling is activated as a function of the ratio of bound to unbound receptor concentrations (Casali and Struhl, 2004). As in our previous study, the variable [Signal] denotes the concentration of a factor that models pathway activity at the intracellular level (see Nahmad and Stathopoulos (2009) for further details). At the steady state, the set of Equations (3.5) reduce to the following second-order equation, only valid within the anterior compartment ($x>0$),

$$D\frac{d^2[\mathrm{Hh}]_{\mathrm{ss}}}{dx^2}-\frac{\chi\,[\mathrm{Hh}]_{\mathrm{ss}}}{\beta_{\mathrm{Ptc}}+\gamma_{\mathrm{Hh\_Ptc}}[\mathrm{Hh}]_{\mathrm{ss}}}\left[\alpha_{ptc0}+\frac{\alpha_{ptc}[\mathrm{Hh}]_{\mathrm{ss}}^{nm}}{\eta\left[\kappa^n+[\mathrm{Hh}]_{\mathrm{ss}}^n\right]^m+[\mathrm{Hh}]_{\mathrm{ss}}^{nm}}\right]-\beta_{\mathrm{Hh}}[\mathrm{Hh}]_{\mathrm{ss}}=0, \qquad (3.6)$$

with $\chi=\frac{T_{\mathrm{Ptc}}\gamma_{\mathrm{Hh\_Ptc}}}{\beta_{ptc}}$, $\kappa=\frac{k_{\mathrm{Signal}}\beta_{\mathrm{Hh\_Ptc}}}{\gamma_{\mathrm{Hh\_Ptc}}}$, and $\eta=\frac{k_{ptc}\beta_{\mathrm{Signal}}}{\alpha_{\mathrm{Signal}}}$. This equation is nonlinear and an analytical solution may be difficult (or impossible) to obtain. However, near the anterior-posterior boundary ($0< x <<1$), we can assume that Hh exists at sufficiently high levels so that $[\mathrm{Hh}]_{\mathrm{SS}}^{\mathrm{n}} >> \kappa^{\mathrm{n}}$ holds in this region (see parameter values in Supporting Table 1). Under this assumption, one of the nonlinear terms in Equation (3.6) can be approximated by a constant,

$$\frac{\alpha_{ptc}[\mathrm{Hh}]_{\mathrm{ss}}^{nm}}{\eta\left[\kappa^n+[\mathrm{Hh}]_{\mathrm{ss}}^n\right]^m+[\mathrm{Hh}]_{\mathrm{ss}}^{nm}}\approx\frac{\alpha_{ptc}}{\eta+1}.$$

The other nonlinear term in Equation (2.6) can be linearized (via a Taylor expansion) around a point where the condition $[\mathrm{Hh}]_{\mathrm{SS}}^{\mathrm{n}} >> \kappa^{\mathrm{n}}$ is satisfied (see details in the Supporting Text). Under these approximations, it can be shown that near to the AP boundary the steady-state gradient can be approximately modeled by the following linear equation:

$$\frac{d^2[\mathrm{Hh}]_{\mathrm{SS}}}{dx^2}-\mathrm{B}[\mathrm{Hh}]_{\mathrm{SS}}-\mathrm{C}=0, \qquad (3.7)$$

with

$$\mathrm{B}=\frac{\beta_{\mathrm{Hh}}}{D}\left[1+\frac{T_{\mathrm{Ptc}}\gamma_{\mathrm{Hh\_Ptc}}}{\beta_{ptc}\left(3\beta_{\mathrm{Hh}}\beta_{\mathrm{Ptc}}+\gamma_{\mathrm{Hh\_Ptc}}\alpha_{\mathrm{Hh}}\right)}\left(\alpha_{ptc0}+\frac{\alpha_{ptc}\alpha_{\mathrm{Signal}}}{\alpha_{\mathrm{Signal}}+k_{ptc}\beta_{\mathrm{Signal}}}\right)\left(3-\frac{\gamma_{\mathrm{Hh\_Ptc}}\alpha_{\mathrm{Hh}}}{3\beta_{\mathrm{Hh}}\beta_{\mathrm{Ptc}}+\gamma_{\mathrm{Hh\_Ptc}}\alpha_{\mathrm{Hh}}}\right)\right]$$

and $\mathrm{C}=\frac{3\beta_{\mathrm{Hh}}T_{\mathrm{Ptc}}\gamma_{\mathrm{Hh\_Ptc}}^2\alpha_{\mathrm{Hh}}^2}{\beta_{ptc}D\left(3\beta_{\mathrm{Hh}}\beta_{\mathrm{Ptc}}+\gamma_{\mathrm{Hh\_Ptc}}\alpha_{\mathrm{Hh}}\right)^2}\left(\alpha_{ptc0}+\frac{\alpha_{ptc}\alpha_{\mathrm{Signal}}}{\alpha_{\mathrm{Signal}}+k_{ptc}\beta_{\mathrm{Signal}}}\right)$ (see Supporting Text for

details). Using appropriate boundary conditions (see Methods section), the solution of Equation (3.7) is given by:

$$[\mathrm{Hh}]_{\mathrm{SS}}(x) = \mathrm{A}\exp\left[-\sqrt{\mathrm{B}}x\right] - \frac{\mathrm{C}}{\mathrm{B}}, \qquad (3.8)$$

with $\mathrm{A} = \dfrac{\dfrac{\alpha_{\mathrm{Hh}}}{\beta_{\mathrm{Hh}}} + \dfrac{\mathrm{C}}{\mathrm{B}}}{1 + \sqrt{\dfrac{\mathrm{B}D}{\beta_{\mathrm{Hh}}}}\coth\left(\sqrt{\dfrac{\beta_{\mathrm{Hh}}}{D}}L_{\mathrm{P}}\right)}$ and L_{P} is the width of the posterior compartment (see Supporting Text). In fact, the numerical solution of Equation (3.6) (using the parameters values in Supporting Table 2.1) is well approximated by the exact solution of the linearization [Equation (3.8)] close to the anterior-posterior boundary (Fig. 3.3B). A steady-state perturbation will maintain the Hh gradient approximately invariant near the anterior-posterior boundary if Equation (3.8) is unaffected by the perturbation, this is, if A, $\sqrt{\mathrm{B}}$, and $\dfrac{\mathrm{C}}{\mathrm{B}}$ remain constant. Thus, under these approximations, the steady-state invariant set of the linearized system is given by:

$$\mathrm{B}' = \frac{\beta'_{\mathrm{Hh}}}{D'}\left[1 + \frac{T'_{\mathrm{Ptc}}\gamma'_{\mathrm{Hh\_Ptc}}\zeta'}{\beta'_{ptc}\left(3\beta'_{\mathrm{Hh}}\beta'_{\mathrm{Ptc}} + \gamma'_{\mathrm{Hh\_Ptc}}\alpha'_{\mathrm{Hh}}\right)}\left(3 - \frac{\gamma'_{\mathrm{Hh\_Ptc}}\alpha'_{\mathrm{Hh}}}{3\beta'_{\mathrm{Hh}}\beta'_{\mathrm{Ptc}} + \gamma'_{\mathrm{Hh\_Ptc}}\alpha'_{\mathrm{Hh}}}\right)\right] = \text{constant1}$$

$$\mathrm{C}' = \frac{3\beta'_{\mathrm{Hh}}T'_{\mathrm{Ptc}}\gamma'^{2}_{\mathrm{Hh\_Ptc}}\alpha'^{2}_{\mathrm{Hh}}\zeta'}{\beta'_{ptc}D'\left(3\beta'_{\mathrm{Hh}}\beta'_{\mathrm{Ptc}} + \gamma'_{\mathrm{Hh\_Ptc}}\alpha'_{\mathrm{Hh}}\right)^{2}} = \text{constant2} \qquad (3.9)$$

$$\mathrm{A}' = \frac{\dfrac{\alpha'_{\mathrm{Hh}}}{\beta'_{\mathrm{Hh}}} + \dfrac{\mathrm{C}'}{\mathrm{B}'}}{1 + \sqrt{\dfrac{D'\,\mathrm{B}'}{\beta'_{\mathrm{Hh}}}}\coth\left(\sqrt{\dfrac{\beta'_{\mathrm{Hh}}}{D'}}L_{\mathrm{P}}\right)} = \text{constant3},$$

where constant1, constant2, and constant3 are given by the wild-type parameter values and $\zeta' = \alpha'_{ptc0} + \dfrac{\alpha'_{ptc}\alpha'_{\mathrm{Signal}}}{\alpha'_{\mathrm{Signal}} + k'_{ptc}\beta'_{\mathrm{Signal}}}$. Although any set of perturbed parameter values that satisfy these equations will maintain the approximated steady-state gradient unchanged,

the steady-state invariant set defined by Equations (3.9) is not very useful in practice because it involves more than fifteen parameters. Therefore, it is convenient to study particular subsets of the set defined by Equations (3.9). As a first case, consider,

$$(\alpha'_{ptc},\alpha'_{ptc},\beta'_{ptc}) = (\delta\tilde{\alpha}_{ptc0},\delta\tilde{\alpha}_{ptc},\delta\tilde{\beta}_{ptc}), \quad \text{for any } \delta > 0 \qquad (3.10)$$

with $\tilde{\alpha}_{ptc0}$, $\tilde{\alpha}_{ptc}$, and $\tilde{\beta}_{ptc}$ denoting the wild-type parameter values and all other parameters kept unperturbed (i.e. at their wild-type values). By substitution into Equations (3.9), it is clear that Equation (3.10) represents a steady-state invariant subset of the linearized system. In fact, Equation (3.10) also leaves invariant the original steady-state equation of the system [Equation (3.6)] and therefore, it is an exact steady-state invariant subset of the system. Geometrically, Equation (3.10) represents a line in the α_{ptc0}–α_{ptc}–β_{ptc} parameter subspace (Fig. 3.3C). Numerical simulations suggest that a few-fold changes in δ affect the duration but have little effect in the amplitude of the overshoot (Fig. 3.3D,E). In particular, we noted that the duration of the overshoot increases rapidly as δ decreases (δ<1), but decreases slowly as δ increases (δ >1). Therefore, perturbations along this steady-state invariant subset provide the opportunity to study the role of signal duration in more detail.

An even simpler case of a steady-state invariant subset of the linearized system can be obtained by noticing that the system of Equations (3.9) does not involve the degradation rate of the Hh-Ptc complex, $\beta_{\text{Hh\_Ptc}}$. Therefore, under these approximations, the steady-state solution does not depend on the value of $\beta_{\text{Hh\_Ptc}}$. For simplicity, consider the approximate steady-state invariant subset given by:

$$\beta'_{\text{Hh\_Ptc}} = \delta\tilde{\beta}_{\text{Hh\_Ptc}}, \qquad \text{for } 0<\delta<1 \qquad (3.11)$$

with all other parameters held constant at their wild-type values (Fig. 3.3F). The constraint $0< \delta <1$ was enforced so that the assumption $[Hh]^n_{SS} >> \kappa^n$ remains valid. In contrast to the subset defined by Equation (3.10), perturbations along the subset described by Equation (3.11) will affect the amplitude of the overshoot, but its duration will be maintained relatively constant (Fig. 3.3G,H). The simplicity of this subset permits the design of a genetic steady-state invariant perturbation. The *ptc*^{14} allele has been characterized as a mutant that is defective in endocytosis-dependent internalization and degradation of the Hh-Ptc complex, suggesting that the stability of the Hh-Ptc complex is increased in Ptc^{14} mutants (Torroja et al., 2004). Importantly, other properties of the Ptc protein appear unaffected in *ptc*^{14} mutant clones. For example, Ptc^{14} proteins bind Hh and repress Hh signal transduction in a similar manner than wild-type Ptc (Torroja et al., 2004). Furthermore, Ptc^{14} is not over expressed in anterior clones away from the AP boundary, suggesting that unbound Ptc^{14} degradation is normal. This genetic evidence suggests that β_{Hh_Ptc} decreases in *ptc*^{14} mutants, while other parameters approximately maintain their wild-type values. Therefore, we predict that *ptc*^{14} mutants satisfy Equation (3.11) and can be considered as a steady-state invariant perturbation of the system near the AP boundary. Based on our modeling results, perturbations along this steady-state invariant subset affect the amplitude of the overshoot, but not the overall shape and duration of the transient response suggesting that more anterior cells would be transiently exposed to the signal (Fig. 3.3G,H). Experiments using *ptc*^{14} mutant clones abutting the anterior-posterior show that the expression domains of Hh target genes expand in the region of these clones (Torroja et al., 2004), consistent with the predictions of our model and our simulations (Nahmad and Stathopoulos, 2009; Fig. 3.3G).

Other subsets can be similarly obtained from Equations (3.9) and their effects on transient dynamics can be systematically analyzed. However, sets involving more parameters are difficult to visualize and perturbations along these subsets may not be easily achieved by experimental manipulations (see below).

3.4 Analysis of Steady-State Invariant Sets

The problem of computing the steady-state invariant set from a given model is in general non-trivial. Although the example of the single morphogen gradient established by diffusion and degradation [Equation (3.1)] is not intended to represent any biological morphogen of interest, it was chosen because the steady-state invariant set can be computed exactly. However, in most cases a solution to the steady-state problem (equation (B2) in Box 3.1) cannot be obtained analytically. Nonetheless, there are different manners to overcome this problem and get a partial or approximate set of steady-state invariant perturbations. One easy way to obtain at least a steady-state invariant subset of a system is to simply inspect the steady-state equation and ask which parameter perturbations leave the equation invariant. For example, perturbations that satisfy Equation (3.10) leave the steady-state problem [Equation (3.6)] unchanged. In this case, there is no need to know the solution of the steady-state equation, but in general, this approach will only provide a subset of steady-state invariant perturbations. We will say that a steady-state invariant set is *direct* if it can be deduced from the steady-state equation. Note that Equation (3.4) is a direct subset of Equation (3.1), and from the steady-state solution (3.2), we verified that it contains all the steady-state invariant perturbations of the system. But this is not true in general. An interesting theoretical

challenge for the future will be to find conditions to determine in which cases the full steady-state invariant set is direct, i.e., when we can obtain all steady-state invariant perturbations of the system without the need of solving the equations.

Alternatively, as we did for Equation (3.6), an approximate steady-state invariant set can be obtained by linearization. One advantage of this approach is that subsets may be more simple and useful for experiment design (e.g., Equation (3.11)). However, unlike exact steady-state invariant sets that are valid throughout the developing field, these approximations are rather local (Fig. 3.3B).

Finally, another approach is to compute the exact steady-state invariant set by spatially discretizing the system, i.e., turning the problem (Equation (B1) in Box 3.1) into a system of ordinary differential equations. In fact, this is the way in which we defined steady-state invariant sets in general in Box 3.1. Using this approach, the property of steady-state invariance needs not to be global, i.e., it can be considered in a desired subset of the whole developmental field and this might often be convenient in practice. For example, some genetic perturbations are lethal to the organism, but can be studied in a specific developmental context (e.g., using mosaic genetic analysis). Another advantage is that embryos and tissues are composed by discrete entities (cells), so that modelling the system in this way might be well justified in this kind of problem.

In practice, it would be convenient to know, based on the geometry of the steady-state invariant set, how difficult is to design a genetic experiment that causes a steady-state invariant perturbation in the system. In other words, how likely is it for a random parameter perturbation to be steady-state invariant? A geometric notion that provides

insight into this question is the concept of codimension*. Intuitively, the codimension of a geometric set tells us how large the dimension of space where the set is embedded is compared to the dimension of the set. For example, the codimension of a sphere is one in a three-dimensional space, but n-2 if considered in a space of dimension n. For the practical purposes of this study, we define the codimension of a set as follows. Let M be a steady-state invariant set that affects *s* parameters and can be parameterized by *r* variables, then the codimension of M is defined as *codim*(M)=*s*-*r*. For instance, the steady-state invariant subsets defined by Equations (3.10) and (3.11) depend on three (α_{ptc0}, α_{ptc}, and β_{ptc}) and one ($\beta_{\mathrm{Hh\_Ptc}}$) parameters, respectively, and both are parameterized by the single variable δ. Therefore, their codimensions are two and zero, respectively. Intuitively, the codimension of a set is inversely related to the concept of *degrees of freedom*, i.e., the number of parameters that can be arbitrarily varied without abandoning the set. In general, steady-state invariant sets of small codimensions (or large degrees of freedom) would be expected to be more suitable in practice because they provide further flexibility in generating steady-state invariant perturbations. The extreme scenario is when the codimension is zero and any perturbation of the parameters involved is in fact steady-state invariant. This scenario is potentially very useful for experimental design because such perturbations do not require precise tuning of parameter values. For example, the fact that the codimension of the subset defined by Equation (3.11) is zero allowed us to propose a concrete experiment (using the ptc^{14} allele) to locally introduce steady-state invariant perturbations in this system.

* Steady-state invariant sets are defined by algebraic equations and therefore the concepts of dimension and codimension can be rigorously defined (see Supporting Text).

3.5 Concluding Remarks

There is recently much interest in the problem of how the dynamics of morphogen gradients contribute to developmental patterning (reviewed by Kutejova et al., 2009). In this paper, I presented a general theoretical approach that may help to identify mutations that affect the transient establishment of morphogen gradients without changing their equilibrium distribution. Although the experimental implementation of these tools to study the role of morphogen gradient dynamics in developmental pattern formation is left to future studies, I provided details of how they can be implemented in practical systems. In particular, the analysis of steady-state invariant subsets in a model of Hh signalling in the *Drosophila* wing provides the opportunity to decouple two properties of the Hh gradient overshoot, namely, duration and amplitude. The duration of the overshoot can be modulated in a steady-state invariant manner by varying the rates of *ptc* production and degradation (Fig. 3.3C-E). Furthermore, the amplitude of the overshoot can be affected by reducing the rate of Ptc-dependent Hh internalization and degradation. In fact, previous experiments in which a mutant form of Ptc (Ptc^{14}), that is defective in Ptc-mediated Hh endocytosis, but otherwise appears to function normally, provides an example of an experimental steady-state invariant perturbation in this system.

Another interesting application of these tools is to consider steady-state invariant sets as parameter perturbations to which the system exhibits robustness. For instance, in engineering it is often desirable to design systems in which the steady state is robust to a certain class of perturbations. Therefore, the converse problem, namely, to construct a dynamical system that will maintain a desired set of perturbations invariant poses an interesting challenge for the future. The context in which the converse problem has been

studied in some detail is robust control theory and there are several examples in which imposing invariance into the steady-state values of some variables constrains the dynamic properties of the system. One of the most studied examples is 'perfect adaptation' in bacterial chemotaxis (Barkai and Leibler, 1997; Alon et al., 1999). For instance, a well-known result in control theory is that the steady-state error in some desired signal remains negligible despite external perturbations or variations in internal components if and only if the error dynamics are governed by integral feedback and this has been shown to apply to perfect adaptation in chemotaxis (Yi et al., 2000). Furthermore, a recent report provides structural conditions on biochemical reaction network dynamics to guarantee invariance of particular steady-state concentrations (Shinar and Feinberg, 2010). Finally, it is likely that evolution has faced and solved this converse problem in selecting for optimal mechanisms for developmental patterning; in some systems, it is possible that natural selection has minimized the effects of certain classes of genetic perturbations to maintain invariant some essential gene expression patterns. Alternatively, natural selection may have taken advantage of the diversity of morphogen dynamics to evolve the mechanisms of developmental pattern formation.

3.6 Outlook

It is broadly recognized that physics and engineering have not only clearly benefited from mathematics, but also have substantially motivated the development of new mathematical theories and concepts. Although the use of mathematical modelling has become a common practice in biological research in general, and in developmental biology in particular (Tomlin and Axelrod, 2007; Ibañes and Izpisúa-Belmonte, 2008; Oates et al.,

2009), some theoreticians hope that problems in biology will contribute to the development of new mathematics in the 21st century (Cohen, 2004; Sturmfels, 2005). The theory of steady-state invariant sets introduced here was motivated by the problem of whether or not morphogen dynamics contribute to developmental patterning. Nonetheless, the applications of the tools presented here are not limited to the design of experimental perturbations and/or to test the role of transient signals in developmental patterning, but may be broadly applicable to a large class of problems and will hopefully depict interesting research avenues in dynamical systems theory.

Chapter 4

Spatial Scaling of Dorsal-Ventral Patterns in the Early *Drosophila* Embryo

Animal populations naturally display variations in the size of their individuals, but these changes in total size are often compensated by proportional changes in organ or tissue sizes. This phenomenon, commonly referred to as scaling, is widespread in animals, but the mechanisms by which cells acquire *relative* positional coordinates -- so that patterns correlate with the size of the field -- are poorly understood. Patterning of the dorsal-ventral (DV) axis in the early *Drosophila* embryo depends on the nuclear distribution of the maternal factor Dorsal (dl). Using quantitative fluorescent *in situ* hybridization data, we investigate how the location of dl target genes depends on natural variations in the size of the DV axis. We show that the borders of the dl target genes *vnd* and *sog* scale with the size of the system, while the *ind* borders correlate, but do not strictly scale with the length of the DV axis. Our results suggest that scaling in this system is a gene-dependent rather than a position-dependent property. The width of the nuclear dl gradient also correlates with axis length, but is not sufficient to explain strict scaling of DV patterns directly in a concentration-dependent manner. Using a system in which a gradient of nuclear dl is ectopically generated along the anterior-posterior (AP) axis, we asked whether scaling solely depends on the patterning cascade downstream of dl or if other endogenous factors contribute to spatial scaling along the DV axis. We found that dl nuclear gradient exhibits much variability and does not scale with respect to the AP axis in these embryos. Strikingly, however, the posterior border of the *vnd* pattern scales precisely with the length of the AP axis. Since the ectopic dl gradient is the only source

of DV positional information in these embryos, we conclude that factors downstream of dl provide spatial information relative to the length of the axis.

4.1 Introduction

Scaling, the ability of pattern to correlate with size in an embryonic field, is exhibited at different levels of organization in animal development. At the level of a single organism, animals often display the ability to reorganize their patterning programs after surgical manipulations; for example, amphibian embryos that are cut in half or fused to other embryos maintain the proportions of their patterns and give rise to anatomically normal animals of different sizes (Spemann, 1938). Another aspect of scaling at the single animal level is the ability of patterns to accommodate changes in size as a result of tissue growth. Many developing systems that are genetically or environmentally manipulated to over- or under-grow are able to maintain the proportions of their patterns invariant. For instance, fly larvae that are poorly fed produce flies with smaller wings, but the wing venation pattern remains largely unaffected (Robertson, 1963).

A different aspect of scaling phenomena is exhibited at the species level; groups of closely related species that differ substantially in egg size give rise to anatomically similar animals despite the fact that they use much of the same genetic circuitry (Carroll et al., 2005). A particular case of this form of scaling is the ability of a population of embryos from a single species to maintain pattern proportions despite natural variations in the size of their individuals. However, there is a fundamental difference between scaling across species and scaling within a species; while scaling across species can be afforded by the adaptation of patterning molecules to evolutionary changes in size,

scaling within a homogeneous population of organisms must rely on a mechanism of establishing positional information using a system of relative, rather than absolute coordinates. Although this form of scaling is widespread in the animal kingdom, the detailed mechanisms by which cells acquire positional information relative to size remain largely unknown.

The *Drosophila* embryo has become a useful system to study spatial scaling of patterns in response to natural variations in embryo size as it provides the following advantages. First, the size of an embryo remains practically unchanged once it is laid and, therefore, a single measurement of axis length is enough to describe the "size" of the system over the whole patterning process. Second, gene expression patterns can be measured quantitatively with resolution that is not yet possible in other systems. Recent studies have compared scaling of Bicoid (Bcd)-dependent patterns along the AP axis in *Drosophila* embryos with scaling of the Bcd gradient itself. For example, a study on closely related *Drosophila* species shows that segmentation patterns in the embryo scale along the AP axis despite that the diffusion properties of Bcd were predicted to be the same in different species (Gregor et al., 2005; Gregor et al., 2008). Further studies have demonstrated that gap gene patterns scale despite natural variations of egg length, even within the same species (Gregor et al., 2007; He et al., 2008; Holloway et al., 2006; Lott et al., 2007; de Lachapelle and Bergmann, 2010), suggesting that the property of scaling in this system is likely to depend on a mechanism of "sensing" the size of the embryo, rather than on the evolution of the biochemical properties of the Bcd morphogen. These studies have established the *Drosophila* embryo as a model system to study scaling of pattern in response to natural variations in size.

Although scaling along the AP axis of the *Drosophila* embryo has been recently the focus of much attention, little is known about scaling along the dorsal-ventral (DV) axis. DV patterning in the fly embryo is orchestrated by the maternal factor Dorsal (dl), a NF-κB homolog (reviewed by Moussian and Roth, 2005). Maternal dl is ubiquitously present in the embryo cytoplasm where it is sequestered by the IκB homolog, Cactus. However, upon activation of the Toll transmembrane receptor in the ventral side of the embryo by the Spätzle morphogen, Cactus is targeted to degradation thereby allowing dl to enter ventral nuclei in the periphery of the embryo (Roth et al., 1989; Steward, 1989; Rushlow et al., 1989). In the nucleus, dl acts as a transcription factor and is required to activate mesoderm (*snail*, *twist*), mesectoderm (*sim*), and neuroectoderm (*rhomboid*, *brinker*, *vnd*, *ind*) differentiation genes in different domains of expression (reviewed by Stathopoulos and Levine, 2005). The nuclear dl distribution displays a concentration gradient that peaks at the ventral midline and decays dorsally, suggesting that dl acts directly as a morphogen gradient (reviewed by Reeves and Stathopoulos, 2009). Moreover, dl has been shown to be *sufficient* to establish different patterns of gene expression in the embryos that have no other source of DV positional information (Huang et al., 1996; Stathopoulos and Levine, 2002). In this study, we use the *Drosophila* embryo as a model to study spatial scaling of DV patterns with respect to natural variations in embryo size. We provide evidence that scaling in this system depends on each particular gene rather than on its location. In addition, we show that the length-scale of the nuclear dl gradient scales with embryo size, but it is not sufficient to explain scaling of dl target genes. We propose that factors downstream of dl contribute to scaling of DV patterns with respect to size in this system.

4.2 Materials and Methods

Fly Stocks

Two "wild-type" populations of embryos were considered. One population comprised embryos of *yw* genotype and the other comprised embryos from the India strain. India embryos are a wild-type strain of *Drosophila melanogaster* that are about 25% larger than the laboratory wild-type strain (*w1118*) along the AP axis (Lott et al., 2007). For the experiments in which the dl gradient is ectopically generated along the AP axis, we collected embryos from females of genotype *wind*[M88]/*wind*[E4]; hsp83>Toll10b bcd 3' UTR. These embryos lacked normal DV patterning due to maternal loss-of-function of the *windbeutel* (*wind*) gene (*wind*[M88] and *wind*[E4] are null alleles; Nilson and Schupbach, 1998). Females carrying the *hsp83*>Toll10b *bcd* 3' UTR (HTB) transgene lay embryos that express an activated form of Toll (Toll10b) maternally-driven by the *hsp83* promoter in the anterior pole of the egg using the *bcd* localization sequence (Huang et al., 1996).

Fixation and Fluorescent *in situ* Hybridization

Two-four hour old embryos were fixed using formaldehyde solution using standard techniques. Fluorescent *in situ* hybridization was performed according to standard protocols using digoxigenin-, biotin- and fluorescin-labelled riboprobes for *sog*, *ind*, and *vnd*. Primary antibodies used were sheep anti-digoxigenin (1:500, Roche), mouse anti-biotin (1:500, Roche) rabbit anti-fluorescin (1:500, Invitrogen), mouse anti-dorsal (1:10, Hybridoma Bank Developmental Studies at the University of Iowa), and rabbit anti-

Histone H3 (1:1000, Abcam). Secondary antibodies used were Alexa Fluor 488 anti-mouse, Alexa Fluor 555 anti-sheep, and Alexa Fluor 647 anti-rabbit (1:1000, Invitrogen).

Embryo Sectioning and Mounting

Fluorescently stained embryos were individually sectioned in 70% glycerol using a sharp razor blade under a dissecting microscope (except for the embryos from *wind*; HTB mothers which were kept as whole-mounts). Sections were taken approximately at 50% egg length and about 150 mm thick (as estimated from comparing with the diameter of the embryo). "Wild-type" sections (and whole embryos from *wind*; HTB mothers) were mounted in 70% glycerol on a glass slide with a cover glass supported by two pieces of double-sided tape in each side to minimize deformation of the sample.

Image Processing, Measurements, and Data Analysis

Statistical analysis was performed using standard tools and functions from MATLAB. Images of fluorescent embryos or sections were taken using a LSM 5 Pascal confocal microscope. Imaging of each sample was performed under identical conditions. To reduce temporal-dependent fluctuations in gene expression, only embryos from late nuclear cycle 14 (marked by expression of *ind*) were considered in the analysis. For "wild-type" cross sections, we acquired an average of 15 z-stacks from the center of the specimen (where deformation of the embryo due to sectioning does not affect the embryo's morphology) using a 40X-oil objective. Z-stacks were then orthogonally projected and gene expression profiles were obtained using MATLAB. Quantification of nuclear dorsal levels in cross sections relative to Histone H3 levels was performed as in a

previous study (Liberman et al., 2009). Measurements of embryo circumference were estimated by calculating the pseudoarclength of 50-100 points found to be on the perimeter of the embryo. In order to obtain the location of the boundaries of the patterns, each gene expression profile was fitted to a stereotypical profile of the specific pattern as described previously (Liberman et al., 2009) and the borders of gene expression were computed as the points of half-maximal decay of the fitted profiles. The location of the ventral midline was found as the average of the midpoints between dorsal and ventral borders of each gene or as the center of the peak of the dorsal gradient.

For whole-mount embryos, we acquired z-stacks from the top of the embryo to about 50% depth using a 20X objective. Each embryo "shell" was then "computationally-unrolled" as described in a previous study (Liberman et al., 2009) to take into account the embryo curvature. The length of the AP axis in each embryo was obtained by computing the average size of the "unrolled" sheet and the positions of the gene expression boundaries were obtained as described above for cross sections. The distance from the anterior pole of the embryo to the locations of target genes was obtained from the "unrolled" sheet and therefore corresponded to distances measured on the surface of the embryo. Quantification of the dl nuclear gradient in whole-mount embryos was obtained by adapting the algorithm of nuclear dl quantification in wild-type embryos published before (Liberman et al., 2009). In embryos from *wind*; HTB females, the nuclear dl gradient is fitted to a Hill function of the form,

$$f(x) = \frac{Ax^m}{k^m + x^m}$$

and the "width" of the gradient is defined as the half-maximal value of the Hill function, "k."

Scaling Criterion

We devised a criterion to determine quantitatively whether or not the location of a certain pattern *scale* with respect to natural variations in the length of the DV axis. For each embryo (labeled by the index i), let X_i be the measured location of a certain pattern with respect to a reference point (in this case, the absolute distance from the border of a certain gene measured to the ventral midline), and let L_i be the length of the embryo's DV axis (estimated by the semi-circumference at approximately mid-embryo along the AP axis). If the population of embryos is sufficiently large, it is possible to study how X_i and L_i are statistically correlated using simple regression analysis. "Perfect scaling" corresponds to the case in which the following linear model holds,

$$X_i = x\, L_i \qquad \text{for all } i, \qquad (4.1)$$

where x is a constant that represents the *relative position* of the pattern. Conversely, if X_i remains unchanged with L_i (i.e., if X_i=x for all i), then X_i and L_i are *not* statistically correlated, and therefore, the location of the pattern is *independent* of embryo size. However, these scenarios are just extreme hypothetical situations and, in practice, there is a continuous range of scaling behaviors in between. A more general and realistic situation is that the pair (X_i, L_i) is linearly correlated while not necessarily obeying the strict scaling condition (4.1), i.e.,

$$X_i = m\, L_i + b \qquad \text{for all } i \qquad (4.2)$$

with m and b some parameters determined by fitting the data to the linear model (4.2). Note that when $|b|$ is "sufficiently" small, the model (4.2) approximates the perfect scaling case (4.1). Note that the model (4.2) also includes the case in which positional

values are independent of size when m=0, which in practice correspond to the case when $b \approx \overline{X}$, where $\overline{X}$ is the mean of the X_i's. However, it is not always possible to make an accurate decision about scalability; for example, if the variability of the positional data (X_i) is "larger" (either due to measurement errors or internal noise) than the range of embryo sizes along the DV axis (L_i) (see below).

We define three steps that provide a simple quantitative criterion to determine scaling in this system:

1. *Scalability Test:* A decision about scalability of the dataset (X_i, L_i) can be made if the range of L_i's is larger than the variation in positional values, X_i's. This is, we say that the dataset (X_i, L_i) *passes* the scalability test if

$$S \equiv \frac{2\,\Delta x\,\overline{L}}{\mathrm{r}(L)} < 1,$$

with Δx the standard deviation of the scaled positions $x_i = \frac{X_i}{L_i}$, $\overline{L}$ is the mean of the L_i's, and r(L) is the "range" of the L_i's as defined by $L_{\max}$ - $L_{\min,}$ where $L_{\max}$, $L_{\min}$ denote the extremes of the distribution of lengths (centered at $\overline{L}$) encompassing 80% of the L_i's. The quantity S will be referred as the *scalability factor*.

2. *Simple linear regression*. A dataset that passes the scalability test is then fitted to a linear model,

$$X = \hat{m}L + \hat{b}, \qquad (4.3)$$

where $\hat{m}$ and $\hat{b}$ are the least-squares estimates of the regression. By construction, the least-squares approximation (4.3) is satisfied by $X = \overline{X}$ and $L = \overline{L}$. Thus, if we write $\hat{b} = \alpha\overline{L}$, then Equation (4.3) evaluated at the mean values takes the following form,

$$\overline{X} = (\hat{m} + \alpha)\overline{L}.$$

Therefore, α is a measure of "how much" the estimated slope would need to be corrected (in units of axis length) in order to have perfect scaling at the point of center of mass ($\overline{X}, \overline{L}$). For practical purposes, we say that a dataset (X_i, L_i) exhibits *strict scaling* if $|\alpha| \leq 0.05$, meaning that linear model of the data differs from the perfect scaling case by at most 5% of the total axis length.

3. *Scaling significance*. Because of the statistical nature of the data, under certain circumstances scaling may be explained by chance, due to random variations in the positional data. This depends on the relative position of the pattern (approximated by $x = \frac{\overline{X}}{\overline{L}}$); confidence about strict scaling increases with the distance from the pattern to the reference point and can be captured in the following quantity,

$$C \equiv \left(1 - S\frac{\overline{L}}{\overline{X}}\right)100\% \qquad \text{if } S\frac{\overline{L}}{\overline{X}} \leq 1 \text{ and } C \equiv 0\% \text{ otherwise.}$$

As the scalability factor S is a measure of the maximum slope that can be generated solely by variability in the positional data, the *scaling percentage, C,* is the percentage of data that *cannot* be explained by the variability in the positional data (see Supporting Fig. 4.1).

4.3 Results

Determining Scaling from Quantitative Measurements of Gene Expression

Using fixed cross sections of wild-type embryos, we quantified the expression levels of three dl target genes that pattern the neuroectoderm of the embryo and measured the positions of their dorsal and ventral borders with respect to the ventral midline along the circumference (Fig. 4.1A,B). We also measured the length of the DV axis as the semi-

circumference of the cross section for each embryo (Fig. 4.1A). In order to study the correlation between pattern locations and size, we devised a criterion to determine scaling of pattern locations with respect to the length of the DV axis in a homogeneous population of embryos (see Materials and Methods for details). Briefly, the criterion determines scalability from three statistical measures. First, the *scalability factor, S*, determines if the range of lengths along the DV axis is larger than the variability of the positional data (scalability test). If the scalability test fails (i.e., if $S>1$) then we cannot conclude anything about the scalability of the pattern location from the data. Second, the *scaling compensation value,* α, measures how positional data compensate to changes in the length of the DV axis based on a linear model of the data. Perfect scaling corresponds to the case in which $\alpha=0$. If $\alpha>0$, then changes in the length of the axis are *undercompensated* by changes in the position of the pattern. Conversely, $\alpha<0$ corresponds to the case in which changes in the length of the axis are *overcompensated* by changes in the position of the pattern. Third, the *scaling percentage, C,* provides a measure of the percentage of data that exhibits scaling beyond what can be explained by chance (i.e., by random fluctuations in our measurements of positional data). This criterion provides a precise definition of scaling from our quantitative gene expression data.

sog and *vnd* Strictly Scale with the Length of the DV Axis, while *ind* Expression Exhibits Overcompensation

Based on our measurements of the position of gene expression patterns with respect to the ventral midline (Fig. 4.1B), we find that the locations of the dorsal borders of *vnd* and *sog* scale almost strictly with the perimeter of the semi-circumference (i.e., the relative

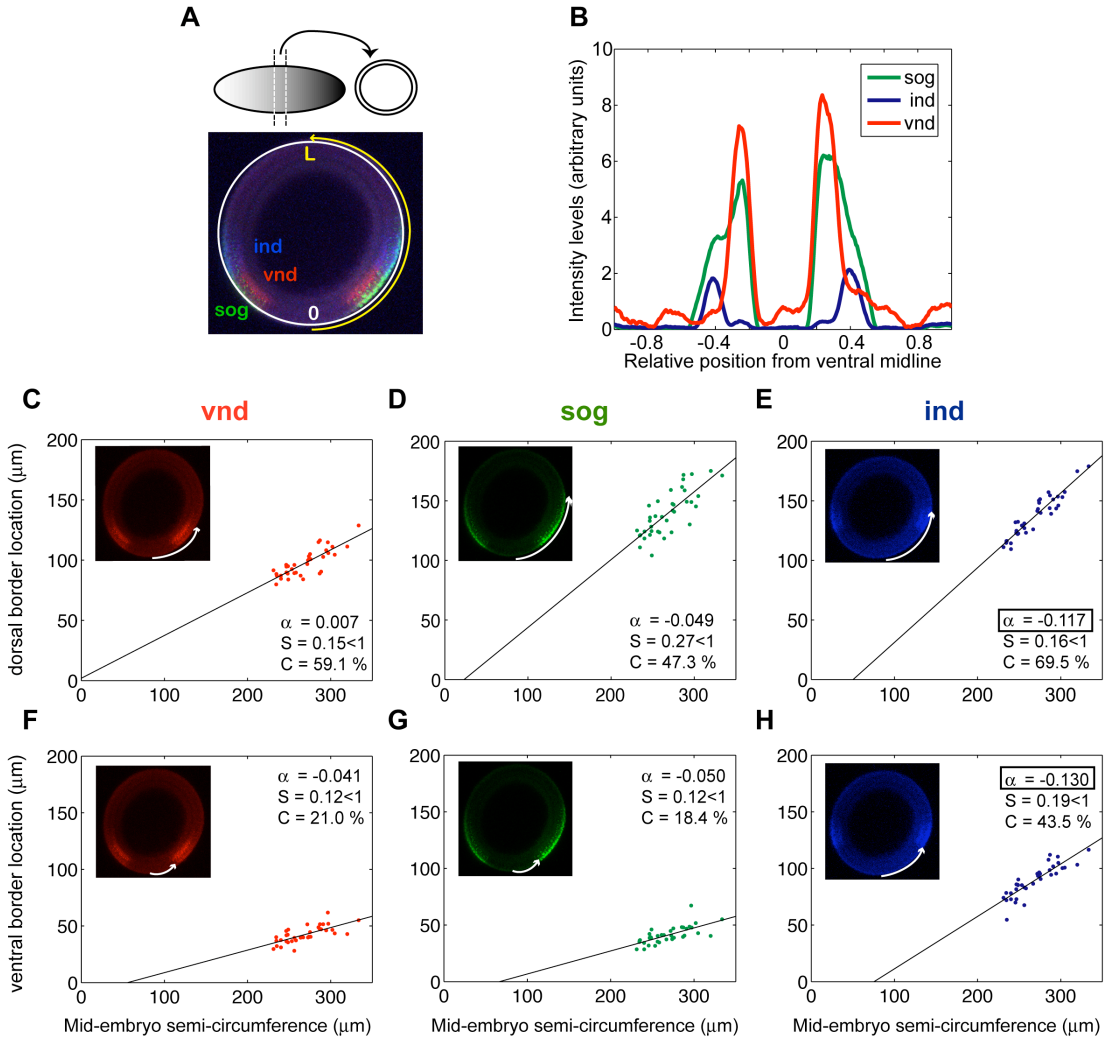

Figure 4.1 Scaling of DV patterns in wild-type embryos.

(A) Fluorescent *in situ* hybridization in a wild-type (*yw*) embryo using *sog* (green), *vnd* (red) and *ind* (blue) probes. Fixed embryos of *yw* phenotype were sectioned approximately at 50% egg length and mounted upright for imaging. The length of the DV axis was measured as half the perimeter of the polygon that encompasses the cross section. Using the ventral midline as a reference point (x = 0), we measured the location of gene expression boundaries around the circumference. **(B)** Gene expression profile around the embryo cross section extracted from the image in (A) in units of DV axis length, L. **(C-H)** Dorsal (C-E) and ventral (F-H) border locations of *vnd* (C,F), *sog* (D,G), and *ind* (E,H), plotted against the length of the DV axis. Each data point displayed corresponds to the average of the distance to each of the two lateral expression domains. Black lines correspond to the least-squares fit of the data. The results of the scaling

criterion applied to each dataset are shown in each panel. By convention, *strict scaling* occurs if $S<1$ and $0.050 \leq \alpha \leq 0.050$.

---

positions are within 5% ($|\alpha| < 0.05$) of the expected (strict scaling) locations with ~50% or more of scaling percentage; Fig. 4.1C,D). Similarly, the locations of the ventral borders of *vnd* and *sog* appear to strictly scale with size, although the scaling percentages of these data are somehow lower (~20%; Fig. 4.1F,G). Collectively, these data provide evidence that the ratios of the "width" of the *vnd* and *sog* patterns to the length of the DV axis remain constant. The positions of the *ind* borders also correlate with changes in the size of the embryo, but this correlation exhibits overcompensation, i.e., variations in the length of the axis result in larger "shifts" of the borders' locations compared to those expected by strict scaling (Fig. 4.1E,H). Therefore, the extent to which scaling is attained depends on the genetic identity of each pattern rather than on its position within the axis (see Discussion).

The dl Gradient also Scales with Respect to the Length of the Embryo Circumference, but it is Insufficient to Explain Scaling of its Target Genes

Since dl controls patterning of the DV axis, we examined whether scaling of *sog* and *vnd* was a direct consequence of scaling of the dl gradient. The dl gradient has a bell-shaped profile that can be empirically fitted to a Gaussian distribution of the form

$$dl(x) = A\exp\left[-\frac{x^2}{2\sigma^2}\right] + B, \qquad (4.4)$$

with A denoting the amplitude of the gradient and σ denoting its "width" or decay length (Liberman et al., 2009; Fig. 4.2A,B). As a consequence of the dl-gradient shape, any two gradients of widths σ and $(1+\gamma)\sigma$ (with γ a small perturbation) are shifted from one

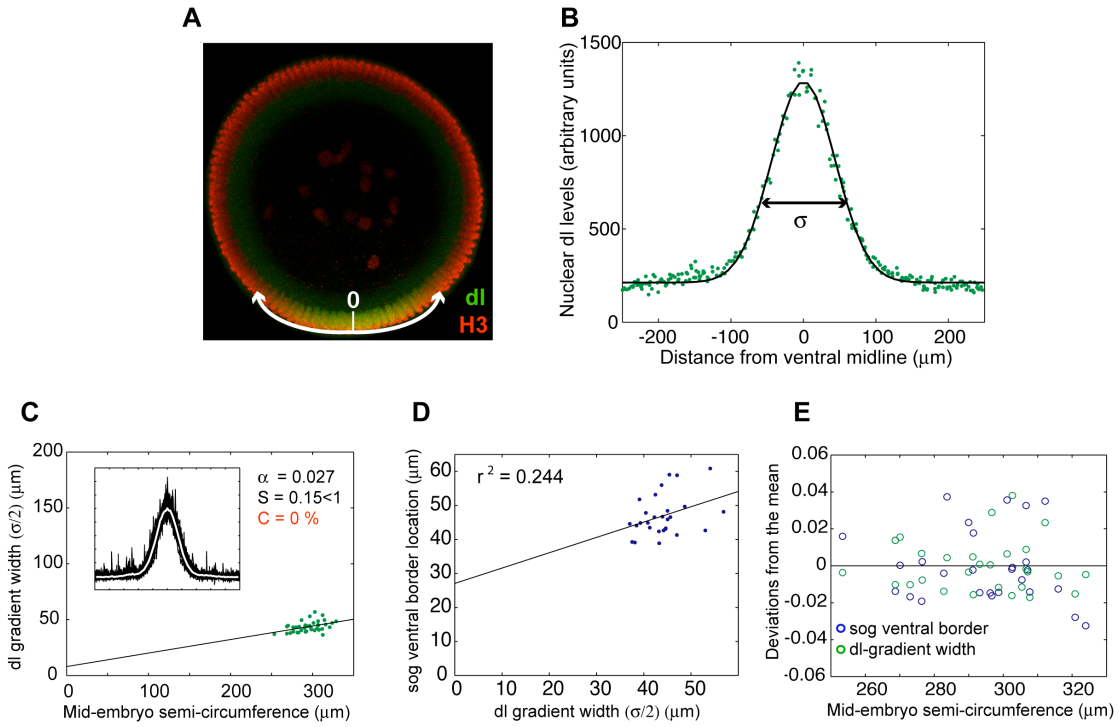

Figure 4.2 Scaling of the nuclear dl gradient in wild-type embryos.

(A) Immunostaining of a wild-type (*yw*) cross section taken at mid-embryo using dl (green) and Histone H3 (red) antibodies to quantify nuclear dl intensity levels. **(B)** Quantification of nuclear dl levels around the cross section circumference using the ventral midline as a reference point (x = 0). Each (green) data point corresponds to the average dl intensity in each nucleus detected by the segmentation algorithm displayed according to its distance from the reference point (x = 0). Black curve indicates the best fit of a Gaussian function of the form of Equation (4.4) characterized by the decay-length, σ. **(C)** "Widths" of the nuclear dl gradient defined as half of the decay-length (σ/2) of the fitted Gaussian curve plotted against the length of the DV axis. Inset shows the intensity profiles of all the embryos considered (n=38). **(D)** Position of the ventral border of *sog* compared to the width of the nuclear dl gradient in the same embryos. The black line represents the least-squares fit to the data points (and *r* denotes the correlation coefficient). **(E)** Precision in the width of the dl gradient vs. precision in determining the ventral boundary of *sog*. Each data point in the graph corresponds to the difference between scaled position (X_i / L_i) of the ventral border of *sog* in an embryo and the mean relative location (or the difference between scaled widths (σ_i / L_i) in an embryo and the mean scaled width) as a function of the mid-embryo semi-circumferences (L_i).

another by exactly the same proportion (1+γ) at any concentration threshold. For example, two gradients whose widths differ by 10% will differ by exactly 10% at the concentrations required to define different patterns of gene expression. Therefore, it is reasonable to use the width of the gradient, σ, as an indicator of how the dl gradient is affected by variations in the length of the DV circumference. We quantified the nuclear levels of dl in fixed cross sections of wild-type embryos and found that the width of the gradient scales with the size of the axis (Fig. 4.2C). However, we found that these data have a scaling percentage of C=0%, i.e., it is not possible to rule out that scaling of these data can be fully explained by the internal variability or experimental error in the measurements of the dl widths. A way to increase the scaling percentage C is to consider a broader range of DV axis lengths. We attempted to increase r(L), by considering the wild-type strain India, whose embryos are ~25 % larger along the AP axis compared to the laboratory strain (Lott et al., 2007). However, we did not find any significant difference in length along the DV axis (see Supporting Fig. 4.2). Nonetheless, we asked if the presumptive scaling of the dl-gradient width could explain scaling of the target gene expression patterns. We stained wild-type embryos simultaneously with dl/Histone H3 antibodies and *sog* RNA probe and asked whether or not the width of the dl gradient correlates with the ventral position of *sog*. Our data show that the location of the ventral border of *sog* is slightly correlated with the width of the dl gradient (r^2=0.244; Fig. 4.2D). However, this correlation is not sufficient to explain scaling of this pattern with respect to the length of the DV axis because changes in dl gradient widths are under-compensated by changes in the location of the *sog* expression pattern (Fig. 4.2D).

These data also provide the opportunity to compare the precision of the dl gradient with the precision in determining the ventral location of the *sog* pattern. We found that the precision in defining the location of the ventral border of *sog* is similar to the precision of the width of the gradient (Fig. 4.2E). This observation demonstrates that the dl gradient could be able to determine the relative location of the ventral border of *sog* with the observed precision. Therefore, the positional information encoded by dl is insufficient to determine the relative position of the *sog* pattern in a concentration-dependent manner.

Taken together, our results reveal that the width of the dl gradient scales with respect to the DV circumference, but scaling of the ventral border of *sog* cannot be explained by a proportional shift of the dl gradient, and suggest that other factors participate in establishing the relative location of this pattern. For example, it is possible that dl contributes to setting the location of the borders of gene expression factors, but additional factors are required to "sharpen" this location as a function of the length of the DV axis.

Scaling of DV Patterns Depends on Factors Downstream of the Toll Pathway

Our data suggest that additional factors are required to determine the relative location of gene expression patterns. Previous models suggest that scaling might be explained by a combination of gradients emanating from opposite ends of a single axis (Aegerter-Wilmsen et al., 2005; Hörstadius, 1939; McHale et al., 2006; Wolpert, 1969). In order to test whether a gradient established from the dorsal side of the embryo contributes to scaling of dl target genes, we use a genetic background in which DV patterning is

ectopically established along the AP axis. Embryos from females that are mutants for at least one of the factors that disrupt DV patterning [such as *windbeutel* (*wind*)] and in addition, carry the HTB transgene (a maternal promoter Hsp83 used to express an activated form of the Toll receptor (Toll10b) using the *bcd* localization sequence), exhibit a full range of DV patterns along the AP axis (Huang et al., 1996). While ectopic DV patterns along the AP axis in embryos of this genetic background cannot be directly compared to endogenous patterning along the DV axis of wild-type embryos, this system allowed us to investigate whether or not endogenous factors are required for scaling of dl-target genes. Since activated Toll is the only source of ectopic DV positional information in these embryos, we would expect that the dl-target genes will lose their ability to scale with respect to the length of the axis if scaling were dependent on additional endogenous factors (e.g., an opposing gradient emanating from dorsal regions of the embryo). We quantified the gradient of nuclear dl in whole-mount embryos from *wind*; HTB mothers and observed several differences with respect of the endogenous dl gradient (Fig. 4.3A-C). First, the overall shape of the gradient is "bimodal" instead of Gaussian (Fig. 4.3B). Second, we observed a very high embryo-to-embryo variability in the range of the dl nuclear gradient. Figure 4.3B shows representative nuclear dl gradients from three different embryos in which such variability is clearly exhibited. Third, unlike in the wild-type case, the width of the ectopic dl gradient does not correlate with the length of the AP axis (Fig. 4.3C).

Next, we measured the distance from the anterior pole of the embryo to the "posterior" borders of *vnd*, *sog*, and *ind* (Fig. 4.3D), i.e., those that would correspond to the dorsal borders in wild-type embryos. Strikingly, the location of the *vnd* border strictly

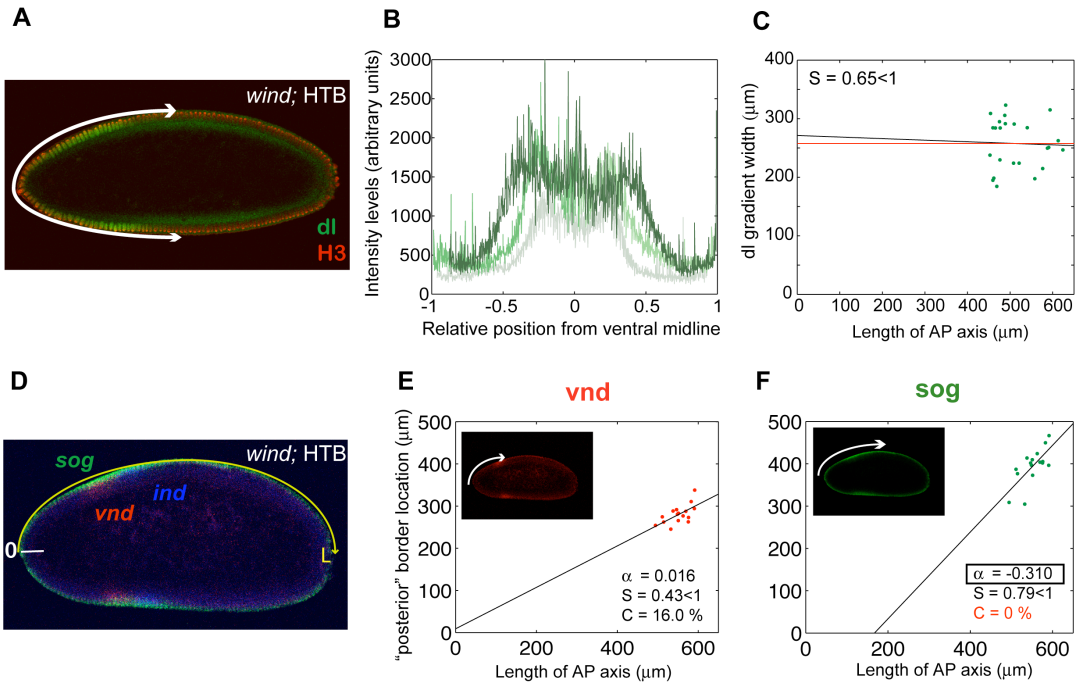

Figure 4.3 Scaling of dl and dl-target genes along the AP axis in embryos from *wind*; HTB females

(A) Immunostaining of an embryo from a *wind*; HTB female using dl (green) and Histone H3 (red) antibodies to quantify nuclear dl intensity levels. **(B)** Intensity profiles from three different embryos that illustrate the variability in the width of the nuclear dl gradient in this genetic background. **(C)** In contrast to the wild-type case, the nuclear dl gradients in this genetic background are fitted to the shape of a Hill function and the "width" is defined as the fitted parameter *k* in the Hill equation (see Materials and Methods). The width of the nuclear dl gradient in these embryos is plotted against the length of the AP axis along the surface of the embryo. The least-squares fit of the data (black line) is similar to a horizontal line that defines the mean width (red line). **(D)** Fluorescent *in situ* hybridization in an embryo from a *wind*; HTB female using *sog* (green), *vnd* (red) and *ind* (blue) probes. The location of borders of gene expression and the length of the AP axis were measured on the surface of the embryo using the anterior pole as a reference point (x = 0). **(E, F)** The position of the posterior borders of *vnd* (E) and *sog* (F) are plotted against the length of the AP axis. Black lines correspond to the least-squares fit of the data. The numerical results of the scaling criterion applied to each dataset are shown in each panel.

scales with the length of the AP axis (Fig. 4.3E). Although the level of scaling percentage in this case is significantly lower than in the wild-type case, this result is remarkable considering that the scalability of the dl gradient widths is completely abolished in this system (Fig. 4.3C). In contrast, the borders of *sog* and *ind* do not seem to scale along the AP axis and exhibit a high degree of embryo-to-embryo variability (Fig. 4.3F and data not shown). The result that *vnd* scales in this system suggests that the mechanism for "sensing" the size of the embryo to establish relative positional information must depend on factors downstream of Toll signaling activation.

4.4 Discussion

A balanced relationship between pattern and size in embryonic development is essential to produce well-proportioned organisms. Although this relationship has been extensively studied in embryological systems such as frogs and sea urchins by dissection and transplantation experiments (reviewed by De Robertis, 2006), little is known about the interplay between pattern and size in natural populations. In this work, we investigated the correlation between patterns of gene expression and embryonic length along the DV axis in the *Drosophila* embryo. In summary, our results provide evidence that the dl-target genes *vnd* and *sog*, as well as the dl gradient itself, exhibit scaling over a range of embryo sizes. However, our data show that scaling of the dl gradient is neither necessary nor sufficient to explain scaling of gene expression patterns along the DV axis. We propose that gene-specific feedback mechanisms operate downstream of the dl gradient to provide positional information relative to the size of the system.

Spatial Scaling of DV Patterns is a Gene-Dependent rather than a Position-Dependent Property

Our data provide evidence that while the ventral boundaries of *sog* and *vnd* coincide (Fig. 4.1B) and scale with respect to the DV circumference (Fig. 4.1F,G), under certain conditions (e.g., in embryos from *wind*; HTB females) scaling of one border does not imply scaling of the other. Similarly, the dorsal border of *vnd* often coincides with the ventral border of *ind*, but our data show that these boundaries have different scaling behaviors (Fig. 4.1C,H). These results support the idea that scaling in this system depends on the gene in question rather than on its location.

Interestingly, this conclusion is in contrast with a recent study on scaling of gap genes along the AP axis of the *Drosophila* embryo that suggest that scaling in the posterior half of the embryo occurs regardless of the gene assayed (de Lachapelle and Bergmann, 2010). Another intriguing difference between our findings on DV patterning and recent work on scaling along the AP axis is the role of the participating morphogens. In the case of Bcd, there is recent evidence that its distribution scales precisely along the AP axis and correlates with the positions of target gene expression (Gregor et al., 2007; He et al., 2008; He et al., 2010). In contrast, while our data suggest that the nuclear dl gradient might scale with the embryo circumference, scaling of the gradient does not necessarily imply scaling of target genes (Fig. 4.2C,D).

Mechanisms of Spatial Scaling along the DV Axis

While the role of dl as the main player in DV patterning in the *Drosophila* embryo cannot be questioned, our results challenge the idea that a gradient of dl provides directly enough positional information to explain scaling of the DV patterns assayed. In particular, our

observations that scalability of the dl gradient does not imply scalability of gene expression patterns leave doubts regarding the mechanisms of establishing relative positional information in this system.

Although our data do not reveal the mechanisms underlying scaling in this system, it does restrict the set of possible scenarios. For example, our observation that the ventral border of *vnd* scales in embryos from *wind*; HTB mothers suggest that the mechanism of scaling of this border should depend on factors that are downstream of Toll signaling. In particular, our data rule out the possibility that two independent gradients emanating from opposing regions establish relative coordinates of positional information in the system (Wolpert, 1969). However, we cannot discard the possibility that two "interdependent" gradients are involved –for instance, an opposing gradient that depends on dl may be required for scaling. One attractive candidate for this opposing gradient is *decapentaplegic* (*dpp*), a member of the TGF-β family. *dpp* expression is restricted to the dorsal-most part of the embryo by dl, and key regulators of Dpp signaling such as *sog* and *brinker* are also under direct transcriptional control by dl (François et al., 1994; Jazwinska et al., 1999). These facts suggest that *dpp* could take part in a feedback mechanism that contributes to establishing a scale-free coordinate system along the DV axis. However, our preliminary results do not show defects on *vnd* scaling in *brk*, *sog* double mutant embryos (data not shown).

Origin of Relative Positional Information in DV Patterning

The elegance of the Classical Morphogen model relies on providing patterning information from a single input: the concentration distribution of the morphogen. As a

consequence, a gradient that scales with size results in patterns of gene expression that scale accordingly. In contrast to this view, our data suggest that positional information relative to the length of the DV axis cannot be established from the simple readout of the dl nuclear gradient (Fig. 4.4A). Instead, our results suggest that the dl gradient can only *instruct* directly a region that is subsequently "sharpened" to a precise location by downstream mechanisms that are specific to each gene (Fig. 4.4B). For example, scaling of the border of *sog* should depend on scaling of the dl-gradient because *sog* scaling is disrupted in embryos from *wind*; HTB mothers (Fig. 4.3F). However, the dl-gradient is insufficient to determine the relative position of *sog* boundaries (at least linearly in a concentration-dependent manner), as the *sog* ventral border does not compensate as much as it would be predicted by a direct readout of the nuclear dl gradient (Fig. 4.2D). Perhaps, scaling of the dl-gradient ensures scaling of other factors (e.g., repressors of *sog* expression) that directly result in scaling of *sog* borders along the DV circumference (Fig. 4.4B). The case of *vnd* is even more dramatic as it does not appear to require scaling of the dl gradient (Fig. 4.3E) suggesting that downstream factors can self-organize scaling of the ventral border of *vnd* with respect to axis length. Some obvious candidates to fulfill the role of these downstream factors that are already known to participate in "sharpening" the ventral borders of *vnd* and *sog* are the transcription factors Twist and Snail (von Ohlen and Doe, 2000; Cowden and Levine, 2003). Future work will determine whether or not Twist and Snail are required for determining the location of the ventral borders of *sog* and *snail* in coordinates relative to the length of the axis.

While the cases examined here do not appear to rely on scaling of the dl gradient to ensure scaling of target gene expression, we cannot rule out that other dl target genes

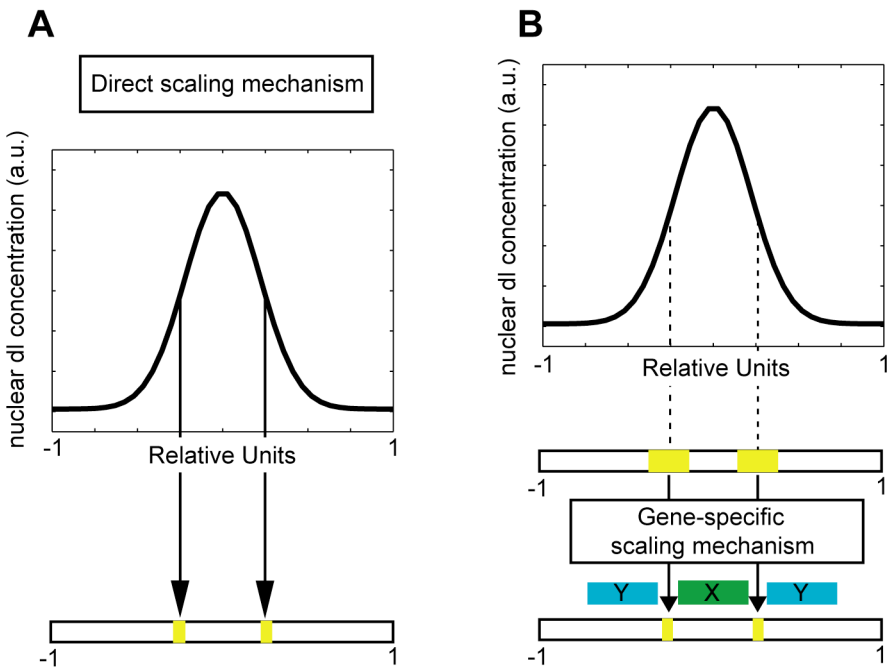

Figure 4.4 Models of spatial scaling of DV patterns in *Drosophila.*

(A) In the *direct scaling mechanism*, a scaled dl gradient defines scaled locations of gene expression. The mechanism of scaling in this case is probably upstream of dl (e.g., scaling of the *pipe* domain in ovarian egg chambers). Although it is possible that some dl-target genes scale as a consequence of nuclear dl scaling, none of the genes assayed here correspond to this case. **(B)** Scaling of the DV patterns studied here is gene-specific. Even if the dl gradient scales with the length of the DV axis, additional downstream factors X and Y could be required for scaling of other dl-target genes. These factors are likely gene-specific, rather than position-specific.

---

scale as a direct consequence of scaling of the dl gradient (Fig. 4.4A). Therefore, an important question is how a scale-invariant dl gradient is established in the first place. One possibility is that feedback mechanisms exist that ensure that the dl gradient accommodate to the size of the embryo (see Ben-Zvi and Barkai (2010), for example). Our data however, do not support the idea that feedback interactions downstream of dl control scaling of the nuclear dl gradient itself because the gradient fails to scale in

embryos from *wind*; HTB females. Another possibility that is consistent with previous studies is that scaling of the dl gradient results from scaling of an upstream factor in the DV signaling cascade. In ovarian egg chambers, *pipe* is expressed in the 40% ventral most region of the follicular epithelium around the oocyte irrespective of egg size (Nilson and Schupbach, 1998; Peri et al., 2002). Since *pipe* predefines the location of the nuclear dl gradient in the embryo, these studies suggest that scaling of the dl gradient may result from scaling of the *pipe* expression domain in the oocyte. Thus, it is conceivable that an ancestral mechanism of scaling that originates in the oocyte and results in scaling of the dl gradient and other dl-dependent patterns diverged at some time in evolution in order to provide more complex mechanisms that ensure the proper establishment of relative positional information in a gene-specific manner.

Chapter 5

Discussion

In a developing organism, cells require information about their relative position in order to function and differentiate appropriately. Despite the discovery that key signaling pathways act as organizers of pattern formation in several systems, the details of how this positional information is distributed, processed, and interpreted by cells in a developing field remain little understood. In this thesis, we use a combination of theoretical tools and experimental work in *Drosophila* to investigate the origin and interpretation of positional information, the role of temporal changes in signaling activity on patterning, and the relationship between the location of patterns and the size of the system. Our contributions to these fundamental questions can be briefly summarized as follows (see details below):

- In Chapter 2, we challenge the prevailing idea that the Hh morphogen establishes positional information in a dose-dependent manner and proposed a model in which gradient dynamics, resulting from the Hh gene network architecture, determines pattern formation in the *Drosophila* wing disc.

- Chapter 3 introduces a general theoretical framework to design genetic experiments that isolate the effects of transient vs. steady-state signals on developmental patterning. This formalism is not limited to the study of signal dynamics and may be generally applicable to other problems.

- In Chapter 4, we investigate spatial scaling of gene expression patterns due to natural variations in the length of the DV axis in the *Drosophila* embryo. In contrast to

recent studies on scaling along the AP axis (de Lachapelle and Bergmann, 2010), we show that scaling in this system is a gene-dependent, rather than a position-dependent property. We propose that gene-specific scaling mechanisms depend on factors downstream of the Toll signaling pathway.

Mathematical Modeling as a Hypotheses-Generating Tool[*]

Mathematical modeling and theoretical biology have led efforts to investigate the question of how patterns emerge during development (Turing, 1952; Wolpert, 1968), and today, there is no doubt that the interplay between theory and experiment has significantly advanced our current understanding of developmental processes (Green, 2002; Ibañes and Izpisúa-Belmonte, 2006). A common approach has been to use available experimental data to devise mathematical models that can be employed as predictors of experimental results (Fig. 5.1A). Typically, these models are then used to explore properties of the system that are not easily exploited by experimentation. Alternatively, mathematical models can be formulated to discriminate between different interpretations of an experiment (Fig. 5.1B). Although the use of mathematical models as *predictors* (Fig. 5.1A**)** or *interpreters* (Fig. 5.1B) of experimental data have often resulted in important contributions to developmental biology, they have also been subject of skepticism from experimentalists. A major criticism to these approaches is that conclusions arise from the models themselves, and as such, depend on the details of their

[*] This section, originally published as part of "Nahmad M. and Stathopoulos A. Establishing positional information through gradient dynamics: A lesson from the Hedgehog signaling pathway. Fly 4:4; 1-5 © 2010 Landes Biosciences," is reproduced under the terms of the license agreement between the authors and the publishers.

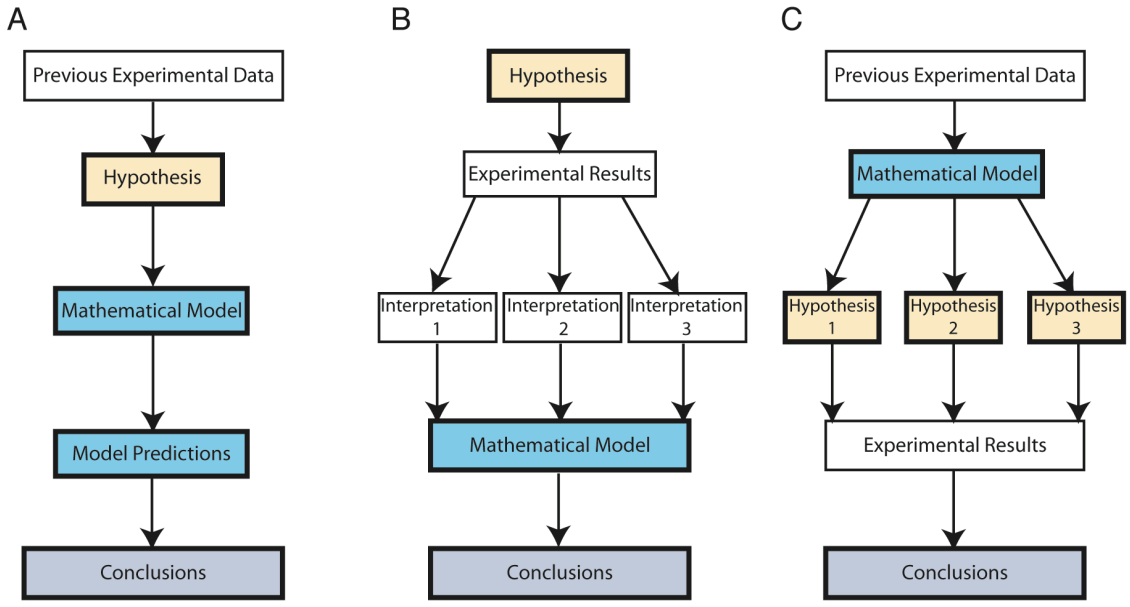

Figure 5.1. Different methodologies for using mathematical modeling in biological research.

(A) The mathematical model is used as a *predictor* of new experimental results. As new experimental data become available, the model is validated or refined. This approach is typically used to build general mathematical models that explain the phenomenon of interest. (B) The mathematical model as an *interpreter* of experimental data. In this case, the mathematical model is used to test the feasibility of different interpretations of an experiment. (C) Mathematical modeling as a *hypotheses-generating tool*. In this approach, the mathematical model is used to propose different hypotheses, but does not favor any particular one. Unlike the methodologies depicted in (A) or (B), in (C) conclusions are only derived from experimental data.

---

mathematical formulation and their accuracy to represent the biological phenomenon.

In our study of the interpretation of Hh signaling in the *Drosophila* wing disc (Nahmad and Stathopoulos, 2009; see Chapter 2), we used mathematical modeling as a tool to formulate hypotheses that could be tested through direct experimentation (Fig. 5.1C). Importantly, these hypotheses would not be straightforward to propose without the mathematical model. Specifically, we modeled the Hh signaling pathway using a

system of partial differential equations and found that under certain assumptions (i.e., the value of a critical parameter), interpretation of the Hh gradient in a concentration-dependent manner was not possible. Furthermore, the model suggested that the formation of the gradient follows some unusual dynamics due to a property of the gene network architecture associated with the Hh signaling pathway, namely, that the Hh receptor and antagonist, *ptc*, was transcriptionally upregulated in response to Hh signaling. The gradient initially expands due to low Ptc levels, but then retracts as a result of Ptc accumulation, which leads to the sequestration and degradation of free extracellular Hh (Fig. 2.2E). Moreover, we showed experimentally that if Hh-dependent *ptc* upregulation is impaired, then the signal fails to establish different domains of gene expression (Fig. 2.3F). Thus, the model did not predict that the dynamics of the gradient were required for the interpretation of the signal, but rather prompted us to investigate it. In contrast to other modeling approaches that have utilized mathematical models as predictors of unknown data (Fig. 5.1A), or to interpret unclear experiments (Fig. 5.1B), in our study the model was used as a motor to propose non-trivial hypotheses (Fig. 5.1C). Our approach is somewhat similar to model-based experimental design strategies in which mathematical models are used to define possible experiments that can be performed. Although these approaches have become widely used in systems biology in the post-genomic era (Kitano, 2002; Kreutz and Timmer, 2009), our approach - to employ mathematical modeling as a tool to guide experimental research - is not common in the context of developmental biology.

A Network Architecture-Based Model of Hh-Dependent Patterning[*]

The most important conceptual contribution of our work on Hh signaling (Chapter 2), in our opinion, is the idea that the shape of the gradient is not the major factor contributing to pattern formation in this system. It is widely recognized that developmental patterning is tightly controlled by feedback components inherent within the gene regulatory network of the system (Kutejova et al., 2009). These feedback interactions have been shown to be essential for generating sharp boundaries of gene expression and to ensure reproducibility and precision under genetic or environmental perturbations. However, most models of morphogen-mediated developmental patterning are built under the main hypothesis that pattern formation is a function of the morphogen concentration profiles. In particular, changes in patterning are usually directly associated with changes in the morphogen distribution, and properties such as precision, robustness, or size-dependent scaling are generally studied assuming that the shape of the morphogen gradient is the predominant factor (Houchmandzadeh et al., 2002; Eldar et al., 2003; Bollenbach et al., 2008; Ben-Zvi et al., 2008). Our study suggests that Hh-dependent patterning in the *Drosophila* wing disc depends on temporal changes of the morphogen profile but, unlike the classical morphogen model, it does not primarily depend on concentration thresholds defined by the distribution of the gradient; instead, patterning is controlled directly by the architecture associated with the Hh gene network, particularly by the feedback that results from Hh-dependent *ptc* upregulation and Ptc-dependent ligand sequestration. Therefore, our model backs up a recent study (Smith et al., 2007) that supports the idea

[*] This section, originally published as part of "Nahmad M. and Stathopoulos A. Establishing positional information through gradient dynamics: A lesson from the Hedgehog signaling pathway. Fly 4:4; 1-5 © 2010 Landes Biosciences," is reproduced under the terms of the license agreement between the authors and the publishers.

that pattern formation is inherent within the gene regulatory network of the system and implicates that the shape of the Hh concentration profile is not the primary source of positional information.

Steady-State Invariant Perturbations as a Tool to Study Morphogen Dynamics

The major challenge in modelling-based experimental design is not just that mathematical models can only capture a simplified view of the natural phenomenon, but that they are tightly constrained by the experiments that can actually be performed. The hope of the theoretical approach presented in Chapter 3 is to use it as a tool to design genetic experiments that separate transient from equilibrium effects in developmental patterning. The problem of computing invariant subsets that correspond to experimentally testable genetic perturbations is in general very difficult; even in the cases in which the steady-state invariant set can be obtained either exactly or approximately, it is unclear if the design of such a genetic experiment is possible (i.e., one in which the affected kinetic parameters remain on the steady-state invariant set). Experimentally, genetic perturbations that are expected to satisfy many constraints on independent kinetic parameters are difficult to realize. For instance, in our example of a free morphogen established by diffusion and linear degradation [Equation (3.1)], only those perturbations in which all three parameters are altered in the same proportion remain on the steady-state invariant set [Equation (3.4)]. Despite the simplicity of this example, a genetic perturbation subject to these constrains (i.e., such that Equation (3.4) holds) is very difficult to achieve experimentally because kinetic rates, in general, may not be precisely tuned using standard genetic techniques. Although this example is not of biological

interest, it illustrates a general conceptual problem of modeling-based experimental design: models that are simple enough so that the steady-state invariant set can be fully computed do not necessarily predict simple genetic experiments. On the other hand, in our model of Hh signaling, the steady-state invariant set cannot be computed exactly and yet, an approximate steady-state invariant subset that involves only one "freely" tuneable parameter can be obtained [Equation (3.11)] and the genetic design of steady-state invariant perturbations is plausible.

The theoretical approach presented in Chapter 3 faces some challenges that may limit its applicability. For example, the geometry of steady-state invariant sets depends on the details of the mathematical model. As these models are based on simplified representations of the developing system, a steady-state invariant perturbation predicted by the theory may not be so experimentally. Therefore, these tools should be used as a predictor of steady-state invariant genetic perturbations but appropriate control experiments should be performed to show that the steady-state distribution of the signal is in fact unchanged by the proposed perturbation. Another assumption of this theoretical approach is that the steady state is reached within a relevant developmental timescale, but this may not necessarily be the case. For example, the nuclear concentration of the transcription factor, Dorsal, in the early *Drosophila* embryo does not appear to reach a steady-state distribution by the time that gene expression patterns are specified (Liberman et al., 2009). However, in the cases when equilibrium is not reached within the patterning timescale, it is clear that positional information is established by signaling dynamics and that additional mechanisms are required to explain patterning in these systems.

Spatial Scaling along the DV Axis of the *Drosophila* Embryo is a Gene-Specific Property

Our finding in Chapter 4 that scaling of dl-target genes with respect to the embryo circumference depends on specific genes, rather than on particular positions along the DV axis, implies that scaling in this system does not result from the interpretation of position from a global system of scaled coordinates like in the French Flag problem (c.f. Wolpert, 1968). Instead, our results suggest that different genes may use different coordinate systems to establish their positional information in the embryo. An intriguing example is the comparison of the dorsal border of *vnd* vs. the ventral border of *ind* because previous studies suggest that *vnd* sets this border of *ind* (von Ohlen and Doe, 2000; Cowden and Levine, 2003). However, our data indicate that despite strict scaling of the dorsal border of *vnd* with the length of the DV axis (Fig. 4.1C), the ventral border of *ind* displays overcompensation and thus does not scale (Fig. 4.1H). One explanation for this result is that *vnd* and *ind* use different coordinate systems to specify the locations of their borders. For example, *vnd* may use feedback interactions downstream of dl to ensure precise scaling, whereas *ind* may employ another system of coordinates; for example, EGFR signaling has been suggested to play a role in *ind* expression (as *egfr* mutant embryos do not express *ind*) (von Ohlen and Doe, 2000).

Similarly, while more data are required to verify whether or not the dl gradient scales in wild-type embryos, our result that the dorsal border of *vnd* scales in embryos that ectopically express dl along the AP axis (in which it is clear that scaling of the dl gradient along the AP axis *does not* occur; see Fig. 4.3B,C,E) shows that dl scaling is not required to ensure scaling of the *vnd* pattern. In contrast, the dorsal border of *sog*, which conclusively scales in wild-type embryos (Fig. 4.1D), fails to scale in this genetic

background (Fig. 4.3F). This suggests that gene-specific coordinates are used to determine positional information with respect to the size of the embryo.

A Gene-Specific Model to Explain Scaling of the Ventral Border of *sog*

Although our experiments in Chapter 4 do not uncover any particular mechanism of scaling, we can speculate about gene-specific mechanisms of scaling in this system. For example, the ventral border of *sog* cannot be explained directly by concentration thresholds of the dl gradient in wild-type embryos (Fig. 4.2D), suggesting that additional factors contribute to scaling of this pattern. We suggest that scaling of the *sog* ventral border is an indirect consequence of scaling of the *snail* gene, which encodes the mesoderm-specific transcription factor implicated in sharpening borders of gene expression in ventrolateral patterns. However, the generation of sharp boundaries does not imply scaling (or viceversa). If scaling of the dl gradient width results in scaling of the *snail* border, then *snail* scaling would be a direct consequence of scaling of the nuclear dl gradient (Fig. 4.4A), while *snail* would work as gene-specific intermediary in scaling of the ventral border of *sog* (see Fig. 4.4B with X=*snail*).

Chapter 6

Future Directions

Besides our contributions discussed in previous chapters to the problem of developmental pattern formation, this work has also brought new questions that remain unanswered. The purpose of this Chapter is to highlight some problems that will likely provide new insights into the field and will be interesting to consider in follow-up studies.

6.1 Future Directions for Chapter 2

Genetic Characterization of the "Memory Module"

The Overshoot Model proposed in Chapter 2 to explain the interpretation of the Hh morphogen in the *Drosophila* wing disc depends on two network subcircuits or "modules" (see Fig. 2.7B). The Overshoot Module causes a delay in Hh-dependent *ptc* upregulation that results in a transient overshoot of the Hh gradient. The Hh overshoot is essential to expose a subset of cells transiently to the signal, but the Overshoot Module fails to explain patterning if this subset of cells is not able to "recall" its history of Hh signaling exposure. The maintenance of this transient state likely depends on a positive feedback loop on *dpp* transcription that maintains expression of *dpp* once the transient signal ceases. However, the genetic players that participate in this transcriptional subcircuit or "Memory Module" have not yet been identified.

One way to identify novel players in the Memory Module is to use a candidate approach, this is, to investigate if "memory" of *dpp* expression persists after some

candidates are impaired one at a time. For example, one natural candidate is *dpp* itself, as it encodes a signaling molecule that could enhance its own expression after it is activated by a transient Hh signal. However, in Chapter 2 we provided evidence against this possibility (see Supporting Figure 2.3). Other possible candidates include members of other signaling pathways that participate in wing disc patterning, such as Wingless and EGFR.

A more direct approach to identify potential transcriptional players in the "Memory Module" is through cis-regulatory analysis; if genetic players exist that determine memory of *dpp* expression through a transcriptional feedback loop, we should be able to identify the region in the *dpp* enhancer DNA where these players bind and activate transcription of *dpp*. Cis-regulatory studies on the *dpp* enhancer have identified a "minimal enhancer" (800 base pairs long) that is capable of reproducing the normal pattern of *dpp* in wing discs (Müller and Basler, 2000). Preliminary data suggest that this minimal element does support memory of *dpp* expression after the inactivation of Hh signaling using the hh^{ts} system described in Chapter 2 (data not shown). However, the confirmation and continuation of this work is left to immediate future studies.

Another possibility is that the "Memory Module" does not require other transcription factors, but instead employs regulation of the existing ones. For example, it is possible that the mechanism for *dpp* memory is provided by the differential responsiveness of Hh target genes to the activator (Ci155) and repressor (Ci75) forms of the transcription factor Ci. Unlike other Hh target genes, *dpp* does not require activation by Ci155 (as *ci* clones located anywhere within the anterior compartment of the wing disc express), but presence of the repressor form Ci75 is sufficient to abolish *dpp* expression

(Méthot and Basler, 1999). These data suggest the existence of (ubiquitous) transcription factors that activate *dpp* expression in the absence of Ci75 and propose a potential mechanism by which *dpp* expression may be maintained upon transient Hh signaling activation; perhaps there is a Hh-dependent factor (e.g., a ligase or a protease) that impairs the activity of Ci75 in the *dpp* domain. One potential factor is *roadkill* (*rdx*), a Hh-target gene that encodes a subunit of a E3 ubiquitin ligase that targets Ci to degradation via the proteasome ubiquitin pathway (Kent et al., 2006; Zhang et al., 2006). Ubiquitous Rdx upregulation causes loss of *ptc* expression and expansion of the *dpp* domain (Kent et al., 2006). However, some evidence argues against the role of rdx as a key player in the "Memory Module." First, Rdx preferentially promotes destruction of full length Ci than Ci75 (Kent et al., 2006). Moreover, *rdx* is normally expressed in a narrow domain abutting the AP boundary of the wing disc, a region of sustained Hh signaling activity (Kent et al., 2006; Zhang et al., 2006).

When Does the Hh Overshoot Occur *in vivo*?[*]

Our study in Chapter 2 provides evidence for the existence of a Hh gradient overshoot upon reinitialization of the gradient using a temperature-sensitive *hh* allele, but when such a dynamic shift in the gradient occurs during normal development remains to be identified. Alternatively, it is also possible that the overshoot occurs multiple times in wing disc development. Such oscillations in the range of the signal may occur if Hh-dependent Ptc upregulation becomes sufficiently strong so that Hh signaling is repressed

[*] This section, originally published as part of "Nahmad M. and Stathopoulos A. Establishing positional information through gradient dynamics: A lesson from the Hedgehog signaling pathway. Fly 4:4; 1-5 © 2010 Landes Biosciences," is reproduced under the terms of the license agreement between the authors and the publishers.

completely, and thus that expression of *ptc* is interrupted - allowing for multiple rounds of Hh gradient expansion and refinement. However, this periodic behavior of Ptc expression has not been reported and, furthermore, we suggest that such regulation is unlikely to occur in a synchronized manner. These important aspects will require direct temporal examination of Hh gradient formation and Ptc expression in living tissues over a long period of time, but this remains technically challenging.

Integration of Patterning by the Overshoot Model with Tissue Growth[*]

Another important problem that will require further investigation is how this model accommodates tissue growth. In particular, if cells that experience a transient Hh signaling retain *dpp* expression by some 'memory' mechanism, whether or not this is retained after cell division, is still in question. Our data show that the time-scale of the overshoot (~6 hours) is shorter than the average cellular proliferation rate in the wing disc during the third instar (~8.5 hours; González-Gaitán et al., 1994); therefore, the dynamics of the gradient should not be directly affected by tissue growth. However, it remains unclear why all the cells derived from *dpp*-expressing progenitors do not retain *dpp* expression; a fraction of cells that are sufficiently close to the AP boundary (where Hh signaling is ON) may end up located farther away from it as a result of tissue growth (where Hh signaling is OFF). One possible explanation is that cells expressing *dpp* maintain their relative position in the wing disc as a result of cell affinity, but their progeny eventually lose the ability to maintain *dpp* expression and are pushed away from

[*] This section, originally published as part of "Nahmad M. and Stathopoulos A. Establishing positional information through gradient dynamics: A lesson from the Hedgehog signaling pathway. Fly 4:4; 1-5 © 2010 Landes Biosciences," is reproduced under the terms of the license agreement between the authors and the publishers.

the anterior-posterior boundary. In fact, the hypothesis that *dpp*-expressing cells attempt to remain together during wing disc development is supported by a study that suggest that *dpp*-expressing cells may regulate a cell adhesion molecule that is necessary to avoid intermixing of anterior and posterior cells (Dahmann and Basler, 2000). However, it is unclear if the progenitors of *dpp*-expressing cells that are no longer exposed to Hh would lose their ability to maintain *dpp* expression. In summary, the relationship between patterns and growth, and particularly, how *dpp* 'memory' is affected by cell proliferation deserves further investigation as well.

The Overshoot Model in Other Patterning Systems[*]

Our model of Hh-dependent patterning in the *Drosophila* wing disc primarily depends on a particular gene network architecture, rather than on Hh concentration thresholds. Numerous studies in different developmental contexts have revealed that the Hh signaling gene network architecture is largely conserved from flies to humans. In particular, Hh-dependent *ptc* upregulation is a common feature in all the systems studied so far. Thus, an exciting question for the future is whether similar models of pattern formation hold for systems with equivalent network architectures, or the principles of developmental pattern formation evolved despite the conservation of gene network topologies. Interestingly, recent data from the vertebrate neural tube suggest that cells determine their fate by integrating the strength of Hh signaling over time (Dessaud et al., 2010), while another study in the same system reported that some positional information

[*] This section, originally published as part of "Nahmad M. and Stathopoulos A. Establishing positional information through gradient dynamics: A lesson from the Hedgehog signaling pathway. Fly 4:4; 1-5 © 2010 Landes Biosciences," is reproduced under the terms of the license agreement between the authors and the publishers.

is lost when *ptc* is not upregulated in response to Hh signaling (Jeong and McMahon, 2005). These results are in close agreement with our model of Hh patterning in the *Drosophila* wing disc (Chapter 2), but additional studies will reveal if developmental patterning in other Hh-dependent systems employs similar principles.

6.2 Future Directions for Chapter 3

A technical challenge that deserves further discussion in the future is how to analyze and visualize steady-state invariant sets in realistic models of developmental patterning. This problem is common in practice because steady-state invariant sets are usually contained in high dimensional spaces. For example, the dimension of the parameter space of our highly simplified model of Hh signaling is 16. More realistic models may involve an even larger number of parameters making the resulting steady-state invariant set difficult to analyse and visualise. Our analysis in Chapter 3 reduces to the study of subsets [Equations (3.10) and (3.11)] that are contained in particular parameter subspaces, but an interesting future direction is to use theoretical tools (e.g., nonlinear extensions of Principal Component Analysis; see Kruger et al., 2007, for a review) to reduce high-dimensional steady-state invariant sets to sets of lower dimensions that are easier to visualise and more useful for experimental design.

6.3 Future Directions for Chapter 4

The work presented in Chapter 4 is an unfinished project that will soon be considered for publication. However, there are some points that require additional experimental support that are currently in progress. For example, the confidence of some of the results (based

on the value of the scaling percentage) is relatively low, partly because the number of embryos considered is not appropriate. In particular, we would like to determine with greater confidence if scaling of the nuclear dl gradient can be confirmed by adding more data to the sample. In addition, it will be useful to investigate the correlation between the width of the dl gradient and the other target genes under study.

Our conclusion that spatial scaling of DV patterns is gene-dependent raises questions about the scalability of other genes in the system. Some candidates include *twist*, *snail*, *rhomboid*, and *brinker*. For example, it would be useful to determine if there are genes whose scalability can be explained by the nuclear dl gradient and whether their scaling can be used to establish scaling of other genes. As DV genes affect each others patterns through a network of complex interactions (reviewed by Stathopoulos and Levine 2005), it is likely that they contribute to each other's ability to scale with respect to the length of the DV axis. Particularly, we would like to test our model that *snail* acts as an intermediate factor to establish scaling of *sog* (see Chapter 5).

We are trying to identify gene-specific scaling mechanisms using a candidate approach, in which scaling of *vnd*, *sog*, and *ind* is assayed in different mutant backgrounds. One limitation of this approach is that the process to screen for scaling using embryo cross sections is very slow, making it difficult to design a large screen that can help in the identification of molecular players that are required for scaling. The search for genetic players that affect scaling in this system is also technically difficult because it is likely that mutants that affect scaling also affect other aspects of patterning, such that the effects on scaling and patterning cannot be genetically separated. On the

technical side, it would be useful to improve our methods to screen faster and more reliably for factors that affect scaling.

There is no doubt that the use of multidisciplinary and quantitative tools will provide new insights into the mechanisms of pattern formation and promise a fruitful path to the future of developmental biology. But this approach is still in its infancy. Our ability to measure gene expression with high temporal and spatial resolution is still very limited even in well-characterized model systems. However, future studies will surely provide a more quantitative picture of animal development that will contribute to a better understanding of the relationship between positional signals and animal design.

Bibliography

Aegerter-Wilmsen T., Aegerter C.M., Bisseling T. (2005). Model for the robust establishment of precise proportions in the early Drosophila embryo. J Theor Biol. 234: 13-19.

Ahn S., Joyner A. L. (2004). Dynamic changes in the response of cells to positive hedgehog signaling during mouse limb patterning. Cell. 118: 505-516.

Akam M. (1987). The molecular basis for metameric pattern in the Drosophila embryo. Development. 101: 1-22.

Alon U., Surette M.G., Barkai N., Leibler S. (1999). Robustness in bacterial chemotaxis. Nature. 397: 168-171.

Apionishev S., Katanayeva N.M., Marks S.A., Kalderon D., Tomlinson A. (2005). Drosophila Smoothened phosphorylation sites essential for Hedgehog signal transduction. Nat Cell Biol. 7: 86–92.

Ashe H. L., Briscoe J. (2006). The interpretation of morphogen gradients. Development. 133: 385-394.

Barkai N., Liebler S. (1997). Robustness in simple biochemical networks. Nature. 387: 913-917.

Belvin M.P., Jin Y., Anderson K.V. (1995). Cactus protein degradation mediates Drosophila dorsal-ventral signaling. Genes Dev. 9: 783-793.

Ben-Zvi D., Barkai N. (2010). Scaling of morphogen gradients by an expansion-

repression integral feedback control. Proc Natl Acad Sci U S A. 107: 6924-6929.

Ben-Zvi D., Shilo B.Z., Fainsod A., Barkai N. (2008). Scaling of the BMP activation gradient in Xenopus embryos. Nature. 453: 1205-1211.

Bergmann A., Stein D., Geisler R., Hagenmaier S., Schmid B., et al. (1996). A gradient of cytoplasmic Cactus degradation establishes the nuclear localization gradient of the dorsal morphogen in Drosophila. Mech Dev. 60: 109-123.

Bergmann S., Sandler O., Sberro H., Shnider S., Schejter E., et al. (2007). Pre-steady-state decoding of the Bicoid morphogen gradient. PLoS Biol. 5: e46. doi:10.1371/journal.pbio. 0050046.

Biehs B., Francois V., Bier E. (1996). The Drosophila short gastrulation gene prevents Dpp from autoactivating and suppressing neurogenesis in the neuroectoderm. Genes Dev 10: 2922–2934.

Bier E., Jan L.Y., Jan Y.N. (1990). Rhomboid, a gene required for dorsoventral axis establishment and peripheral nervous system development in Drosophila melanogaster. Genes Dev. 4: 190-203.

Bijlsma M.F., Spek C.A., Zivkovic D., van de Water S., Rezaee F, Peppelenbosch M. P. (2006). Repression of smoothened by patched-dependent (pro-)vitamin D3 secretion. PLoS Biol. 4:e232.

Blair S.S. (1992). Engrailed expression in the anterior lineage compartment of the developing wing blade of Drosophila. Development. 115:21–33.

Bollenbach T., Pantazis P., Kicheva A., Bökel C., González-Gaitán M., Jülicher F. (2008). Precision of the Dpp gradient. Development. 135: 1137-1146.

Bolouri H. (2008). Embryonic pattern formation without morphogens. Bioessays. 30: 412-417.

Bourillot P.Y., Garret N., Gurdon J.B. (2002). A chaniging morphogen gradient is interpreted by continuous transduction flow. Development. 129: 2167-2180.

Brand A.H., Perrimon N. (1993). Targeted gene expression as a means of altering cell fates and generating dominant phenotypes. Development. 118: 401-415.

Bryant P.J. (1969). Mosaicism. Bioscience. 19: 1126.

Burke R., Nellen D., Bellotto M., Hafen E., Senti K.A., et al. (1999). Dispatched, a novel sterol-sensing domain protein dedicated to the release of cholesterol-modified hedgehog from signaling cells. Cell. 99: 803–815.

Capdevila J., Estrada M.P., Sanchez-Herrero E., Guerrero I. (1994). The Drosophila segment polarity gene patched interacts with decapentaplegic in wing development. EMBO J. 13: 71–82.

Carroll S.B., Grenier J.K., Weatherbee S.D. (2005). From DNA to diversity: molecular genetics and the evolution of animal design. 2nd Edition. Blackwell Publishing. Malden, MA.

Casali A., Struhl G. (2004). Reading the Hedgehog morphogen gradient by measuring the ratio of bound to unbound Patched protein. Nature. 431: 76-80.

Chamoun Z., Mann R.K., Nellen D., von Kessler D.P., Bellotto M., et al. (2001). Skinny hedgehog, an acyltransferase required for palmitoylation and activity of the hedgehog signal. Science. 293: 2080–2084.

Chen Y., Struhl G. (1996). Dual roles for patched in sequestering and transducing Hedgehog. Cell. 87: 553–563.

Child C. M. (1941). Patterns and Problems of Development. Chicago University Press. Chicago, IL.

Chuang P.T., McMahon A.P. (1999) Vertebrate Hedgehog signalling modulated by induction of a Hedgehog-binding protein. Nature. 397: 617–621.

Cohen J.E. (2004). Mathematics is biology's next microscope, only better; biology is mathematics' next physics, only better. PLoS Biol. 2: e439.

Cooke J. (1995). Morphogens in vertebrate development: how do they work? Bioessays. 17: 93–96.

Cowden J., Levine M. (2003). Ventral dominance governs sequential patterns of gene expression across the dorsal-ventral axis of the neuroectoderm in the Drosophila embryo. Dev Biol. 262: 335-349.

Dahmann C., Basler K. (2000). Opposing transcriptional outputs of Hedgehog signalling and engrailed control compartmental cell sorting at the Drosophila A/P boundary. Cell. 100: 411-422.

Dalcq A.M. (1938). Form and causality in early development. Cambridge University Press. Cambridge, UK.

Dalcq A., Pasteels J.J. (1937). Une conception nouvelle des bases physiologiques de la morphogénese. Arch Biol. 48:669–710.

Davidson E.H. (2006). The Regulatory Genome: Gene Regulatory Networks in Development and Evolution. Academic Press. Burlington, MA.

de Celis J.F., Ruiz-Gomez M. (1995) groucho and hedgehog regulate engrailed expression in the anterior compartment of the Drosophila wing. Development. 121: 3467–3476.

de Lachapelle A.M., Bergmann S. (2010). Precision and scaling in morphogen gradient read-out. Mol Syst Biol. 6: 351.

De Robertis E.M. (2006). Spemann's organizer and self-regulation in amphibian embryos. Nat Rev Mol Cell Biol. 7:296-302.

Denef N., Neubuser D., Perez L., Cohen S.M. (2000). Hedgehog induces opposite changes in turnover and subcellular localization of patched and smoothened. Cell. 102: 521–531.

Dessaud E., Ribes V., Balaskas N., Yang L.L., Pierani A., et al. (2010). Dynamic assignment and maintenance of positional identity in the ventral neural tube by the morphogen sonic hedgehog. PLoS Biol. 8: 1000382.

Dessaud E., Yang L.L., Hill K., Cox B., Ulloa F., et al. (2007). Interpretation of the sonic hedgehog morphogen gradient by a temporal adaptation mechanism. Nature. 450: 717–720.

Drier E.A., Huang L.H., Steward R. (1999). Nuclear import of the Drosophila Rel protein

Dorsal is regulated by phosphorylation. Genes Dev. 13: 556-568.

Driever W., Nüsslein-Volhard C. (1988a). A gradient of bicoid protein in Drosophila embryos. Cell. 54: 83-93

Driever W., Nüsslein-Volhard C. (1988b). The bicoid protein determines position in the Drosophila embryo in a concentration-dependent manner. Cell. 54: 95-104.

Drossopoulou G., Lewis K.E., Sanz-Ezquerro J.J., Nikbakht N., McMahon A.P., et al. (2000) A model for anteroposterior patterning of the vertebrate limb based on sequential long- and short-range Shh signalling and Bmp signalling. Development. 127: 1337–1348.

Dyson S., Gurdon J.B. (1998). The interpretation of position in a morphogen gradient as revealed by occupancy of activin receptors. Cell. 93: 557–568.

Edwards D.N., Towb P., Wasserman S.A. (1997) An activity-dependent network of interactions links the Rel protein Dorsal with its cytoplasmic regulators. Development. 124: 3855-3864.

Eldar A., Rosin D., Shilo B.Z., Barkai N. (2003). Self-enhanced ligand degradation underlies robustness of morphogen gradients. Dev Cell. 5: 635-646.

Ferguson E.L., Anderson K.V. (1992). Decapentaplegic acts as a morphogen to organize dorsal-ventral pattern in the Drosophila embryo. Cell. 71: 451-461.

Fischer J.A., Giniger E., Maniatis T., Ptashne M. (1988). GAL4 activates transcription in Drosophila. Nature. 332: 853-856.

Francois V., Solloway M., O'Neill J.W., Emery J., Bier E. (1994). Dorsal-ventral

patterning of the Drosophila embryo depends on a putative negative growth factor encoded by the short gastrulation gene. Genes Dev. 8: 2602-2616.

García-Bellido A. (1975). Genetic control of wing disc development in Drosophila. Ciba Found Symp. 0: 161-182.

Gierer A., Meinhardt H. (1972) A theory of biological pattern formation. Kybernetik. 12: 30-39.

Golembo M., Schweitzer R., Freeman M., Shilo B.Z. (1996). Argos transcription is induced by the Drosophila EGF receptor pathway to form an inhibitory feedback loop. Development. 122: 223–230.

Gonzalez A., Chaouiya C., Thieffry D. (2008). Logical modelling of the role of the Hh pathway in the patterning of the Drosophila wing disc. Bioinformatics. 24: 234–240.

González-Gaitán M., Capdevila M.P., García-Bellido A. (1994). Cell proliferation patterns in the wing disc of Drosophila. Mech Dev. 46: 183-200.

Green J. (2002). Morphogen gradients, positional information and Xenopus: interplay of theory and experiment. Dev Dyn. 225: 392-408.

Green J., Smith J.C. (1990). Graded changes in dose of a Xenopus activin elicit stepwise transitions in embryonic cell fate. Nature. 347: 391–394.

Gregor T., Bialek W., de Ruyter van Steveninck R.R., Tank D.W., Wieschaus E.F. (2005). Diffusion and scaling during early embryonic pattern formation. Proc Natl Acad Sci U S A. 102: 18403-18407.

Gregor T., McGregor A.P., Wieschaus E.F. (2008). Shape and function of the Bicoid

morphogen gradient in dipteran species with different sized embryos. Dev Biol. 316:350-358.

Gregor T., Tank D.W., Wieschaus E.F., Bialek W. (2007). Probing the limits to positional information. Cell. 130: 153-164.

Gregor T., Wieschaus E.F., McGregor A.P., Tank D.W. (2007). Stability and nuclear dynamics of the bicoid morphogen gradient. Cell 130: 141-152.

Grier A., Meinhardt H. (1972). A theory of biological pattern formation. Kybernetik 12: 30-39.

Gunbin K.V., Omelyanchuk L.V., Kogai V.V., Fadeev S.I., Kolchanov N.A. (2007). Model of the reception of hedgehog morphogen concentration gradient: comparison with an extended range of experimental data. J Bioinform Comput Biol. 5: 491-506.

Gurdon J.B., Bourillot P.Y. (2001). Morphogen gradient interpretation. Nature. 413: 797-803.

Gurdon J.B., Dyson S., St Johnston D. (1998). Cells' perception of position in a concentration gradient. Cell. 95: 159-162.

Gurdon J.B., Harger P., Mitchell A., Lemaire P. (1994). Activin signaling and response to a morphogen gradient. Nature. 371: 487-492.

Gurdon J.B., Mitchell A., Mahony D. (1995). Direct and continuous assessment by cells of their position in a morphogen gradient. Nature. 376: 520–521.

Gurdon J.B, Standley H., Dyson S., Butler K., Langon T., et al. (1999). Single cells can sense their position in a morphogen gradient. Development. 126: 5309-5317.

Gustafson T. (1965). In: The Biochemistry of Development. Weber E. (ed.). Academic Press. New York, NY. p.139.

Han C., Belenkaya T.Y., Wang B., Lin X. (2004). Drosophila glypicans control the cell-to-cell movement of Hedgehog by a dynamin-independent process. Development. 131: 601-611.

Harfe B.D., Scherz P.J., Nissim S., Tian H., McMahon A.P., et al. (2004). Evidence for an expansion-based temporal Shh gradient in specifying vertebrate digit identities. Cell. 118: 517-528.

Harvey S.A., Smith J.C. (2009). Visualisation and quantification of morphogen gradient formation in the Zebrafish. PLoS Biol. 7: e1000101.

He F., Wen Y., Cheung D., Deng J., Lu L.J., et al. (2010). Distance measurements via the morphogen gradient of Bicoid in Drosophila embryos. BMC Dev Biol.10: 80.

He F., Wen Y., Deng J., Lin X., Lu L.J., et al. (2008). Probing intrinsic properties of a robust morphogen gradient in Drosophila. Dev Cell. 15: 558-567.

Hepker J., Blackman R.K., Holmgren R. (1999). Cubitus interruptus is necessary but not sufficient for direct activation of a wing-specific decapentaplegic enhancer. Development. 126: 3669-3677.

Ho K.S., Suyama K., Fish M., Scott M.P. (2005). Differential regulation of Hedgehog target gene transcription by Costal2 and Suppressor of Fused. Development. 132: 1401-1412.

Holloway D.M, Harrison L.G, Kosman D, Vanario-Alonso C.E, Spirov A.V. (2006). Analysis of pattern precision shows that Drosophila segmentation develops substantial independence from gradients of maternal gene products. Dev Dyn. 235: 2949-2960.

Horstadius S. (1939). The mechanics of sea urchin development, studied by operative method. Biol Rev. 14: 132–179.

Houchmandzadeh B., Wieschaus E., Liebler S. (2002). Establishment of developmental precision and proportions in the early Drosophila embryo. Nature. 415: 798-802.

Hsiung F., Ramirez-Weber F.A., Iwaki D.D., Kornberg T.B. (2005). Dependence of Drosophila wing imaginal disc cytonemes on Decapentaplegic. Nature. 437: 560–563.

Huang A.M., Rusch J., Levine M. (1997). An anteroposterior Dorsal gradient in the Drosophila embryo. Genes Dev. 11: 1963-1973.

Huangfu D., Liu A., Rakeman A.S. , Murcia N.S., Niswander L., Anderson K.V. (2003). Hedgehog signalling in the mouse requires intraflagellar transport proteins. Nature. 426: 83-87.

Huxley J.S., de Beer G.R. (1934). The Elements of Experimental Embryology. Cambridge University Press. Cambridge, UK.

Ibañes M., Izpisúa-Belmonte J.C. (2008). Theoretical and experimental approaches to understand morphogen gradients. Mol Syst Biol. 4: 176.

Imler J.L., Zheng L. (2004). Biology of Toll receptors: lessons from insects and mammals. J Leukoc Biol. 75: 18-26.

Ingham P.W., McMahon A.P. (2001). Hedgehog signaling in animal development: paradigms and principles. Genes Dev. 15: 3059-3087.

Ip Y.T., Park R.E., Kosman D., Bier E., Levine M. (1992). The dorsal gradient morphogen regulates stripes of rhomboid expression in the presumptive neuroectoderm of the Drosophila embryo. Genes Dev. 6: 1728-1739.

Jacob F., Monod J. (1961). Genetic regulatory mechanisms in the synthesis of proteins. J Mol Biol. 3: 318-356.

Jaeger J., Reinitz J. (2006). On the dynamic nature of positional information. Bioessays. 28: 1102-11.

Jaeger J., Surkova S., Blagov M., Janssens H., Kosman D., et al. (2004) Dynamic control of positional information in the early Drosophila embryo. Nature. 430: 368–371.

Jazwinska A., Rushlow C., Roth S. (1999). The role of brinker in mediating the graded response to Dpp in early Drosophila embryos. Development. 126: 3323–3334.

Jaźwińska A., Rushlow C., Roth S. (1999). The role of brinker in mediating the graded response to Dpp in early Drosophila embryos. Development. 126: 3323-3334.

Jeong J., McMahon A.P. (2005). Growth and pattern of the mammalian neural tube are governed by partially overlapping feedback activities of the hedgehog antagonists Patched1 and Hhip1. Development. 132: 143-154.

Jia J., Tong C,, Wang B., Luo L., Jiang J. (2004). Hedgehog signalling activity of Smoothened requires phosphorylation by protein kinase A and casein kinase I. Nature 432: 1045-1050.

Jiang J., Hui C.C. (2008). Hedgehog signaling in development and cancer. Dev Cell. 15: 801-812.

Jiang J., Kosman D., Ip Y.T., Levine M. (1991). The dorsal morphogen gradient regulates the mesoderm determinant twist in early Drosophila embryos. Genes Dev. 5: 1881-1891.

Johnson R.L., Grenier J.K., Scott M.P. (1995). patched overexpression alters wing disc size and pattern: transcriptional and post-transcriptional effects on hedgehog targets. Development 121: 4161-4170.

Kanodia J.S., Rikhy R., Kim Y., Lund V.K., DeLotto R., et al. (2009). Dynamics of the Dorsal morphogen gradient. Proc Natl Acad Sci USA. 106: 21707-21712.

Kent D., Bush E.W., Hooper J.E. (2006). Roadkill attenuates Hedgehog responses through degradation of Cubitus interruptus. Development. 133: 2001-2010.

Kicheva A., González-Gaitán M. (2008). The Decapentaplegic morphogen gradient: a precise definition. Curr Opin Cell Biol. 20: 137-143.

Kicheva A., Pantazis P., Bollenbach T., Kalaidzidis Y., Bittig T., Jülicher F., González-Gaitán M. (2007). Kinetics of morphogen gradient formation. Science. 315: 521-525.

Kitano H. (2002). Systems biology: a brief overview. Science. 295: 1662-1664.

Kondo S., Asai R. (1995). A reaction-diffusion wave on the skin of the marine angelfish Pomacanthus. Nature. 376: 765-768.

Kornberg T.B., Guha A. (2007). Understanding morphogen gradients: a problem of dispersion and containment. Curr Opin Genet Dev. 17: 264-271.

Kreutz C., Timmer J. (2009). Systems biology: experimental design. FEBS J. 276: 923-942.

Kruger U., Zhang J., Xie L. (2007). Developments and applications of nonlinear Principal Component Analysis: A review. In: Principal manifolds for data visualization and dimension-reduction, Gorban A., et al. (eds.) pp. 1-44. Berlin-Heidelberg: Springer.

Kutejova E., Briscoe E., Kicheva A. (2009). Temporal dynamics of patterning by morphogen gradients. Curr Opin Genet Dev. 19: 315-322.

Lai K., Robertson M.J., Schaffer D.V. (2004). The sonic hedgehog signaling system as a bistable genetic switch. Biophys J. 86: 2748–2757.

Lander A.D., Nie Q., Wan F.Y. (2002). Do morphogen gradients arise from diffusion? Dev Cell. 2: 785-796.

Lander A.D. (2007). Morpheus unbound: reimagining the morphogen gradient. Cell. 128: 245-256.

Lawrence P.A. (1966). Development and determination of hairs and bristles in the milkweed bug, Oncopeltus fasciatus (Lygaeidae, Hemiptera). J Cell Sci. 1: 475-498.

Lawrence P.A. (1992). The Making of a Fly. Blackwell Publishing. Oxford, UK.

Lawrence P.A. (2001). Morphogens: how big is the big picture? Nat Cell Biol. 3: E151-154.

Lawrence P.A., Struhl G. (1996). Morphogens, compartments, and pattern: lessons from Drosophila? Cell. 85: 951–961.

Levine M., Davidson E.H. (2005). Gene regulatory networks for development. Proc Natl Acad Sci U S A. 102: 4936-4942.

Lewis J., Slack J.M., Wolpert L. (1977). Thresholds in development. J Theor Biol. 65: 579–590.

Liberman L.M., Reeves G.T., Stathopoulos A. (2009). Quantitative imaging of the Dorsal nuclear gradient reveals limitations to threshold-dependent patterning in Drosophila. Proc Natl Acad Sci USA. 106: 22317-22322.

Lott S.E., Kreitman M., Palsson A., Alekseeva E., Ludwig M.Z. (2007). Canalization of segmentation and its evolution in Drosophila. Proc Natl Acad Sci USA. 104: 10926-10931.

Ma C., Zhou Y., Beachy P.A., Moses K. (1993). The segment polarity gene hedgehog is required for progression of the morphogenetic furrow in the developing Drosophila eye. Cell. 75: 927-938.

McGuire S.E., Roman G., Davis R.L. (2004). Gene expression systems in Drosophila: a synthesis of time and space. Trends Genet. 20: 384-391.

McHale P., Rappel W.J., Levine H. (2006). Embryonic pattern scaling achieved by oppositely directed morphogen gradients. Phys Biol. 3: 107-120.

Meinhardt H. (1978). Space-dependent cell determination under the control of a morphogen gradient. J Theor Biol. 74: 307-321.

Meinhardt, H. (1983). Cell determination boundaries as organizing regions for secondary

embryonic fields. Dev Biol. 96: 375-385.

Meinhardt H. (2004). Different strategies for midline formation in bilaterians. Nat Rev Neurosci. 5: 502-510.

Methot N., Basler K. (1999). Hedgehog controls limb development by regulating the activities of distinct transcriptional activator and repressor forms of Cubitus interruptus. Cell. 96: 819-831.

Methot N., Basler K. (2001). An absolute requirement for Cubitus interruptus in Hedgehog signaling. Development. 128: 733-742.

Morata G., Lawrence P.A. (1975). Control of compartment development by the engrailed gene in Drosophila. Nature. 255: 614-617.

Morgan T.H. (1934). Embryology and Genetics. Columbia University Press. New York, NY.

Morgan T.H. (1897). Regeneration in oligochaete worms. Science. 6: 692-693.

Morisato D. (2001). Spätzle regulates the shape of the Dorsal gradient in the Drosophila embryo. Development. 128: 2309-2319.

Moussian B., Roth S. (2005). Dorsoventral axis formation in the Drosophila embryo--shaping and transducing a morphogen gradient. Curr Biol. 15: 887-899.

Müller B., Basler K. (2000). The repressor and activator forms of Cubitus interruptus control Hedgehog target genes through common generic gli-binding sites. Development. 127: 2999-3007.

Mullor J.L., Calleja M., Capdevila J., Guerrero I. (1997). Hedgehog activity, independent of decapentaplegic, participates in wing disc patterning. Development. 124: 1227-1237.

Mullor J.L., Guerrero I. (2000). A gain-of-function mutant of patched dissects different responses to the hedgehog gradient. Dev Biol. 228: 211-224.

Nahmad M., Stathopoulos A. (2009). Dynamic interpretation of Hedgehog signaling in the Drosophila wing disc. PLoS Biol. 7: 1000202; DOI:10.1371/journal. pbio.1000202.

Nakagoshi H., Shirai T., Nabeshima Y., Matsuzaki F. (2002). Refinement of wingless expression by a wingless- and notch-responsive homeodomain protein, defective proventriculus. Dev Biol. 249: 44-56.

Nedham J. (1942). Biochemistry and Morphogenesis. Cambridge University Press. Cambridge, UK.

Nellen D., Burke R., Struhl G., Basler K. (1996). Direct and long-range action of a DPP morphogen gradient. Cell. 85: 357-368.

Nilson L.A., Schüpbach T. (1998). Localized requirements for windbeutel and pipe reveal a dorsoventral prepattern within the follicular epithelium of the Drosophila ovary. Cell. 93: 253-262.

Nusslein-Volhard C., Wieschaus E. (1980). Mutations affecting segment number and polarity in Drosophila. Nature. 287: 795–801.

Oates A.C., Gorfinkiel N., González-Gaitán M., Heisenberg C.P. (2009). Quantitative approaches in developmental biology. Nat Rev Genet. 10: 517-530.

Pan D.J., Huang J.D., Courey A.J. (1991). Functional analysis of the Drosophila twist

promoter reveals a dorsal-binding ventral activator region. Genes Dev. 5: 1892-1901.

Panakova D., Sprong H., Marois E., Thiele C., Eaton S. (2005). Lipoprotein particles are required for Hedgehog and Wingless signalling. Nature. 435: 58–65.

Peri F., Technau M., Roth S. (2002). Mechanisms of Gurken-dependent pipe regulation and the robustness of dorsoventral patterning in Drosophila. Development. 129: 2965-2975.

Price J.V., Clifford R.J., Schüpbach T. (1989) The maternal ventralizing locus torpedo is allelic to faint little ball, an embryonic lethal, and encodes the Drosophila EGF receptor homolog. Cell. 56: 1085-1092.

Reach M., Galindo R.L., Towb P., Allen J.L., Karin M., Wasserman S.A. (1996). A gradient of cactus protein degradation establishes dorsoventral polarity in the Drosophila embryo. Dev Biol. 180: 353-364.

Reeves G.T., Stathopoulos A. (2009). Graded dorsal and differential gene regulation in the Drosophila embryo. Cold Spring Harb Perspect Biol. 1: a000836.

Reversade B., De Robertis E.M. (2005). Regulation of ADMP and BMP2/4/7 at opposite embryonic poles generates a self-regulating morphogenetic field. Cell. 123: 1147-1160.

Riddle R.D., Johnson R.L., Laufer E., Tabin C. (1993). Sonic hedgehog mediates the polarizing activity of the ZPA. Cell. 75: 1401–1416.

Roberts P. (1964). Mosaics Involving Aristapedia, a Homeotic Mutant of Drosophila melanogaster. Genetics. 49: 593-598.

Robertson F.W. (1963). The ecological genetics of growth in *Drosophila*. VI. The genetic correlation between the duration of the larval period and body size in relation to larval diet. Gene Res Camb. 4: 74-92.

Roelink H., Porter J.A., Chiang C., Tanabe Y., Chang D.T., et al. (1995). Floor plate and motor neuron induction by different concentrations of the amino-terminal cleavage product of sonic hedgehog autoproteolysis. Cell. 81: 445-455.

Roth S., Stein D., Nüsslein-Volhard C. (1989). A gradient of nuclear localization of the dorsal protein determines dorsoventral pattern in the Drosophila embryo. Cell. 59: 1189-1202.

Rushlow C.A., Han K., Manley J.L., Levine M. (1989). The graded distribution of the dorsal morphogen is initiated by selective nuclear transport in Drosophila. Cell. 59: 1165-1177.

Rushlow C., Frasch M., Doyle H., Levine M. (1987). Maternal regulation of zerknüllt: a homoeobox gene controlling differentiation of dorsal tissues in Drosophila. Nature. 330: 583-586.

Saha K., Schaffer D.V. (2006). Signal dynamics in Sonic Hedgehog tissue patterning. Development. 133: 889-900.

Sander K. (1994). Of gradients and genes: Developmental concepts of Theodor Boveri and his students. Dev Genes Evol. 203: 295-297.

Schejter E.D., Shilo B.Z. (1989). The Drosophila EGF receptor homolog (DER) gene is allelic to faint little ball, a locus essential for embryonic development. Cell. 56: 1093-

1104.

Scherz P.J., McGlinn E., Nissim S., Tabin C.J. (2007). Extended exposure to Sonic hedgehog is required for patterning the posterior digits of the vertebrate limb. Dev Biol. 308: 343-354.

Sen J., Goltz J.S., Stevens L., Stein D. (1998). Spatially restricted expression of pipe in the Drosophila egg chamber defines embryonic dorsal-ventral polarity. Cell. 95: 471-81.

Shimizu K., Gurdon J.B. (1999). A quantitative analysis of signal transduction from activin receptor to nucleus and its relevance to morphogen gradient interpretation. Proc Natl Acad Sci U S A. 96: 6791-6796.

Shinar G., Feinberg M. (2010). Structural sources of robustness in biochemical reaction networks. Science. 327: 1389-1391.

Smith J., Thoedoris C., Davidson E.H. (2007). A gene regulatory network subcircuit drives pattern of gene expression. Science. 318: 794-797.

Sondhi K.C. (1963). The biological foundations of animal patterns. Q Rev Biol. 38: 289-327.

Spemann H. (1938). Embryonic Development and Induction. Yale University Press. New Haven, CT.

Spemann H, Mangold H. (1924). Induction of embryonic primordia by implantation of organizers from a different species. Roux's Arch Entw Mech. 100: 599-638.

Stathopoulos A., Levine M. (2002). Linear signaling in the Toll-Dorsal pathway of

Drosophila: activated Pelle kinase specifies all threshold outputs of gene expression while the bHLH protein Twist specifies a subse.D evelopment. 129: 3411-3419.

Stathopoulos A., Levine M. (2005). Genomic regulatory networks and animal development. Dev Cell. 9:449-462.

Stern C. (1954). Genes and developmental patterns. Proc. 9th Internat Cong Genetics. Part 1. pp. 355-369.

Steward R. (1989). Relocalization of the dorsal protein from the cytoplasm to the nucleus correlates with its function. Cell. 59: 1179-1188.

Strigini M., Cohen S.M. (1997). A Hedgehog activity gradient contributes to AP axial patterning of the Drosophila wing. Development. 124: 4697-4705.

Strutt H., Thomas C., Nakano Y., Stark D., Neave B., et al. (2001). Mutations in the sterol-sensing domain of Patched suggest a role for vesicular trafficking in Smoothened regulation. Curr Biol. 11: 608-613.

Stumpf H.F. (1966). Mechanism by which cells estimate their location within the body. Nature. 212: 430-431.

Stumpf H.F. (1967). On positional determination of cuticle zones within a segment of Galleria mellonella. Dev Biol. 16: 144-167.

Sturmfels B. (2005). Can biology lead to new theorems? Clay Mathematics Institute Annual Report .

Su V.F., Jones K.A., Brodsky M., The I. (2007). Quantitative analysis of Hedgehog gradient formation using an inducible expression system. BMC Dev Biol. 7: 43.

Tabata T., Takei Y. (2004). Morphogens, their identification and regulation. Development. 131: 703-712.

Taipale J., Cooper M.K., Maiti T., Beachy P.A. (2002). Patched acts catalytically to suppress the activity of Smoothened. Nature. 418: 892-897.

Tanimoto H., Itoh S., ten Dijke P., Tabata T. (2000). Hedgehog creates a gradient of DPP activity in Drosophila wing imaginal discs. Mol Cell. 5: 59-71.

Thompson C.R., Reichelt S., Kay R.R. (2004). A demonstration of pattern formation without positional information in Dictyostelium. Dev Growth Differ. 46: 363-369.

Tokunaga C. (1978). Genetic mosaic studies in Drosophila melanogaster, with special reference to the prepattern hypothesis. In: Genetic Mosaics and Cell Differentiation. Gehring W.J. (ed.). Springer-Verlag. Berlin, Germany. pp. 157-204.

Tomlin C.J, Axelrod J.D. (2007). Biology by numbers: mathematical modelling in developmental biology. Nat Rev Genet. 8: 331-340.

Torroja C., Gorfinkiel N., Guerrero I. (2004). Patched controls the Hedgehog gradient by endocytosis in a dynamin-dependent manner, but this internalization does not play a major role in signal transduction. Development. 131: 2395-2408.

Towb P., Galindo R.L., Wasserman S.A. (1998). Recruitment of Tube and Pelle to signaling sites at the surface of the Drosophila embryo. Development. 125: 2443-2550.

Towers M., Mahood R., Yin Y., Tickle C. (2008). Integration of growth and specification in chick wing digit-patterning. Nature. 452: 882-886.

Turing A.M. (1952). The chemical basis of morphogenesis. Phil Trans R Soc Lond B Biol Sci. 237: 37-72.

Varjosalo M., Taipale J. (2008). Hedgehog: functions and mechanisms. Genes Dev. 22: 2454-2472.

Vervoort M. (2000). Hedgehog and wing development in Drosophila: a morphogen at work? Bioessays. 22: 460-468.

Vervoort M., Crozatier M., Valle D., Vincent A. (1999). The COE transcription factor Collier is a mediator of short-range Hedgehog-induced patterning of the Drosophila wing. Curr Biol. 9: 632-639.

von Dassow G., Meir E., Munro E.M., Odell G.M. (2000). The segment polarity network is a robust developmental module. Nature. 406: 188-192.

von Ohlen T., Doe C.Q. (2000). Convergence of dorsal, dpp, and egfr signaling pathways subdivides the drosophila neuroectoderm into three dorsal-ventral columns. Dev Biol. 224: 362-372.

Waddington C.H. (1940). Organisers and Genes. Cambridge University Press. Cambridge, UK.

Waddington C.H. (1956). Principles of Embryology. George Allen & Unwin. London, UK.

Witkowski J. (1985). The hunting of the organizer: an episode in biochemical embryology. TIBS. 10: 379–381.

Wolpert L. (1968). The French Flag problem: a contribution to the discussion on pattern development and regulation. In: Waddington C.H. (ed.). Towards a theoretical biology. Edinburgh University Press. Edinburgh, UK. pp. 125–133.

Wolpert L. (1969). Positional information and the spatial pattern of cellular differentiation. J Theor Biol. 25: 1-47.

Wolpert L. (1971). Positional information and pattern formation. Curr Top Dev Biol. 6: 183-224.

Yi T. M., Huang Y., Simon M. I., Doyle J. (2000). Robust perfect adaptation in bacterial chemotaxis through integral feedback control. Proc Natl Acad Sci USA. 97: 4649-4653.

Yu S.R., Burkhardt M., Nowak M., Ries J., Petrásek Z., et al. (2009). Fgf8 morphogen gradient forms by a source-sink mechanism with freely diffusion molecules. Nature. 461: 533-536.

Zhang Q., Zhang L., Wang B., Ou C.Y., Chien C.T., Jiang J. (2006). A hedgehog-induced BTB protein modulates hedgehog signaling by degrading Ci/Gli transcription factor. Dev Cell. 10: 719-729.

Zhao Y., Tong C., Jiang J. (2007). Hedgehog regulates smoothened activity by inducing a conformational switch. Nature. 450: 252-258.

Zhu A.J., Scott M.P. (2004). Incredible journey: how do developmental signals travel through tissue? Genes Dev. 18: 2985-2997.

Appendices

Supporting Materials for Chapter 2

Supporting Text

Justification of assumptions

We modeled Hh signaling in the wing disc using a system of nonlinear partial differential equations [Equations (2.1)-(2.5)]. The general form of the equations is similar to previous morphogen models of the wing disc [1,2,3,4,5]. Here we discuss the approximations used in the formulation of our mathematical model.

Disc Geometry. Wing discs in *Drosophila* are approximately flat larval tissues. We assumed that anterior-posterior (AP) patterning of the disc can be modeled as a one-dimensional system. Because Hh crosses into the anterior compartment from all positions along the AP boundary, a one-dimensional domain is a good approximation of the complicated disc geometry [6]. The subdivision of wing discs into compartments is much more than a convenient definition. The posterior compartment is defined by the expression of the selector gene *engrailed* and cell populations from different compartments do not seem to intermix during development [7]. Thus, the concepts of compartments and AP boundary are well defined in the system. The AP axis of a third instar wing discs is about 200 μm (~80 cells) long [8,9]. We assumed that the AP boundary divides this one-dimensional domain into two equal parts (of 100 μm each).

From our images, this seems a fair approximation. We do not expect that any of these approximations of the disc geometry affect the conclusions of this study.

Disc Growth. Cells in third instar wing discs proliferate in a uniform manner, approximately one division every 8 hours [10]. Since the time-scale of cell proliferation is slow compared to morphogen gradient formation [11,12], in our model we assumed that patterning and growth can be decoupled, and discs are assumed to have a fixed size. A study suggests that the Dpp gradient in the wing disc is not affected by disc growth [13]. Since the Hh gradient specifies the source of the Dpp gradient, it is likely that the Hh gradient is also not affected by disc growth. It is unclear when the Hh gradient forms during wing disc development. However, as the range of Hh is relatively short, the results do not depend on a precise size/stage of the discs.

Equations. *hedgehog* is transcriptionally activated in every posterior cell by the selector gene *engrailed* and we assume that Hh is produced and secreted at a constant rate in all cells of the posterior compartment [Equation (2.1)]. Hh transport into the anterior compartment is a complex process and requires heparan-sulfate proteoglycans and lipoproteins [14,15], but it is mainly transported extracellularly and not by sequential rounds of dynamin-dependent endocytosis/exocytosis [16,17]. We assume that this transport process can be modeled as an effective diffusion process [Equation (2.1)]. This seems to be a good approximation [4,6].

Ligand-Receptor binding reaction is modeled as a mass-action law; in this case, the rate of Hh_Ptc formation is proportional to the product of [Hh] and [Ptc] [Equations

(2.1)-(2.3)]. Because upon Hh binding to Ptc, the Hh_Ptc complex is internalized and targeted to degradation [16], we modeled the Hh+Ptc→ Hh_Ptc reaction as irreversible, i.e., once the Hh_Ptc complex is formed and internalized, the Ptc receptor cannot be reused and the Hh ligand cannot be re-secreted [Equation (2.1)]. This assumption is supported by experimental data [16], but in any case, assuming that the reaction Hh_Ptc→Hh+Ptc occurs at a slow rate (compared to the inverse reaction) it does not affect the conclusions of this study (data not shown). We modeled the distribution of the receptor Ptc, both mRNA and protein, in space and time. *ptc* is constitutively present at low levels in the anterior compartment, but in addition, it is transcriptionally upregulated by Hh signaling. Hh-dependent *ptc* transcription is modeled using a Hill function that depends on the levels of signaling activity, here represented by the variable [Signal] [Equation (2.1)]. In Equation (2.3), the rate of *ptc* translation is assumed proportional to [*ptc*] as in other studies [18].

A molecular model of how Smo activation depends on Ptc and Hh_Ptc is missing, but a study has reported the ability of Hh-Ptc complexes to titrate the inhibition of Ptc on signal activation [19]. We use these phenomenological observations to model the rate of "Signal" activation as a Hill function of the [Hh_Ptc] to [Ptc] ratio [Equation (2.5)]. Although the choice of this Hill function is not directly justified by chemical reactions, experimental data suggests that the rate of "Signal" activation is a saturation curve that depends on the [Hh_Ptc] to [Ptc] ratio [19] (see also Fig. 2.1D). Numerical simulations suggest that other choices of sigmoid curves do not affect our conclusions (data not shown). We do not include equations for other Hh target genes in Figure 2.1B because their profiles are only outputs of the system and are not required for the analysis.

Initial and Boundary Conditions. The initial conditions of the system are unclear, since many of the genes involved in Hh signaling may be expressed early in wing disc development. Nevertheless, we administered the initial conditions which are demonstrated sufficient to rescue patterning to approximate wild-type conditions when the system is reinitialized artificially using the *hh* temperature sensitive mutation hh^{ts2} [20]. Since *ptc* is expressed in a Hh-independent way at low levels in the anterior compartment, we set the following initial conditions (I.C.) for [*ptc*] and [Ptc],

(I.C. 1) $[ptc](x,0) = \dfrac{S^{+}(x)\alpha_{ptc0}}{\beta_{ptc}} = \dfrac{\alpha_{ptc0}}{\beta_{ptc}}$ for $x > 0$, and zero otherwise,

(I.C. 2) $[\mathrm{Ptc}](x,0) = \dfrac{T_{\mathrm{Ptc}}}{\beta_{\mathrm{Ptc}}}[ptc](x,0)$.

All other terms in the mathematical model are set to zero initially. Unlike other theoretical studies [3,6], we have explicitly included the posterior compartment in our model and simulations. This simplifies (and makes irrelevant) the choice of the posterior boundary condition. Also, because the range of the Hh gradient is short compared to the size of the anterior compartment, the results are largely independent of the choice of the anterior boundary condition. In our simulations, we use zero-flux boundary conditions (B.C.) at $x = \pm 100$ μm,

(B.C.) $\left.\dfrac{\partial[\mathrm{Hh}]}{\partial x}\right|_{x=-100} = \left.\dfrac{\partial[\mathrm{Hh}]}{\partial x}\right|_{x=100} = 0$.

Parameters

The parameter values used in the computer simulations of Equations (2.1)-(2.5) are reported in Supporting Table 2.1. Parameter values were either extracted from the

literature, or estimated from experimental or empirical measurements. In this section, we discuss the estimation of those parameters that are not extracted explicitly from the literature. Third instar wing disc cells have an approximate diameter of 2.5 μm and an approximate volume of 2×10^{-14} litres [6]. When parameters are reported in other units, we use these factors to convert parameters into units of Molar.

Hh effective diffusion coefficient *(D).* The Hh diffusion coefficient has not been measured. For Dpp and Wingless in the wing disc, reported values are 0.1 and 0.5 $\mu m^2/s$, respectively. Hh transport seems more similar to that of Wingless, which also requires lipoparticles [15]. Therefore, we estimated $D = 0.5\ \mu m^2/s$.

Hh production-secretion rate *(α_{Hh}).* We assumed that extracellular levels of Hh are about 1μM in the posterior compartment; this is similar to the levels of Dpp in the source of the Dpp gradient. Since the maximum levels of Hh, Hh_{Max}, are given by $Hh_{Max} = \frac{\alpha_{Hh}}{\beta_{Hh}}$, we have that $\alpha_{Hh} = (1\ \mu M)\beta_{Hh}$.

Hh-Ptc association rate *(γ_{Hh_Ptc}).* We use $\gamma_{Hh\_Ptc} = 0.12\ \mu M^{-1}\ s^{-1}$ as used for analysis of the Dpp system [6].

Hh degradation rate *(β_{Hh}).* The characteristic space-constant, λ, of an exponential concentration gradient is formally defined as the distance at which the concentration drops by a factor of 1/e of its maximal intensity. For a morphogen gradient established by diffusion (D) and linear degradation (β), we have $\lambda^2 = \frac{D}{\beta}$. However, if in addition, Hh is degraded by binding its receptor, we have that the space constant is

$\lambda_{Hh} \approx \sqrt{\frac{D}{\beta_{Hh} + \gamma_{Hh\_Ptc} < Ptc >}}$ where <Ptc> is the average unoccupied Ptc receptors in the Hh operating domain. Based on computer simulations, we estimated an average of 65% unoccupied Ptc. Studies have reported $\lambda_{Hh} \approx 3.5$ μm [21], which permits the following estimation, $\beta_{Hh} \approx \frac{D_{Hh}}{\lambda_{Hh}^2} - \gamma_{Hh} < Ptc >= 3.4 \times 10^{-3}$ s^{-1}.

ptc translation rate (T_{Ptc}). The control of mRNA translation is precisely regulated in different eukaryotic cells. For example, the rate of rabbit globin translation when globin mRNA is injected into Xenopus oocytes is 110 globin proteins per mRNA molecule per hour [22], and this number does not appear to change in different embryonic stages or cell types [23]. Since rabbit globin mRNA is 650 base pairs (bp) [24], we estimated that the rate of translation in eukaryotes is about 20 bp/sec. Thus, T_{Ptc} is obtained using this estimated rate of translation as well as information that the *ptc* mRNA is 5535 bp in length (www.flybase.org).

Ptc and Hh_Ptc degradation rates (β_{Ptc} and $\beta_{Hh\ Ptc}$). It has been proposed that Ptc internalization and degradation is independent of Hh binding [25]. Therefore, we assume that $\beta_{Ptc} = \beta_{Hh\_Ptc}$. We use the receptor degradation rate measured in other vertebrate receptors which is consistent with the rapid turnover of Ptc when Hh signaling is shut off in hh^{ts2} discs [8].

ptc transcription rate (α_{ptc} and α_{ptc0}). In our experiments, Ptc is detected as soon as 2 hours after Hh signal is recovered (Fig. 2.2E) suggesting that [*ptc*] levels can build up within 2 hours. Maximum receptor levels in this system have been estimated at approximately 1,600 per cell [6]; this gives 0.48 μM. Therefore, we can estimate *ptc*

maximum levels as $\frac{\alpha_{ptc}}{\beta_{ptc}} = \frac{(0.48\ \mu\text{M})\beta_{\text{Ptc}}}{T_{\text{Ptc}}} = 0.2\ \mu\text{M}$. If these levels can be reached within approximately 2 hours, then the rate of *ptc* activation is $\alpha_{ptc} = \frac{0.2\ \mu\text{M}}{7200\ \text{s}} \approx 2.7 \times 10^{-5}\ \mu\text{M s}^{-1}$. Finally, the Hh-independent levels in the anterior compartment are about 7-fold lower than in the Hh-induced *ptc* domain [19]. Therefore, we set $\alpha_{ptc0} = \frac{\alpha_{ptc}}{7}$.

ptc degradation rate (β_{ptc}). From the previous computation, $\beta_{ptc} = \frac{\alpha_{ptc}}{0.2\ \mu\text{M}} \approx 1.4 \times 10^{-4}\ \text{s}^{-1}$.

"Signal" activation rate (α_{Signal}). We assume that signal activity depends on the rates of Smo phosphorylation. The maximum levels of pSmo are assumed to be 0.3 μM. Denef et al. [26] showed that a pSmo replaces unphosphorylated Smo within 30 minutes after exposure to Hh in cell culture [26]. Therefore, we estimate $\alpha_{\text{Signal}} = \frac{0.3\ \mu\text{M}}{1800\ \text{s}} \approx 1.7 \times 10^{-4}\ \mu\text{M s}^{-1}$.

"Signal" degradation rate (β_{Signal}). From the last expression, we obtain, $\beta_{\text{Signal}} = \frac{\alpha_{\text{Signal}}}{0.3\mu\text{M}} \approx 5.5 \times 10^{-4}\ \text{s}^{-1}$.

[Signal] level required for *ptc* half-maximal activation (k_{ptc}). We simulated the system and found a value of k_{ptc} to support a *ptc* domain which is 5 cells wide.

Hh_Ptc:Ptc ratio required for half-maximal activation of Signal (k_{Signal}). Casali and Struhl suggested that this ratio is approximately two [19].

Hill coefficients (m and n). We set m=3 [2]. In the text (see also discussion below), we estimated n > 6.8, (n > 4.0 in the more stringent scenario). In all the simulations, however (except for Figure 2.1C), n was set to 6.8.

Steady-State analysis

At the steady state, it is possible to reduce the full model [Equations (2.1-2.5)] to a single equation of [Hh]. Setting the right-hand side of Equations (2.1-2.5) to zero, and making the necessary algebraic substitutions we obtain the following boundary-value problem

$$D\frac{d^2[\mathrm{Hh}]_{\mathrm{ss}}}{dx^2} + S^{-}(x)\alpha_{\mathrm{Hh}} - \frac{\chi\,[\mathrm{Hh}]_{\mathrm{ss}}}{\beta_{\mathrm{Ptc}} + \gamma_{\mathrm{Hh\_Ptc}}[\mathrm{Hh}]_{\mathrm{ss}}}\left[S^{+}(x)\alpha_{ptc0} + \frac{\alpha_{ptc}[\mathrm{Hh}]_{\mathrm{ss}}^{nm}}{\eta\left[\kappa^n + [\mathrm{Hh}]_{\mathrm{ss}}^n\right]^m + [\mathrm{Hh}]_{\mathrm{ss}}^{nm}}\right] - \beta_{\mathrm{Hh}}[\mathrm{Hh}]_{\mathrm{ss}} = 0, \quad \text{(S1)}$$

with $\chi = \frac{T_{\mathrm{Ptc}}\gamma_{\mathrm{Hh\_Ptc}}}{\beta_{ptc}}$, $\kappa = \frac{k_{\mathrm{Signal}}\beta_{\mathrm{Hh\_Ptc}}}{\gamma_{\mathrm{Hh\_Ptc}}}$, and $\eta = \frac{k_{ptc}\beta_{\mathrm{Signal}}}{\alpha_{\mathrm{Signal}}}$, and satisfying the boundary conditions $\left.\frac{\mathrm{d}[\mathrm{Hh}]_{\mathrm{ss}}}{\mathrm{d}x}\right|_{x=-100} = \left.\frac{\mathrm{d}[\mathrm{Hh}]_{\mathrm{ss}}}{\mathrm{d}x}\right|_{x=100} = 0.$

Equation (S1) is still difficult to solve analytically but can be used to compute steady-state profiles numerically. The solution of the full model [Equations (2.1)-(2.5)] approaches the steady-state solution of the last equation and is practically undistinguishable after 8 hours of simulation time (data not shown).

At the steady state, it is also possible to write each variable as an explicit function of $[\mathrm{Hh}]_{\mathrm{ss}}$. An example is the steady-state profile of $[\mathrm{Signal}]_{\mathrm{ss}}$ as a function of the extracellular gradient $[\mathrm{Hh}]_{\mathrm{ss}}$ [Equation (2.6)]. Figure 2.1E shows that based on the estimation of the parameter *n* (Fig. 2.1D and next section), the shape of the $[\mathrm{Signal}]_{\mathrm{ss}}$ profile is step-like. In this situation, the parameter ε defined in Equation (2.6) can be interpreted as a 'switching threshold' (see below for discussion of this concept). If a cell experiences an extracellular concentration of Hh higher than ε, Hh signaling will be

activated in that cell, while if $[Hh]_{ss} < \varepsilon$, then that cell will not be responsive to the Hh pathway. This binary behavior of the system is, of course, only strictly true when $n \to \infty$. In practice, this is only an approximation and therefore cells that experience extracellular Hh levels similar to ε will produce 'intermediate' levels of "Signal." Therefore, it is appropriate to ask what is the size of the region expressing these 'intermediate' levels of "Signal" at steady-state when $n > 6.8$. A simple inspection of Figure 2.1E suggests that $[Signal]_{ss}$ levels change from nearly maximal to nearly minimal within < 3 cell diameters. However, it is not clear what the range of $[Signal]_{ss}$ is that can activate Hh signalling *in vivo*. Morphogen studies in *Xenopus* suggest that 100 active receptors is about the lowest signaling concentration that cells can respond to [27]. If we consider similar numbers for the signal transducer pSmo in our system (which is also a transmembrane molecule), this is about 0.03 μM. In our simulation results of Figure 2.1E, a cell at position 9 would express already lower levels of [Signal] at the steady state. Thus, according to this analysis, we estimate that [Signal] levels drop from nearly maximal to undetectable in less 3 cells. Because this estimation depends on many uncertain parameters, we cannot strictly rule out that some concentration-dependent effects contribute to some extent to the final output. In fact, the small overlap between Col and dppZ detected in Figure 2.3F may be due to a slight concentration-dependent difference between the two target genes.

The steady-state interpretation of the Hh extracellular gradient in terms of Equation (2.6) requires some additional discussion. Since [Hh] refers to free unbound Hh concentration, strictly speaking, Equation (2.6) is not the relationship that describes how cells 'translate' extracellular levels into signaling outputs because cells probably do not

have another way of sensing extracellular Hh concentrations other than by using the receptor Ptc. This does not affect any of the predictions of the model. However, it is important to clarify the meaning of some parameters. For example, the interpretation of ε as the 'switching threshold' is somehow artificial, because cells (presumably) do not have a way to 'measure' unbound extracellular [Hh]. A more appropriate definition of 'switching threshold' may be obtained using an extracellular gradient that cells can sense. Since, all steady-state variables can be written as a function of $[Hh]_{ss}$, we can define more realistic 'switching thresholds.' For example, we can write $[Ptc]_{ss}$ as a function of $[Hh]_{ss}$ and set the switching threshold to be $[Ptc]_{ss}(\varepsilon)$. The switching threshold can also be defined in terms of $[Hh\_Ptc]_{ss}$, $\frac{[Hh\_Ptc]_{ss}}{[Ptc]_{ss}}$, or other combinations. Using the ratiometric model, the natural choice of switching threshold is given by

$$\delta = \frac{[Hh\_Ptc]_{ss}(\varepsilon)}{[Ptc]_{ss}(\varepsilon)} = \frac{\gamma_{Hh\_Ptc}}{\beta_{Hh\_Ptc}}\varepsilon = k_{Signal}. \qquad \text{(S2)}$$

Note that δ and ε are linearly proportional. Indeed, the last equation is just a particular case of a more general property of the system, namely, at steady-state, Equation (2.4) can be written in the form,

$$\frac{[Hh\_Ptc]_{ss}}{[Ptc]_{ss}} = \frac{\gamma_{Hh\_Ptc}}{\beta_{Hh\_Ptc}}\,[Hh]_{ss}. \qquad \text{(S3)}$$

Therefore, defining the switching threshold as ε or δ is equivalent. Nonetheless, δ (and not ε) is used as a 'switching threshold' in Figures 2.3 and 2.5. In any case, we insist that other choices do not affect the concept or the conclusions of this study.

Ratiometric model and estimation of n

Our mathematical analysis depends on the ratiometric model of Hh signaling interpretation [19]. Since this model has caused some controversy in the literature [28], it is appropriate to discuss possible problems that may arise in this treatment. The ratiometric interpretation of Hh signaling is a phenomenological model, this is, it is based on observations about target gene expression, but does not provide a molecular mechanism of Hh signal activation. In the past, it was thought that the levels of free (unliganded) Ptc would control the activity of the signal. In this scenario, signaling activity would not change as long as levels of free Ptc are maintained constant. The ratiometric model is introduced to explain the effect of [Hh_Ptc] levels in cells with a constant background of free Ptc [19]. To a first approximation, the ratiometric model explains how cells would correct the interpretation of a certain concentration of [Ptc] levels when also expressing [Hh_Ptc], but experiments in vertebrates or in different conditions suggest that the ratiometric model is probably not applicable in general. For example, the ratiometric model may be sensitive to total levels of Ptc, as experiments in vertebrates do not seem to obey the predictions of the model [29]. If so, the ratiometric model may not explain some mutants such as *ptc* overexpression. Despite these difficulties, the ratiometric model explains Hh patterning to a good approximation under normal physiological conditions. Because our analysis is based on the wild-type and many important details about Hh transduction are unknown, we argue that for the purpose of this study, the ratiometric model may be used as a phenomenological model of Hh signal interpretation.

An additional consideration is the use of the measurements from Casali and Struhl [19] to estimate the value of n. Here, we give a formal mathematical argument of the lower-bound estimation of n in Figure 2.1D. The basic idea is that n has a geometric meaning in the graph of the Hill function for which n is the Hill coefficient; it is a measure of the steepness of the Hill function. The following proposition shows that, given two points in the curve of the Hill function, it is possible to estimate a lower-bound estimate of n.

Proposition: *Consider the function* $F(x) = \frac{\mathrm{A}x^{\mathrm{n}}}{k^{\mathrm{n}} + x^{\mathrm{n}}}$. *Let x, y be real numbers and without loss of generality take* $x \le y$. *Then,*

$$\frac{F(y) - F(x)}{y - x} \le F'(k) = \frac{\mathrm{An}}{4\mathrm{k}}$$

(If x=y, the left hand side is understood as the limit, i.e., $F'(x) \le F'(k)$*).*

Proof. *By the intermediate value theorem of calculus, there is* $x \le z \le y$ *such that*

$$\frac{F(y) - F(x)}{y - x} \le F'(z).$$

A simple computation shows that the maximum of F'(x) is reached when x=k.
This completes the proof.

Let $\mathrm{F}\left(\frac{\mathrm{Hh\_Ptc}}{\mathrm{Ptc}}\right) = \frac{100\%\left(\frac{[\mathrm{Hh\_Ptc}]}{[\mathrm{Ptc}]}\right)^{\mathrm{n}}}{k_{\mathrm{Signal}}^{n} + \left(\frac{[\mathrm{Hh\_Ptc}]}{[\mathrm{Ptc}]}\right)^{\mathrm{n}}}$. The experiments of Casali and Struhl [19] provide two data points in the graph of F as they made clones of *ptc*$^{-}$ cells in the anterior compartment expressing different amounts of the [Hh_Ptc]/[Ptc] ratio. For $\frac{[\mathrm{Hh\_Ptc}]}{[\mathrm{Ptc}]} = 1.6$, they found no detectable activation of Hh target genes, and for

$\frac{[\text{Hh\_Ptc}]}{[\text{Ptc}]} = 2.7$, they found high expression of Hh outputs. We can, therefore, apply the proposition above to obtain a lower-bound estimate of n. We assumed that F(1.6)=5% and F(2.7)=95% to represent no and full activation of the pathway up to a 5% detection error (95%). Unfortunately, Casali and Struhl did not compare gene expression levels in the $\frac{[\text{Hh\_Ptc}]}{[\text{Ptc}]} = 2.7$ clone to wild-type gene expression in the same disc, but both Col and a reporter of *dpp* appear strongly expressed in these clones [19]. Also, it is not clear whether or not signaling activity is maximal for $\frac{[\text{Hh\_Ptc}]}{[\text{Ptc}]} = 2.7$, since Casali and Struhl did not report whether or not *engrailed* was expressed in clones expressing this ratio. Therefore, the accuracy of the estimate F(2.7) = 95% is unknown. However, reasonable deviations of this choice do not affect our conclusions. For example, setting F(2.7) = 80% gives the lower-bound estimate of n to be 5.7. As other caveats can be found in the use of these data for the estimation of the value of n, we insist that to give an accurate and reliable value of n is not a result or goal of this study. Instead, our estimation of n suggests that the hypothesis that the steady-state [Signal] profile has a step-like shape is reasonable and consistent with experimental findings.

Analysis of the Hh gradient in *ptc*-TPT and *ptc*+TPT discs

Hh signaling in *ptc*-TPT discs can be simulated using our mathematical model, with the exception of Equation (2.2), which is replaced by

$$\frac{\partial[ptc]}{\partial t} = \alpha_{\text{TPT}} - \beta_{ptc}[ptc], \qquad \text{(S4)}$$

and the initial condition (I.C.1) is replaced by $[ptc](x,0) = \frac{\alpha_{\mathrm{TPT}}}{\beta_{ptc}}$. Compared to Equation (2.2), the last equation eliminates all wild-type *ptc* expression and models ubiquitous expression of *ptc* as introduced by the TPT transgene. Chen and Struhl estimated that two copies of the TPT transgene introduce Ptc levels that are less than twofold compared to the maximal levels of Ptc near the AP boundary [30]. Therefore, we set $\alpha_{\mathrm{TPT}} = \frac{\alpha_{ptc}}{5} \approx 5.4 \times 10^{-6}\ \mu\mathrm{M\ s^{-1}}$ in the numerical simulations of Hh signaling in *ptc*-TPT discs.

Regarding the levels introduced by the TPT transgene, it is important to clarify that in a previous report it was observed that dppZ expands further anteriorly with respect to the wild-type pattern (reported as data not shown in ref. [30]). However, in our own experiments we observe that the dppZ domain is slightly reduced with respect to the wild type (Fig. 2.3B,E). This apparent discrepancy may be due by one of the following reasons. First, it is possible that the Chen and Struhl [30] used another insertion of the TPT transgene, for example, one on the second chromosome. Or second, the TPT transgene may have acquired mutations in the past decade that affected the performance of the original transgene. In any case, the predictions of the Overshoot Model are not affected by the strength of the transgene. The Overshoot Model predicts the Col and dppZ patterns to overlap regardless of whether each pattern expands or reduces with respect to the wild type.

Although the profiles shown in Figure 2.3G,H are intended as illustrations of the predictions of the Classical Morphogen Model vs. Overshoot Model in different genetic backgrounds, it is illustrative to estimate the expected size of the dppZ domain that would

not overlap with the Col pattern in *ptc*-TPT discs according to the interpretation of the Classical Morphogen Model. One way of doing this is to measure the size of the Col vs. dppZ domain in wild-type discs and use the numerical simulations to predict the expected non-overlapping region in *ptc*-TPT discs. However, this estimate will depend on the parameter values used in the simulations, as well as in our accuracy to measure the dppZ domain, which is difficult to estimate reliably because unlike Col, in wild-type discs the anterior boundary of the dppZ is not sharp (Fig. 2.3C).

Another way of estimating the difference in Col and dppZ patterns according to the Classical Morphogen model interpretation is to compare the shape of the Hh gradient in the region anterior to the Ptc/Col domain ($x > x_{\text{ptc/col}}$, with $x_{\text{ptc/col}}$ denoting the position of the anterior border of Ptc/Col, which we assume is the same throughout this analysis). As Ptc is not upregulated by Hh signaling in this region, we can assume that Ptc levels are approximately constant (denoted by $[\text{Ptc}]_A$) so that Equation (2.1) at steady-state is linear and given by

$$0 = D\frac{d^2[\text{Hh}]_{SS}}{dx^2} - \left(\gamma_{\text{Hh\_Ptc}}[\text{Ptc}]_A + \beta_{\text{Hh}}\right)[\text{Hh}]_{SS}, \qquad \text{(S5)}$$

subject to the boundary condition $[\text{Hh}]_{SS}(x_{\text{ptc}})=T_1$, which assumes that the Ptc boundary is set by a fixed concentration threshold, denoted by T_1. Equation (S5) has the following solution,

$$[\text{Hh}]_{ss}(x) = T_1 \exp\left[-\frac{x - x_{\text{ptc/col}}}{\lambda}\right] \quad (x > x_{\text{ptc/col}}), \qquad \text{(S6)}$$

where $\lambda = \sqrt{\dfrac{D}{\gamma_{\text{Hh\_Ptc}}[\text{Ptc}]_A + \beta_{\text{Hh}}}}$ is the characteristic length of the gradient. In the context of the Classical Morphogen model, λ is actually a good representation of the width of the

non-overlapping domain. Equations (S5-S6) are also valid in *ptc*+TPT and *ptc*-TPT discs provided that the constant $[Ptc]_A$ is adjusted appropriately. Thus, we can compare what are the expected differences in the Col and dppZ domains in these backgrounds according to the Classical Morphogen model. If we denote $[Ptc]_0$ the anterior Ptc levels in wild-type discs, and assume that the levels of Ptc introduced by the TPT transgene can be denoted by $[Ptc]_{TPT}$ (from measurements of an earlier study using the TPT transgene, it can been estimated that $[Ptc]_{TPT}/[Ptc]_0=1.4$), then the predicted differences in Col/Ptc and dppZ domains in different mutant backgrounds are given by:

$$\lambda_{WT} = \sqrt{\frac{D}{\gamma_{Hh\_Ptc}[Ptc]_0 + \beta_{Hh}}} \qquad \text{(in wild-type discs)}$$

$$\lambda_{ptc\text{-}TPT} = \sqrt{\frac{D}{\gamma_{Hh\_Ptc}[Ptc]_{TPT} + \beta_{Hh}}} \qquad \text{(in } ptc \text{ - TPT discs)} \qquad \text{(S7)}$$

$$\lambda_{ptc+TPT} = \sqrt{\frac{D}{\gamma_{Hh\_Ptc}([Ptc]_0 + [Ptc]_{TPT}) + \beta_{Hh}}} \qquad \text{(in } ptc + \text{TPT discs).}$$

Thus, Equations (S7) provide quantitative proof of our predictions in Figure 2.4A-C, namely, $\lambda_{ptc\text{-}TPT} > \lambda_{ptc+TPT}$ independently on the Ptc levels expressed by the TPT transgene. Our data in Figure 2.4F' show that experimentally $\lambda_{ptc+TPT}$ is at least 3 cells wide, suggesting that the non-overlapping region in *ptc*-TPT would be larger than 3 cells. This prediction is clearly not consistent with the observations in Figure 2.3F', demonstrating that the patterns in these mutant backgrounds cannot be explained by the Classical Morphogen model. Thus, this analysis provides strong support for the Overshoot model over the Classical Morphogen model in this system.

SUPPORTING REFERENCES

1. Lander AD (2007) Morpheus unbound: reimagining the morphogen gradient. Cell 128: 245-256.

2. Eldar A, Rosin D, Shilo BZ, Barkai N (2003) Self-enhanced ligand degradation underlies robustness of morphogen gradients. Dev Cell 5: 635-646.

3. Bollenbach T, Kruse K, Pantazis P, Gonzalez-Gaitan M, Julicher F (2005) Robust formation of morphogen gradients. Phys Rev Lett 94: 018103.

4. Gunbin KV, Omelyanchuk LV, Kogai VV, Fadeev SI, Kolchanov NA (2007) Model of the reception of hedgehog morphogen concentration gradient: comparison with an extended range of experimental data. J Bioinform Comput Biol 5: 491-506.

5. Nahmad M, Glass L, Abouheif E (2008) The dynamics of developmental system drift in the gene network underlying wing polyphenism in ants: a mathematical model. Evol Dev 10: 360-374.

6. Lander AD, Nie Q, Wan FY (2002) Do morphogen gradients arise by diffusion? Dev Cell 2: 785-796.

7. Garcia-Bellido A, Merriam JR (1971) Genetic Analysis of Cell Heredity in Imaginal Discs of Drosophila melanogaster. Proc Natl Acad Sci U S A 68: 2222-2226.

8. Held LI (2002) Imaginal discs : the genetic and cellular logic of pattern formation. Cambridge [England]; New York: Cambridge University Press. xv, 460 p. p.

9. Bollenbach T, Pantazis P, Kicheva A, Bokel C, Gonzalez-Gaitan M, et al. (2008) Precision of the Dpp gradient. Development 135: 1137-1146.

10. Gonzalez-Gaitan M, Capdevila MP, Garcia-Bellido A (1994) Cell proliferation patterns in the wing imaginal disc of Drosophila. Mech Dev 46: 183-200.

11. Teleman AA, Cohen SM (2000) Dpp gradient formation in the Drosophila wing imaginal disc. Cell 103: 971-980.

12. Kicheva A, Pantazis P, Bollenbach T, Kalaidzidis Y, Bittig T, et al. (2007) Kinetics of morphogen gradient formation. Science 315: 521-525.

13. Hufnagel L, Teleman AA, Rouault H, Cohen SM, Shraiman BI (2007) On the mechanism of wing size determination in fly development. Proc Natl Acad Sci U S A 104: 3835-3840.

14. Han C, Belenkaya TY, Wang B, Lin X (2004) Drosophila glypicans control the cell-to-cell movement of Hedgehog by a dynamin-independent process. Development 131: 601-611.

15. Panakova D, Sprong H, Marois E, Thiele C, Eaton S (2005) Lipoprotein particles are required for Hedgehog and Wingless signalling. Nature 435: 58-65.

16. Torroja C, Gorfinkiel N, Guerrero I (2004) Patched controls the Hedgehog gradient by endocytosis in a dynamin-dependent manner, but this internalization does not play a major role in signal transduction. Development 131: 2395-2408.

17. Su VF, Jones KA, Brodsky M, The I (2007) Quantitative analysis of Hedgehog gradient formation using an inducible expression system. BMC Dev Biol 7: 43.

18. von Dassow G, Meir E, Munro EM, Odell GM (2000) The segment polarity network is a robust developmental module. Nature 406: 188-192.

19. Casali A, Struhl G (2004) Reading the Hedgehog morphogen gradient by measuring the ratio of bound to unbound Patched protein. Nature 431: 76-80.

20. Strigini M, Cohen SM (1997) A Hedgehog activity gradient contributes to AP axial patterning of the Drosophila wing. Development 124: 4697-4705.

21. Kicheva A, Gonzalez-Gaitan M (2008) The Decapentaplegic morphogen gradient: a precise definition. Curr Opin Cell Biol 20: 137-143.

22. Gurdon JB (1974) The control of gene expression in animal development. Cambidge, Mass.: Harvard University Press.

23. Lodish HF (1976) Translational control of protein synthesis. Annu Rev Biochem 45: 39-72.

24. Gaskill P, Kabat D (1971) Unexpectedly large size of globin messenger ribonucleic acid. Proc Natl Acad Sci U S A 68: 72-75.

25. Gallet A, Therond PP (2005) Temporal modulation of the Hedgehog morphogen gradient by a patched-dependent targeting to lysosomal compartment. Dev Biol 277: 51-62.

26. Denef N, Neubuser D, Perez L, Cohen SM (2000) Hedgehog induces opposite changes in turnover and subcellular localization of patched and smoothened. Cell 102: 521-531.

27. Dyson S, Gurdon JB (1998) The interpretation of position in a morphogen gradient as revealed by occupancy of activin receptors. Cell 93: 557-568.

28. Zhu AJ, Scott MP (2004) Incredible journey: how do developmental signals travel through tissue? Genes Dev 18: 2985-2997.

29. Taipale J, Cooper MK, Maiti T, Beachy PA (2002) Patched acts catalytically to suppress the activity of Smoothened. Nature 418: 892-897.

30. Chen Y, Struhl G (1996) Dual roles for patched in sequestering and transducing Hedgehog. Cell 87: 553-563.

Supporting Protocol

The following protocol explains how the expression of Ptc was quantified to generate the concentration profiles in Fig. 2.2E. This process was followed with each image manually one at a time. The process was repeated independently twice in each image and the final result was averaged. For each time point, 4-7 discs were analyzed.

1. The original image was passed through a Gaussian filter (medfilt2 in Matlab).
2. Crop a 30X30 pixel box manually from the Posterior compartment of the filtered image and compute the average pixel intensity. This is the background intensity.
3. Subtract the background intensity to the whole filtered image.
4. Crop a 30X30 pixel box manually from the Anterior compartment (far from the AP boundary) of the filtered-background subtracted image and compute the average pixel intensity. This is the "Ptc basal intensity".
5. Crop a 20X80 pixel box that crosses the AP boundary in a place that the posterior border of Ptc looks approximately straight (as the red box in the cartoon of Figure 2.2E). Average the intensities of each of the 20 lines that are perpendicular to the AP boundary.
6. Divide the average intensity at each point by the "Ptc basal intensity". This gives the intensity profiles in units of the "Ptc basal intensity". In Figure 2E, all profiles were plotted on the same relative scale.
7. Finally, the width in Figure 2.2F is defined as the distance between the points that cross an intensity equal to 2 (this is twice the Ptc basal levels). Widths for the same time points were averaged along their standard deviation and are plotted in Figure 2.2F.

Supporting Table 2.1. Wild-type parameter values used in the numerical simulations.

Parameter	Description	Value
D	Hh diffusion coefficient	0.5 $\mu m^2 s^{-1}$
α_{Hh}	Hh maximal activation rate	3.4 x 10^{-3} $\mu M s^{-1}$
α_{ptc}	*ptc* maximal activation rate	2.7 x 10^{-5} $\mu M s^{-1}$
α_{ptc0}	*ptc* basal transcription rate	3.8 x 10^{-6} $\mu M s^{-1}$
α_{Signal}	Signal maximal activation rate	1.6 x 10^{-4} $\mu M s^{-1}$
β_{Hh}	Hh degradation rate	3.3 x 10^{-3} s^{-1}
β_{ptc}	*ptc* degradation rate	1.4 x 10^{-4} s^{-1}
β_{Ptc}	Ptc degradation rate	1.5 x 10^{-3} s^{-1}
β_{Signal}	'Signal' degradation rate	5.5 x 10^{-4} s^{-1}
β_{Hh_Ptc}	Hh_Ptc degradation rate	1.5 x 10^{-3} s^{-1}
γ_{Hh_Ptc}	Association rate, Hh_Ptc complex	7.15 x10^{-2} $\mu M^{-1} s^{-1}$
T_{Ptc}	Ptc translation rate	3.6 x 10^{-3} s^{-1}
k_{ptc}	*ptc* half-maximal activation conc.	0.14 μM
k_{Signal}	[Signal] half-maximal activation	2.135
m	Hill coefficient (*ptc* activation)	3
n	Hill coefficient ('Signal' activation)	6.8

(Parameter values are estimated from previous theoretical and experimental studies; see Nahmad and Stathopoulos (2009) for details).

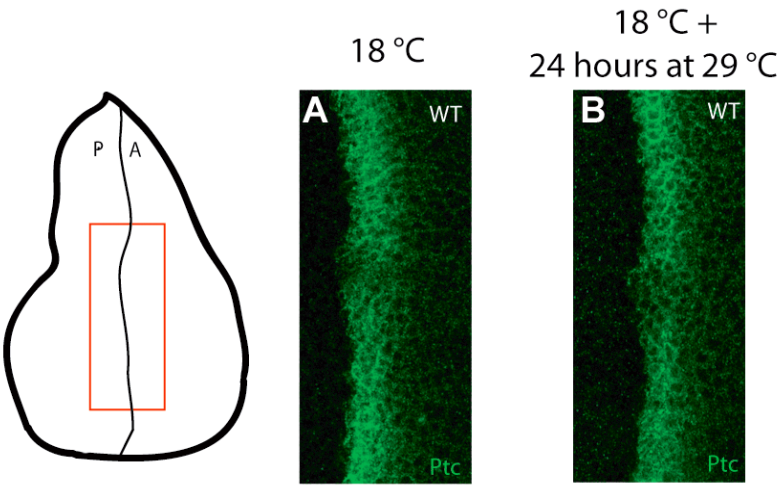

Supporting Fig. 2.1 Temperature changes do not affect Ptc expression.

Wild-type discs from larvae raised at 18°C (A) or from larvae raised at 18°C followed by 24 h at 29°C (B) immunolabeled for Ptc. Fixation, immunostaining, and imaging of discs in (A and B) were performed under identical conditions.

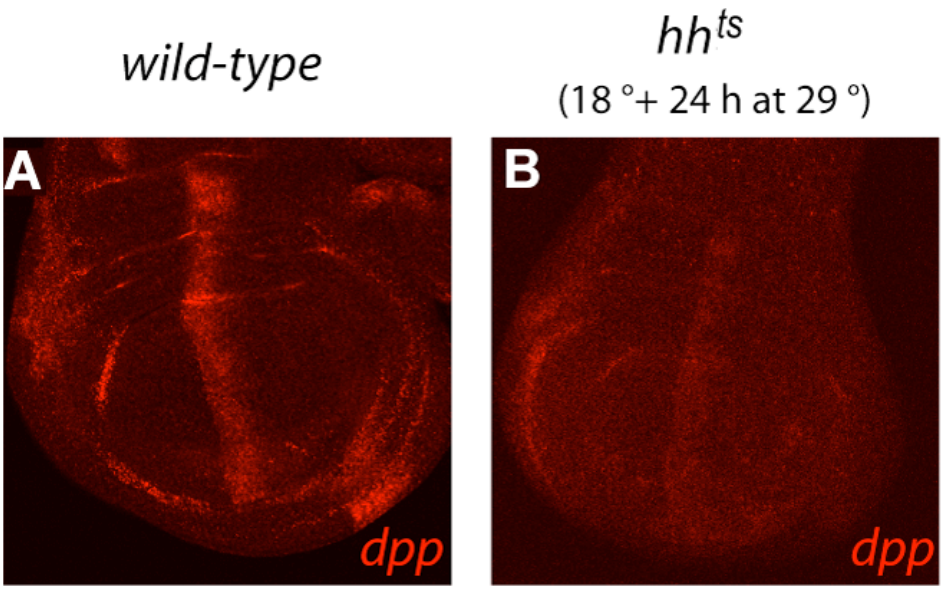

Supporting Fig. 2.2 dpp expression is maintained after Hh signaling is interrupted. In situ hybridization using a riboprobe to dpp in a wild-type disc (A) versus a hhts2 homozygous disc (B) grown at 18°C and exposed to 29°C for the last 24 h of the third larval instar. The domain of dpp expression is similar in (A and B), but the intensity of expression is higher in wild type. If residual Hh levels were to account for this expression, then dpp expression domain would be predicted to shift in expression toward the AP boundary; the full extent of the pattern would not be expected.

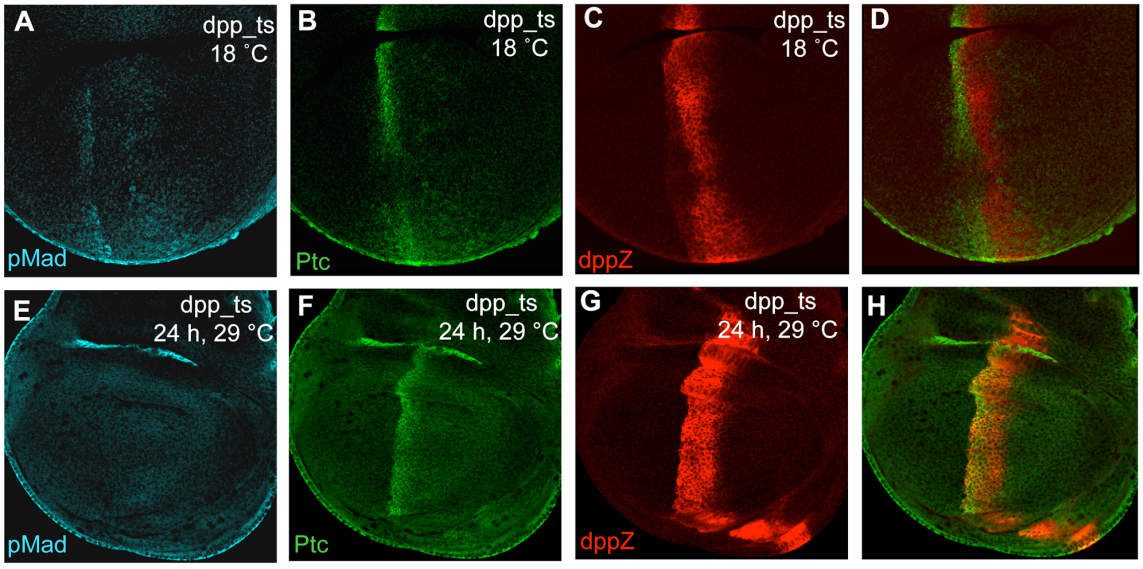

Supporting Fig. 2.3 dppZ and Ptc expression patterns are normal after Dpp signaling interruption.

(A–C) dpp^{hr56}/dpp^{hr4} animals raised at 18°C are normal in Dpp signal transduction assayed by pMAD expression (A) and have normal patterns of Ptc (B) and dppZ (C). (D) Merge of the patterns displayed in (B and C). (E–G) dpp^{hr56}/dpp^{hr4} larvae exposed to restrictive temperature (29°C) for 24 h have lost their pMAD expression pattern (E), and yet, Ptc and dppZ are approximately normal (F and G). The patterns do not overlap, suggesting that Dpp signaling is not required for maintenance of *dpp* expression in the nonoverlapping region. (H) Merge of the patterns displayed in (F and G). In this figure, the dppZ transgene is an insertion on chromosome III, to allow assay in a dpp mutant background.

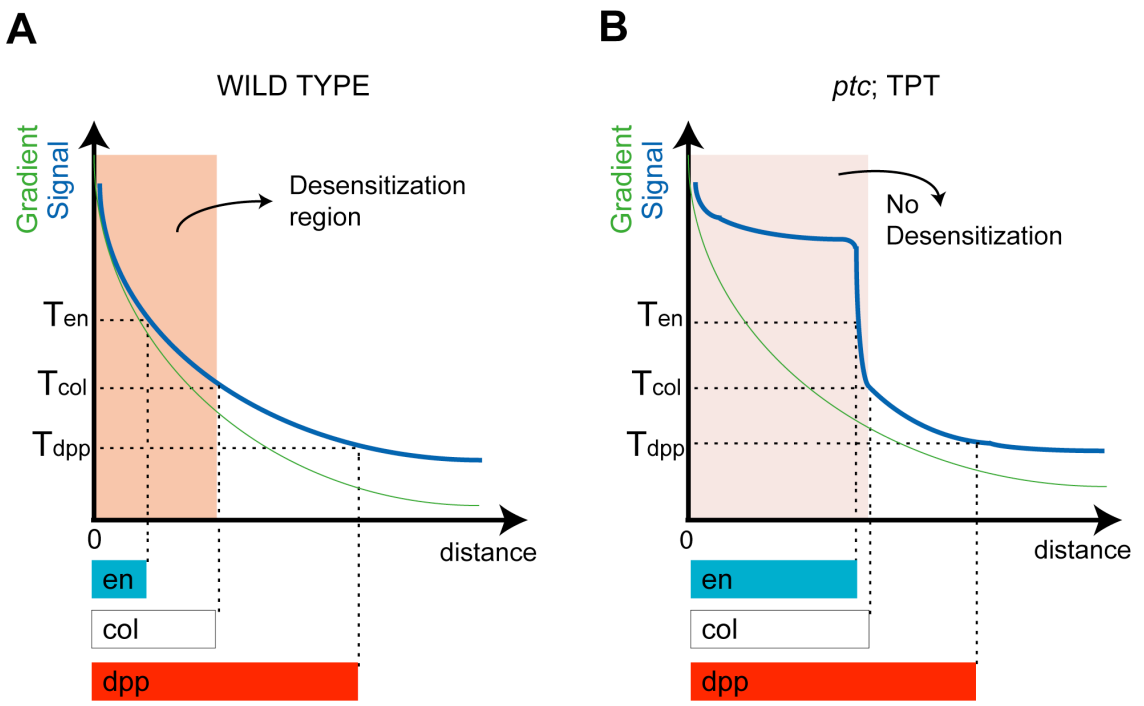

Supporting Fig. 2.4 The overlap of Col and dppZ in *ptc*−TPT discs cannot be explained by the Temporal Adaptation model.

Predictions of Hh patterning in wild-type (A) versus *ptc*−TPT discs (B) according to the Temporal Adaptation model (Dessaud et al., 2007). In wild-type discs (A), Ptc-mediated desensitization is required to map different concentrations of the extracellular gradient (green) into a graded signal response (blue). However, when signal-mediated Ptc up-regulation is impaired, cells are unable to differentially "desensitize" the levels of the signal and respond similarly to different concentrations of the signaling (B). Thus, lack of desensitization in ptc−TPT discs results in the expansion of the highest response (e.g., en; blue) to the extent of the intermediate response (e.g., col; white), but should have little or no effect in the differential establishment of the dppZ and Col borders, because Ptc-mediated desensitization is a cell-autonomous effect.

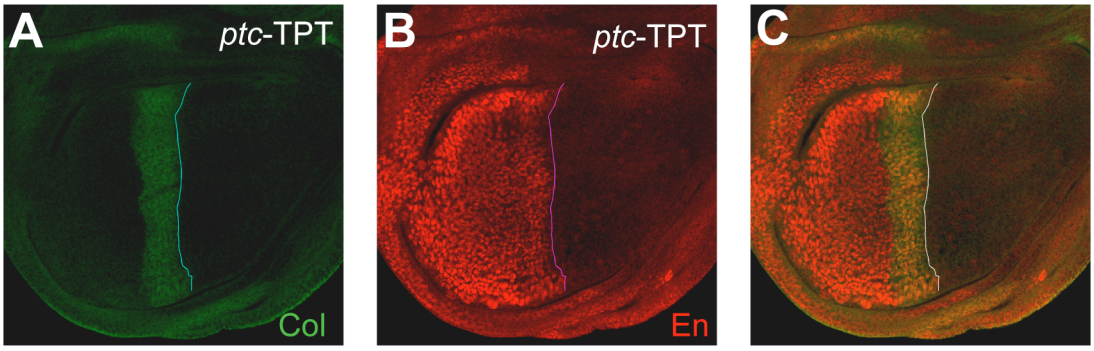

Supporting Fig. 2.5 Col and the anterior pattern of En overlap in *ptc*−TPT discs. Col (A) and En (B) are expressed in nearly the same domain in the anterior compartment in late third instar *ptc*−TPT discs. (C) Merge of panels displayed in (A and B). The line drawn from the Col pattern shows that Col and En approximately share their anterior border.

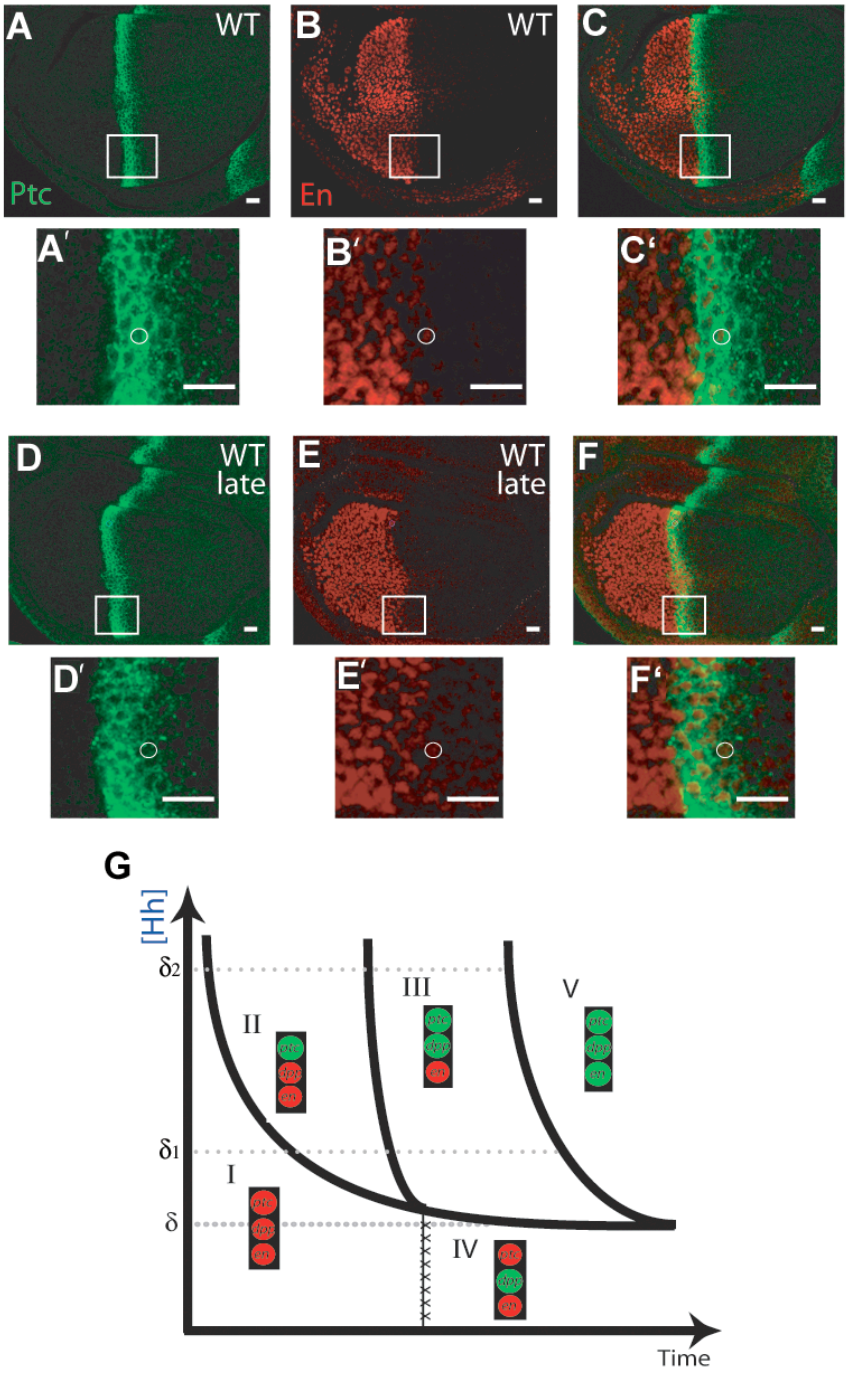

Supporting Fig. 2.6 Hh-dependent expression of Ptc and En approximately overlap in late wild-type discs.

(A and B) Immunostaining of wild-type wing discs from a crawling third instar larva using anti-En (A) and anti-Ptc (B) antibodies. (C) Merge of images in (A and B). (A′–C′)

4× magnification of the white box depicted in (A–C). White circles mark a cell in the anterior border of the En pattern showing that at this time, the En border approximately falls within the domain of Ptc expression, but does not share the same anterior boundary. (D and E) Same as (A and B), but from a third larva close to pupariation. (F) Merge of images in (D and E). (D′–F′) Magnification of the white box in (D–F). Scale bars indicate 10 μm. White circles mark a cell at the anterior boundary of the En pattern, showing that at this time, the En and Ptc anterior borders coincide. (G) Generalization of the state-space model in Figure 2.5 to incorporate *engrailed*. No additional concentration threshold is required to define the en domain of expression. Instead, en seems to be responsive to integration of Hh signaling over time, as it shares an anterior boundary with Ptc, and presumably Col, at later time points. Therefore, cells exposed to two different Hedgehog concentrations δ1 and δ2 above the switching threshold, δ, turn on Hh target gene expression at different time points but eventually activate all target genes (Territory V).

Supporting Materials for Chapter 3

Supporting Text

Linear approximation of the Hh steady-state gradient

Consider the model of Hh signaling in the *Drosophila* wing disc [Equations (3.5)]. At steady-state, simple algebraic substitutions reduce the system of equations to a single piecewise ordinary differential equation,

$$D\frac{d^2[\mathrm{Hh}]_{\mathrm{ss}}}{dx^2} + S^{-}(x)\alpha_{\mathrm{Hh}} - \frac{S^{+}(x)\chi\,[\mathrm{Hh}]_{\mathrm{ss}}}{\beta_{\mathrm{Ptc}} + \gamma_{\mathrm{Hh\_Ptc}}[\mathrm{Hh}]_{\mathrm{ss}}}\left[\alpha_{ptc0} + \frac{\alpha_{ptc}[\mathrm{Hh}]_{\mathrm{ss}}^{nm}}{k_{ptc}\beta_{\mathrm{Signal}}\left[\kappa^n + [\mathrm{Hh}]_{\mathrm{ss}}^n\right]^m + \alpha_{\mathrm{Signal}}[\mathrm{Hh}]_{\mathrm{ss}}^{nm}}\right] - \beta_{\mathrm{Hh}}[\mathrm{Hh}]_{\mathrm{ss}} = 0 \quad \text{(A1)}$$

with $\chi = \frac{T_{\mathrm{Ptc}}\gamma_{\mathrm{Hh\_Ptc}}}{\beta_{ptc}}$ and $\kappa = \frac{k_{\mathrm{Signal}}\beta_{\mathrm{Hh\_Ptc}}}{\gamma_{\mathrm{Hh\_Ptc}}}$. In the anterior compartment, $S^{-}(x) = 0$ and $S^{+}(x) = 1$, and Equation (A1) reduces to Equation (3.6) which can be linearised to obtain an approximate solution for the Hh steady-state gradient near the AP boundary [Equation (3.8)]. Here, we provide the details of this linearization that were omitted in the text. Near the AP boundary, Hh is present at sufficiently high levels that we can assume $[\mathrm{Hh}]_{\mathrm{SS}}^{\mathrm{n}} >> \kappa^{\mathrm{n}}$ (see below) so that the following approximation holds,

$$\frac{\alpha_{ptc}[\mathrm{Hh}]_{\mathrm{ss}}^{nm}}{\eta\left[\kappa^n + [\mathrm{Hh}]_{\mathrm{ss}}^n\right]^m + [\mathrm{Hh}]_{\mathrm{ss}}^{nm}} \approx \frac{\alpha_{ptc}}{\eta + 1}.$$

This expression reduces one nonlinear term in Equation (3.6) to a constant. The other nonlinear term can be approximated by a linear function near a point of interest $\left([\mathrm{Hh}]_{\mathrm{SS}}^0\right)$ via a Taylor expansion:

$$f([\mathrm{Hh}]_{\mathrm{SS}}) = \frac{\chi\,[\mathrm{Hh}]_{\mathrm{ss}}}{\beta_{\mathrm{Ptc}} + \gamma_{\mathrm{Hh\_Ptc}}[\mathrm{Hh}]_{\mathrm{ss}}} \approx f\left([\mathrm{Hh}]^0_{\mathrm{SS}}\right) + \frac{df}{d[\mathrm{Hh}]_{\mathrm{SS}}}\left([\mathrm{Hh}]^0_{\mathrm{SS}}\right)\left([\mathrm{Hh}]_{\mathrm{SS}} - [\mathrm{Hh}]^0_{\mathrm{SS}}\right)$$

$$\approx \frac{\chi}{\beta_{\mathrm{Ptc}} + \gamma_{\mathrm{Hh\_Ptc}}[\mathrm{Hh}]^0_{\mathrm{SS}}}\left[\frac{\gamma_{\mathrm{Hh\_Ptc}}[\mathrm{Hh}]^{0\ 2}_{\mathrm{SS}}}{\beta_{\mathrm{Ptc}} + \gamma_{\mathrm{Hh\_Ptc}}[\mathrm{Hh}]^0_{\mathrm{SS}}} + \left(1 - \frac{\gamma_{\mathrm{Hh\_Ptc}}[\mathrm{Hh}]^0_{\mathrm{SS}}}{\beta_{\mathrm{Ptc}} + \gamma_{\mathrm{Hh\_Ptc}}[\mathrm{Hh}]^0_{\mathrm{SS}}}\right)[\mathrm{Hh}]_{\mathrm{SS}}\right].$$

The maximum $[\mathrm{Hh}]_{\mathrm{SS}}$ levels are limited by the ratio of the Hh production rate (α_{Hh}) to the Hh degradation rate (β_{Hh}) and numerical estimates suggest that $[\mathrm{Hh}]_{\mathrm{SS}}$ rapidly drops to one third of this maximal value within a few cells diameters from the AP boundary (Fig. 3.3B). Therefore, substituting $[\mathrm{Hh}]^0_{\mathrm{SS}} = \frac{1}{3}\frac{\alpha_{\mathrm{Hh}}}{\beta_{\mathrm{Hh}}}$ (which also satisfies the condition of the previous approximation: $\left[\frac{1}{3}\frac{\alpha_{\mathrm{Hh}}}{\beta_{\mathrm{Hh}}}\right]^{\mathrm{n}} >> \kappa^{\mathrm{n}}$ using the parameter values in Supporting Table 2.1) in the Taylor expansion above we get,

$$\frac{\chi\,[\mathrm{Hh}]_{\mathrm{ss}}}{\beta_{\mathrm{Ptc}} + \gamma_{\mathrm{Hh\_Ptc}}[\mathrm{Hh}]_{\mathrm{ss}}} \approx \frac{3\chi\beta_{\mathrm{Hh}}}{3\beta_{\mathrm{Hh}}\beta_{\mathrm{Ptc}} + \alpha_{\mathrm{Hh}}\gamma_{\mathrm{Hh\_Ptc}}}\left[\frac{\gamma_{\mathrm{Hh\_Ptc}}\alpha^2_{\mathrm{Hh}}}{9\beta^2_{\mathrm{Hh}}\beta_{\mathrm{Ptc}} + 3\alpha_{\mathrm{Hh}}\beta_{\mathrm{Hh}}\gamma_{\mathrm{Hh\_Ptc}}} + \left(1 - \frac{\alpha_{\mathrm{Hh}}\gamma_{\mathrm{Hh\_Ptc}}}{3\beta_{\mathrm{Hh}}\beta_{\mathrm{Ptc}} + \alpha_{\mathrm{Hh}}\gamma_{\mathrm{Hh\_Ptc}}}\right)[\mathrm{Hh}]_{\mathrm{SS}}\right].$$

These approximations turn Equation (3.6) into a linear equation [Equation (3.7)] which can be solved analytically once boundary conditions are provided. The boundary condition at the anterior end is completely irrelevant and can be ignored (i.e. assumed at infinity) because the range of the $[\mathrm{Hh}]_{\mathrm{SS}}$ gradient is much shorter than the width of the anterior compartment. However, the solution [Equation (3.8)] is only fully determined once the boundary conditions at x=0 are specified. In fact, the parameter A in Equation (3.8) is determined by imposing continuity of the gradient (and its derivative) at the AP boundary. Note that Equation (A1) in the posterior compartment takes the following simple form:

$$D\frac{d^2[\mathrm{Hh}]_{\mathrm{ss}}}{dx^2} + \alpha_{\mathrm{Hh}} - \beta_{\mathrm{Hh}}[\mathrm{Hh}]_{\mathrm{ss}} = 0.$$

Imposing a zero-flux boundary condition in the posterior end: $\left[\frac{d[\mathrm{Hh}]_{\mathrm{SS}}}{dx}\left(x=-L_{\mathrm{P}}\right)=0\right]$,

the solution of this equation is:

$$[\mathrm{Hh}]_{\mathrm{SS}}(x)=\frac{\alpha_{\mathrm{Hh}}}{\beta_{\mathrm{Hh}}}-\mathrm{M}\cosh\left[\frac{x+L_{\mathrm{P}}}{\sqrt{D/\beta_{\mathrm{Hh}}}}\right] \quad (\text{for } x\le 0), \qquad (\mathrm{A2})$$

with M determined by boundary conditions at x =0. By continuity, Equations (3.8) and (A2) and their derivatives must coincide at x=0. This condition determines A (in Equation (3.8)) and M (in Equation (A2)) uniquely from a system of two algebraic equations:

$$\mathrm{A}-\frac{\mathrm{C}}{\mathrm{B}}=\frac{\alpha_{\mathrm{Hh}}}{\beta_{\mathrm{Hh}}}-\mathrm{M}\cosh\left[\sqrt{\frac{\beta_{\mathrm{Hh}}}{D}}L_{\mathrm{P}}\right]$$
$$\mathrm{A}\sqrt{\mathrm{B}}=\mathrm{M}\sqrt{\frac{\beta_{\mathrm{Hh}}}{D}}\sinh\left[\sqrt{\frac{\beta_{\mathrm{Hh}}}{D}}L_{\mathrm{P}}\right].$$

And simple algebraic substitutions give,

$$\mathrm{A}=\frac{\frac{\alpha_{\mathrm{Hh}}}{\beta_{\mathrm{Hh}}}+\frac{\mathrm{C}}{\mathrm{B}}}{1+\sqrt{\frac{\mathrm{B}D}{\beta_{\mathrm{Hh}}}}\coth\left(\sqrt{\frac{\beta_{\mathrm{Hh}}}{D}}L_{\mathrm{P}}\right)}.$$

This analysis permits to obtain a linear approximation of the Hh gradient near the AP boundary and defines the approximate steady-state invariant set described by Equations (3.9).

Geometric Properties of Steady-State Invariant Sets

Given the practical purposes of the study, we considered steady-state invariant perturbations as a subset of parameter space, but their geometric properties were not

stated in detail. Here, we briefly discuss some general geometrical properties of steady-state invariant sets and discuss potential advantages of a geometric treatment. Steady-state invariant sets are defined by systems of algebraic equations (in many cases by polynomial equations), and therefore, they are real semi-algebraic varieties. As such, geometric properties such as their dimension (or codimension) are well defined. Although a formal treatment of the geometry of steady-state invariant sets is beyond the scope of this study, it is important to realize that there is a vast literature of algebraic and geometric tools to analyze the properties steady-state invariant sets. Future geometric studies may provide insights into practical aspects of steady-state invariant sets. For example, how to decompose steady-state invariant sets into more simple varieties; and the existence of steady-state invariant subsets of codimension zero.

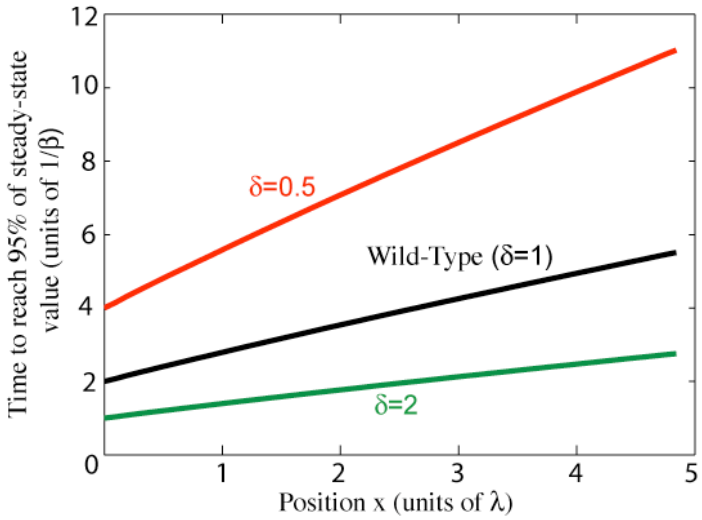

Supporting Fig. 3.1. **The time to reach the steady state is position-dependent.**

In the model of the single morphogen described by Equation (3.1), the time to reach the steady state is position-dependent. Cells located closer to the morphogen source approach the equilibrium faster than cells farther away from it. The same trend is observed for parameter perturbations along the steady-state invariant set (δ=0.5, red line; δ=2, green line). As a consequence of this spatial effect, cells sufficiently far from the source may not reach the equilibrium within the developmental timescale.

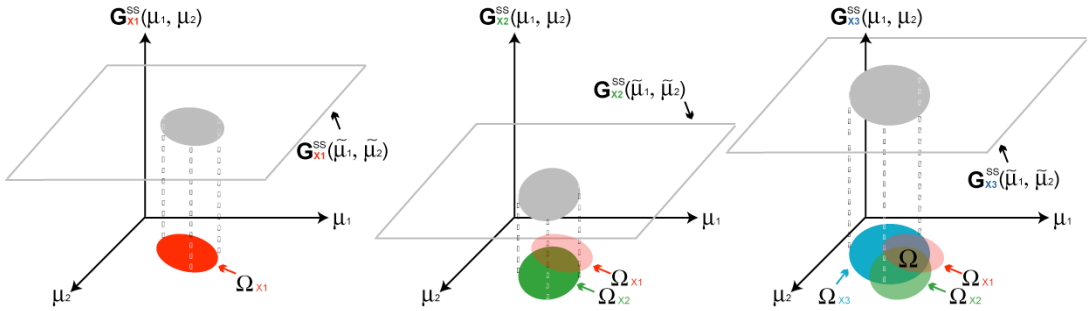

Supporting Fig. 3.2. Geometric visualization of a general steady-state invariant set. For a fixed spatial position, we can obtain the set of parameter values that leave the steady-state solution $\mathbf{G}^{SS}$ unchanged with respect to the wild-type (Equation (B4) in Box 3.1), i.e., the set of points in parameter space that are mapped into the same value of $\mathbf{G}^{SS}$ than the wild-type values. The figure shows a cartoon of these sets for three different points (denoted by Ω_{X1}, Ω_{X2}, and Ω_{X3}). The steady-state invariant set $\boldsymbol{\Omega}$ (in $\mathbf{S}$={X1, X2, X3}) is given by the intersection of those sets (Equation (B5) in Box 3.1).

Supporting Materials for Chapter 4

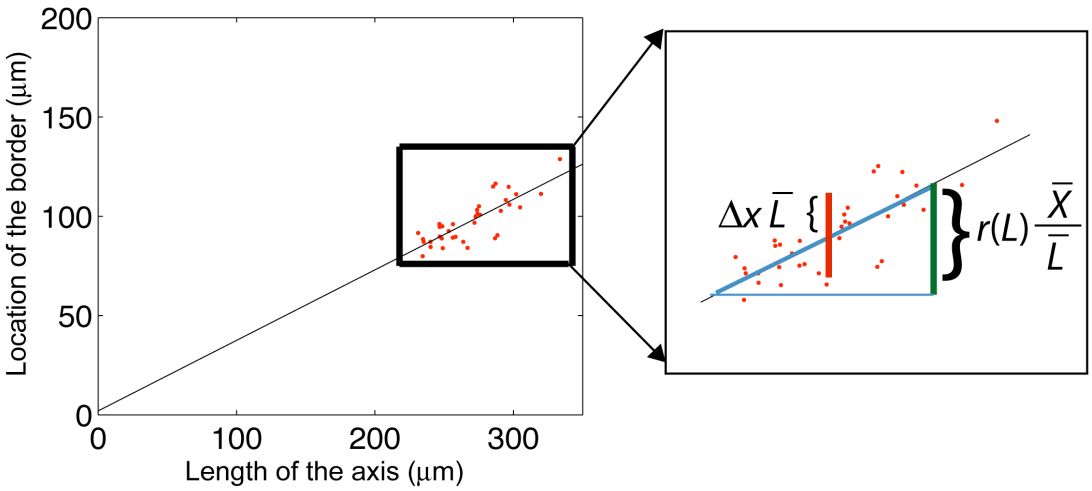

Supporting Fig. 4.1 Derivation of the scaling percentage level.

Given a plot of positional data vs. length of the domain, we can derive the scaling percentage level formula by comparing the variability in the positional data (red bar) to the height of a right triangle (green bar) of base equal to r(L) and slope defined by the ratio of the mean location to the mean axis length. The ratio of the red to green bars represents how much of the data can be explained by chance due to fluctuations in the X_i's. Thus, C is the percentage of scaling data that cannot be explained by variability on the positional data.

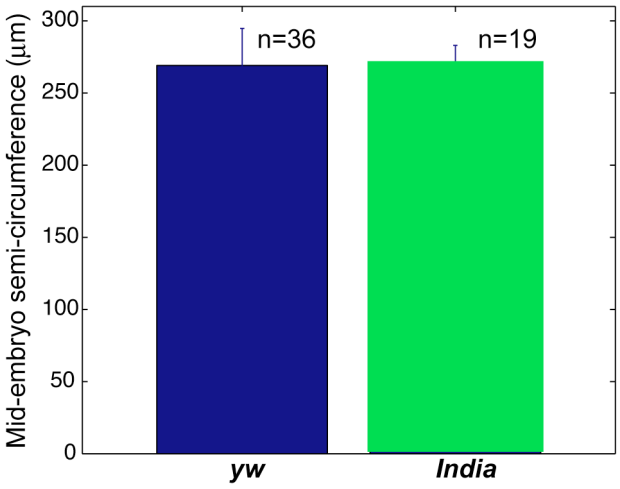

Supporting Fig. 4.2 *yw* and India embryos do not display significant differences in the length of the DV axis.

Although India and *w1118* embryos display significant differences along the AP axis (Lott et al., 2007), measurements from cross sections show that they do not differ significantly in the length of their DV axis.